THE EXPRESSION OF ^{19}F-LABELED BETA-PHOSPHOGLUCOMUTASE AND THE EVALUATION OF ITS INHIBITORS

By

Anna A. Ampaw

Submitted in partial fulfillment of the requirements
for the degree of Master of Science

at

Dalhousie University
Halifax, NS
July 2016

~ Hebrews 13:5-6 ~

TABLE OF CONTENTS

List of Tables

List of Figures

List of Schemes

Abstract

β-Phosphoglucomutase (βPGM) is an isomerase that catalyzes the conversion of β-glucose 1-phosphate to glucose 6-phosphate via a 1,6-bisphosphate intermediate. Incorporation of 5-fluorotryptophan (5FW) into βPGM (ie. 5FWβPGM) as a ^{19}F NMR spectroscopic probe revealed that the ^{19}F nucleus in 5FW is a sensitive probe for monitoring metal fluoride transition state analogue (TSA) complexation and ligand binding. The ability of βPGM to form transition state analogue complexes with novel compounds, β-glucose 1,6*C*-phosphonate, and β-2-deoxy-2-fluoro glucose and mannose 1*C*-phosphonates were examined; however, only β-glucose 1,6*C*-phosphonate (IC_{50} = 186 ± 73 μM) and β-2-deoxy-2-fluoro glucose (2.68 ± 0.04 μM) configured analogs bound to βPGM. All compounds that exhibited complexation with 5FWβPGM by ^{19}F NMR spectroscopy were confirmed as competitive. Approaches to the synthesis of 1,6-bisphosphate and phosphofluoridates analogs as mechanism-based inactivators of 5FWβPGM are described.

List of Abbreviations and Symbols Used

1D	one dimensional
2D	two dimensional
5FW	5-fluorotryptophan
5FWβPGM	5-fluorotryptophan labeled βPGM
Å	ångstrom
α	alpha
β	beta
β2FG1CP	β-2-deoxy-2-fluoro glucose 1*C*-phosphonate
β2FMan1CP	β-2-deoxy-2-fluoro mannose 1*C*-phosphonate
βG16CP	β-glucose 1,6*C*-phosphonate
βG1P	β-glucose 1-phosphate
βG1CP	β-glucose 1*C*-phosphonate
βG1CFsP	(S)-β-glucose 1*C*-fluoromethylene phosphonate
βPGM	β-phosphoglucomutase
ε	extinction coefficient
γ	gamma
δ	chemical shift
Δδ	change in chemical shift
A_{340}	absorbance at 340 nm
AcOH	acetic acid
Ac_2O	acetic anhydride
AIBN	azobisisobutyronitrile
Asp	aspartic acid
ATP	adenosine triphosphate
Bn	benzyl
Bu	butyl
COSY	correlation spectroscopy
cm	centimeter

d	doublet
dd	doublet of doublets
ddd	doublet of doublet of doublets
DBU	1,8-diazabicyclo[5.4.0]undec-7-ene
ddH_2O	distilled deionized water
DEAE	diethylaminoethyl
DIPEA	*N,N*-Diisopropylethylamine
DMAP	4-(Dimethylamino)pyridine
DMF	dimethylformamide
DMSO	dimethyl sulfoxide
DNA	deoxyribonucleic acid
dt	doublet of triplets
DTT	dithiothreitol
EDTA	Ethylenediaminetetraacetic acid
EtOAc	ethyl acetate
^{19}F	fluorine
^{1}H	hydrogen
HMBC	heteronuclear multiple-bond correlation
HSQC	heteronuclear single quantum coherence
IC_{50}	concentration resulting in 50% inhibition
IPTG	isopropyl β-D-1-thiogalactopyranoside
kb	kilobase
k_{cat}	turnover number
K_i	inhibition constant
K_m	Michaelis-Menten constant
L	litre
LB	lysogeny broth
LC	liquid chromatography
m	multipet
MeOH	methanol
MHz	megahertz

MS	mass spectroscopy
MWCO	molecular weight cutoff
$NADP^+$	nicotinamide adenine dinucleotide phosphate
NADPH	reduced nicotinamide adenine dinucleotide phosphate
NMR	nuclear magnetic resonance
NOE	nuclear overhauser effect
OD_{600}	optical density at 600 nm
PAGE	polyacrylamide gel electrophoresis
PCR	polymerase chain reaction
Ph	phenyl
ppm	parts per million
R_f	retention factor
rpm	revolutions per minute
s	singlet
SDS	sodium dodecyl sulfate
S_N1	nucleophilic substitution
t	triplet
TBAB	tetrabutylammonium bromide
TBTU	*N,N,N′,N′*-Tetramethyl-*O*-(benzotriazol-1-yl)uronium tetrafluoroborate
THF	tetrahydrofuran
Thr	threonine
TLC	thin-layer chromatography
TS	transition state
U	units
UV	ultraviolet

Acknowledgments

First and foremost, I would like to thank my supervisor, Dr. David Jakeman, for his continuous support and encouragement over the course of my studies. From the day you flew me to Halifax as a potential graduate student, you have provided me with the opportunity to expand out of my comfort zone and develop my skills as a scientist and a researcher. I would also like to thank my lab mates, past and present, for their inputs on my various projects and for creating a supportive and constructive research environment. Specifically, I would like to thank Jian-She Zhu who continuously advised and encouraged me and provided great discussion towards my project. I would also like to specifically thank Nicole Allward for her large contributions towards my project.

I would like to acknowledge my committee members, Dr. Stephen Bearne and Dr. Bruce Grindley, for their advice and support throughout the course of my work. I would also like to acknowledge Dr. Alejandro Cohen for the time and effort spent in acquiring LC-MS/MS data for my work.

A special thanks goes out to my parents, Ransford and Eva Ampaw, and my sister, Phoebe Ampaw, for listening to my complaints and frustrations during the last few years and for always providing encouraging words to get me through the difficult times. I also thank my friends, old and new, for their support, and the Eghan family for making my move to Halifax easier than anticipated. Last but definitely not least, I thank God for seeing me through my graduate degree.

CHAPTER 1. INTRODUCTION

1.1 Phosphate Transfer Enzymes

Phosphate esters are stable and essential linkages for biological metabolism. These linkages play key roles in genetic materials, cell regulation, and energy reservoirs and their kinetic stability is imperative for various biological roles. The stability is such that the half-life for the spontaneous hydrolysis of phosphorus-oxygen bonds is 10^7 years for diesters and 10^{12} years for monoesters at physiological conditions.[1] Thus, enzymes that cleave the P-O bond of mono- and diesters, for biologically important phosphate-transfer reactions, must significantly enhance the rate of reaction. Rate enhancements for enzyme catalyzed phosphate-transfer reactions have been reported to be as high as ~10^{21},[1] making these enzymes and their mechanisms a focus for research. Phosphate transfer enzymes act on a wide variety of substrates involving a specific donor and an acceptor including water (phosphatases), another substrate (kinases) or another functional group on the same molecule (mutases). Enzymatic phosphoryl transfer reactions have been classified into three distinct mechanisms: dissociative, associative, and concerted.[2] A dissociative phosphoryl transfer mechanism consists of an S_N1-like mechanism involving the formation of a metaphosphate ion followed by an attack from a nucleophile in a rate-determining step (Scheme 1A). In an associative mechanism, a two-step addition-elimination reaction occurs via a phosphorane intermediate (Scheme 1B). This mechanism is usually observed in some enzymatic reactions with triesters and diesters. Lastly, in a concerted mechanism no intermediate is formed, rather, bond formation to the nucleophile and bond fission to the leaving group occur during its transition state

(Scheme 1C). The pathway in which enzyme-catalyzed phosphate transfer reactions occur is dependent on the nature of the nucleophile, electrophile, leaving group, and primarily its catalytic scaffold.

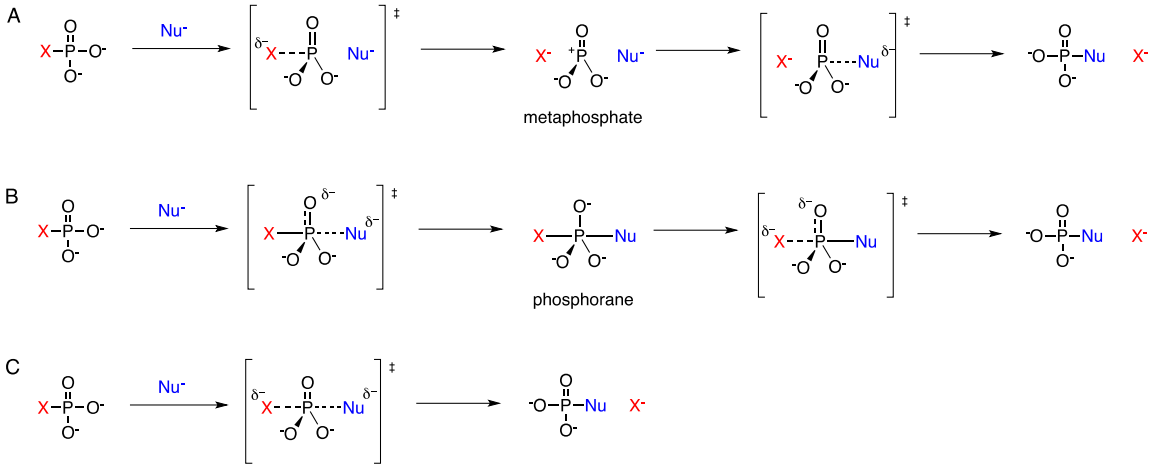

Scheme 1. Three enzymatic phosphoryl transfer mechanisms.[2]

(A) Dissociative mechanism with metaphosphate ion intermediate; (B) associative, addition-elimination mechanism with phosphorane intermediate; (C) concerted mechanism. Nu represents a nucleophile and X represents a leaving group.

1.2 Haloalkanoic Acid Dehalogenase (HAD) Superfamily

A majority of the enzymes that catalyze phosphoryl transfer reactions are members of the HAD superfamily. HAD superfamily enzymes catalyze reactions involving formation of a covalent intermediate with an active site aspartate, which includes enzymes such as phosphoesterases, ATPases, phosphonatases, dehalogenases, phosphomannomutases, and β-phosphoglucomutase. Evolution of this family has allowed for diversification of substrates; however, similarities in core domain structure exist between each enzyme. All members of the HAD family possess a conserved α/β core domain comprised of a central parallel β-sheet flanked by α-helices on both sides.[2,3,4] This conserved pattern supports

the four highly conserved loops comprising the catalytic scaffold, which house the Mg^{2+} cofactor and the two aspartic acid (Asp) residues, one of which acts as a nucleophile and one of which acts as a general acid/base catalyst.[3] Contrarily, the structure of the cap domain varies within the HAD family, allowing members to be grouped further into subfamilies. The evolution of the various cap domain structures is a result of the inability of the core domain to close off the active site from water and recognize its substrate, thus, the cap domain provides a cap-open/cap-closed mechanism allowing for substrate specificity.[3] A unique member of the HAD family, β-phosphoglucomutase (βPGM), has evolved its cap domain to accommodate the binding of two different substrates and to prevent hydrolysis of its phosphorylated aspartic acid residue.

1.3 β-Phosphoglucomutase

β-Phosphoglucomutase (βPGM) is a phosphotransferase isomerase enzyme that catalyzes the conversion of β-glucose 1-phosphate (βG1P) to glucose 6-phosphate (G6P) via an associative mechanism involving a β-glucose 1,6-bisphosphate (βG16P) intermediate (Scheme 2). Its enzyme product, G6P, is a key metabolite that links exopolysaccharide biosynthesis to glycolysis in certain bacteria and prokaryotes.[5,6]

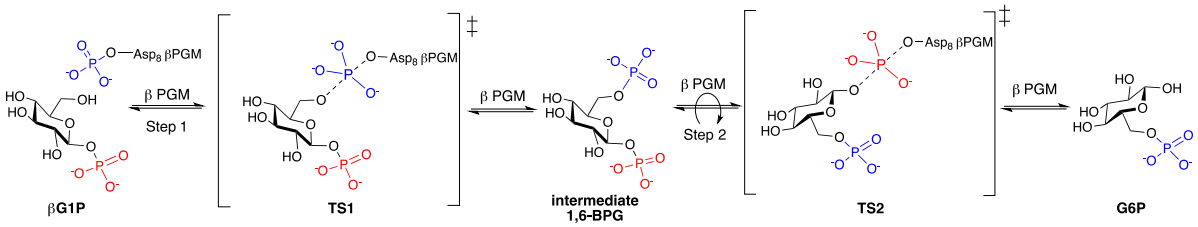

Scheme 2. Enzymatic mechanism of βPGM converting βG1P to G6P via a βG16BP intermediate.

Conversion of substrate to product occurs through a ping pong bi bi mechanism allowing the intermediate to reorient itself in the enzyme active site.

Studies on the enzyme structure of βPGM reveal that the protein is 25 kDa and monomeric, containing a helical cap domain and the HAD family conserved α/β core domain with its active site at the interface of these domains.[4] A superimposition of crystal structures representing the open and closed conformation of βPGM suggest that upon binding of βG1P, the structure of βPGM changes from its "cap-open" conformation to its "cap-closed" conformation by the rigid rotation of its cap domain.[5] In its cap-closed conformation, the phosphorylated aspartic acid residue (Asp8) of βPGM transfers its phosphate to the C-6 hydroxyl of βG1P producing a β-glucose 1,6-bisphosphate (βG16P) intermediate causing the enzyme to convert to its "cap-open" conformation. The open active site triggers βG16P to dissociate from the enzyme, allowing itself to reposition for dephosphorylation of the phosphate at C-1, before it rebinds to the enzyme prompting it to convert back into its "cap-closed" conformation. Removal of the C-1 phosphate group by Asp8 results in release of the product by conversion back into its "cap-open" conformation. Once the product is released, the aspartyl phosphate group remains stable against hydrolysis before another substrate binds to the active site. Allen and coworkers[7] attributed the ability for phosphorylated βPGM to discriminate between substrate and hydrolysis during the exchange of product for substrate to a proposed "hinge model." The "hinge model" suggested that Asp10 acts as a general acid/base catalyst that stabilizes the enzyme in its cap-closed conformation by forming a hydrogen bond with C-1 oxygen. However, in its cap-open conformation, Asp10 is pinned outside of the active site by hydrogen bond formation between the two amino groups of Thr16 and Ala17, thus it

cannot catalyze the phosphoryl transfer to water.[7] Attempts at understanding the two-step mechanism of βPGM have also been made by several kinetic studies[5] and by the use of metal fluorides, which form transition state analog (TSA) complexes by trapping the enzyme in its cap-closed conformation.

1.4 ^{19}F as a Spectroscopic Probe

Fluorine (^{19}F) has been used to probe the structure of proteins in their solvated environment for several years due to its high sensitivity and useful properties. The similarity in size between ^{19}F and ^{1}H nuclei allows for easy substitution into proteins and the absence of naturally occurring fluorine in proteins renders ^{19}F a good spectroscopic probe. Fluorine are spin ½ nuclei that occur at 100% natural abundance and have 83% the sensitivity of ^{1}H allowing for lower protein concentrations and shorter acquisition times for ^{19}F NMR studies compared to multi-dimensional NMR experiments. Fluorine probes can be incorporated as part of the enzyme structure,[8-19] or as fluorinated analogs for natural ligands, substrates, and intermediates.[20-23]

1.4.1 Metal Fluorides as Stable Analogs for Phosphoryl Groups

The formation of stable metal fluoride complexes in the active site of phosphoryl transfer enzymes was first observed in G proteins.[24] X-ray crystallography revealed a square pyramidal AlF_4^- species in the position of the γ-phosphate upon addition of aluminum and fluoride, and similarly, a trigonal bipyramidal MgF_3^- species was observed in the position of the γ-phosphate upon addition of magnesium and fluoride. In the case of G proteins, these metal fluoride species resulted in enzyme activation, however, in other phosphoryl

transfer enzymes, metal fluoride complexes have resulted in enzyme inhibition, providing insight into their transition states. An enzyme's ability to achieve high reaction rates is dependent on its ability to stabilize its transition state, which is often facilitated by the formation of stabilizing non-covalent interactions between the enzyme and its transition state leading to a lower activation energy.[25] Analyzing these interactions can provide information about the enzyme mechanism and structure, however, trapping the enzyme during its transition state can be difficult due to its high energy.[26] Thus, transition state analogs are used to form complexes that lock the enzyme in its high energy state.[21,27-30] Formation of transition state analogs for phosphoryl transfer enzymes has been of interest in an attempt to rationalize their high rate enhancements. Initially, vanadate complexes were used as analogs of phosphates in phosphoryl transfer enzymes;[27,31] however, recent studies have shown that metal fluorides closely mimic the charge and geometry of the covalently bound phosphate such that they can form long-lived complexes with various substrate analogs.[20,32] Although MgF_3^- and AlF_4^- form complexes with different geometries, they are both suitable mimics of the transferring PO_3^- species. AlF_4^- prefers an octahedral shape, and MgF_3^- a trigonal-bipyramidal shape.[22]

1.4.2 Metal Fluoride Transition State Analogs of βPGM

Waltho and coworkers showed that MgF_3^- and AlF_4^- TSA complexes with G6P could be isolated and analyzed (Fig. 1) as a representation of step 2 (TS2) of the enzyme reaction; however, complexes with βG1P were inaccessible as a result of its high rate of reaction.[33] To solve this problem, methylenephosphonate and α-fluoromethylenephosphonate analogs of βG1P were synthesized to enable formation of the TSA complexes (Fig. 1),

inhibiting step 1 (TS1) of the enzymatic reaction.[21] Both step 1 and step 2 TSA complexes are representations of the enzyme in its different cap-closed forms. Crystal structures of both TSA complexes revealed that complexes for step 1 involve direct contact of amino acid residues with the substrate while formation of the step 2 complexes involve two conserved water molecules bridging together the substrate and amino acid residues.[21] The difference in step 1 and step 2 complexes can also be observed by ^{19}F NMR spectroscopy as the ^{19}F chemical shifts are different for G6P and βG1P analog complexes.

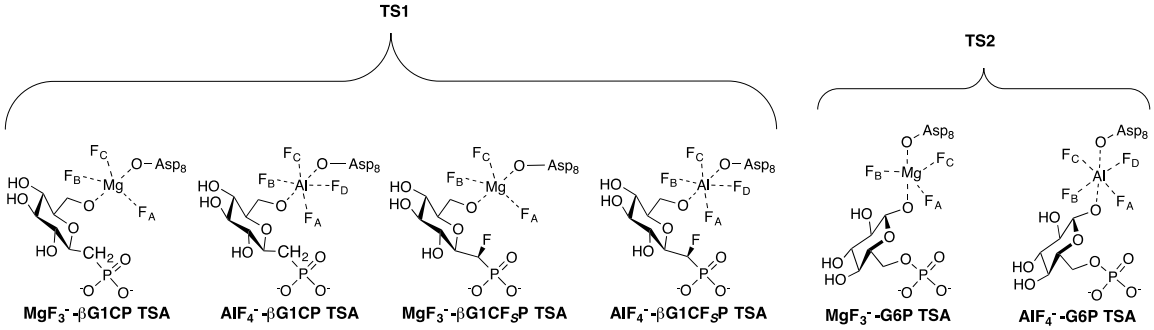

Figure 1. Inhibition of step 1 and 2 of the enzymatic reaction by the formation of TSA complexes.

MgF_3^- and AlF_4^- have a suitable geometry and charge to mimic the aspartyl PO_3^- enabling the formation of a stable complex with βPGM and either G6P,[33] βG1CP,[21] or βG1CF$_S$P.[21]

1.5 Probing Enzyme Conformation with Fluorinated Amino Acids

Although the use of fluorinated ligands provides a spectroscopic probe to detect complex formation, incorporating fluorine into a protein structure via a ^{19}F-labeled amino acid analog provides an effective tool to monitor non-fluorinated ligand binding[14,15] and to analyze protein conformations and dynamics in the ground state.[9,16-19] Studies have shown that fluorine probes located on different domains of the enzyme can provide insight on localized or global structural changes occurring during ligand binding[33] and on

conformational changes inaccessible to crystallography.[17] ^{19}F-Labeled proteins are also advantageous when investigating a protein of an unknown structure. Solvent-exposure experiments[9,10,35] and NOE experiments[21,36,37] can be performed with ^{19}F-labeled proteins to determine intramolecular interactions between amino acid residues or intermolecular interactions between amino acids and solvent or ligands. These advantages combined with the ease of ^{19}F NMR studies on ^{19}F-labeled proteins has made it a more attractive tool than other 1D and 2D NMR studies when investigating protein conformation and protein-ligand interactions.

Fluorine as a spectroscopic probe for βPGM has been explored through the formation of stable metal fluoride complexes; however, it is limited only to substrate and product analogs and lacks any information about the enzyme conformation or stoichiometry. Thus, incorporating a spectroscopic probe into the enzyme structure would allow for the screening and analysis of a wide range of inhibitors without the use of metal fluorides.

1.6 Research Objectives

The objectives for this research are:

- To express fluorine-labeled βPGM and to observe the formation of transition state analog complexes using ^{19}F NMR spectroscopy
- To synthesize non-covalent inhibitors and to explore the synthesis of mechanism-based inactivators of βPGM
- To perform kinetic analysis on fluorine-labeled βPGM and evaluate synthetic non-covalent inhibitors

CHAPTER 2. RESULTS AND DISCUSSION: ^{19}F-LABELED βPGM NMR STUDIES

Excerpts of this section were taken from Ampaw, A.; Bhattasali, D.; Cohen, A.; Jakeman, D. L. *Submitted to Chem. Sci.* **2016.**

2.1 Expression of His_6-Tag in βPGM

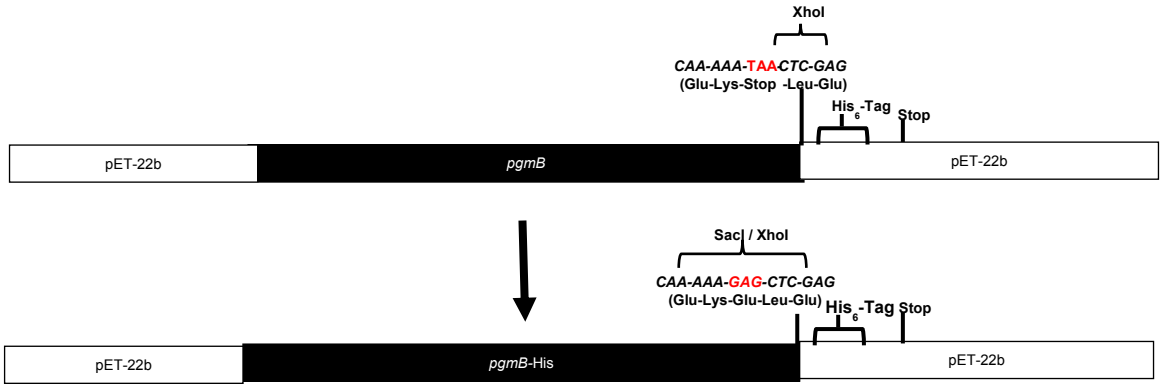

Figure 2. Pictorial representation of pET-22b(+)*_pgmB*-His mutation.

The highlighted base pairs were altered to convert a stop codon to Glu and to add the restriction site SacI.

pET22b(+)*_pgmB,* the gene used to express βPGM from *Lactococcus lactis,* was received as a gift from the University of Sheffield with a stop codon located before its C-terminal histidine$_6$-tag (His_6-tag). To allow for a convenient method of purification, the stop codon was removed via site-directed mutagenesis. The stop codon was converted to a glutamic acid residue while incorporating a unique restriction site (Fig. 2). PCR amplification of oligonucleotide primers and the pET22b(+)*_pgmB* template resulted in a

mutant that was confirmed by plasmid digestion with restriction enzymes SacI and PstI (Fig. 3).

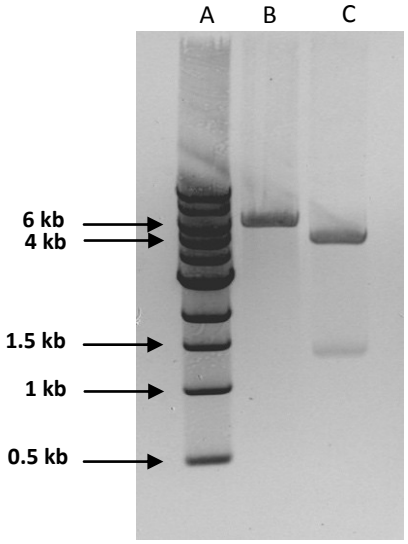

Figure 3. 1% agarose gel of pET-22b_pgmB and pET-22b_pgmB-His digested with restriction enzymes.

(A) 1 kb DNA ladder; (B) pET-22b_pgmB digested with PstI and SacI; (C) pET-22b_pgmB-His digested with PstI and SacI.

2.2 Expression of ^{19}F-labeled βPGM

Incorporation of fluorine into the βPGM enzyme was accomplished by the use of 5-fluorotryptophan (5FW). The βPGM structure contains two tryptophan residues, W24 and W216. Analysis of a previously solved crystal structure of βPGM with a TSA complex (PDB ID code 4C4R)[21] reveals that W24 is on the enzyme cap domain and W216 is on the enzyme core domain. W24 is ~3 Å from the active site, allowing the indole nitrogen to form a hydrogen bond with the substrate during catalysis while W216 is on the outer surface of the core domain, ~22 Å from the active site, and is not in direct contact with the substrate (Fig. 4). Since the two tryptophan residues are located on

different domains, we anticipated that their difference in environment would result in two distinct ^{19}F resonances by ^{19}F NMR spectroscopy.

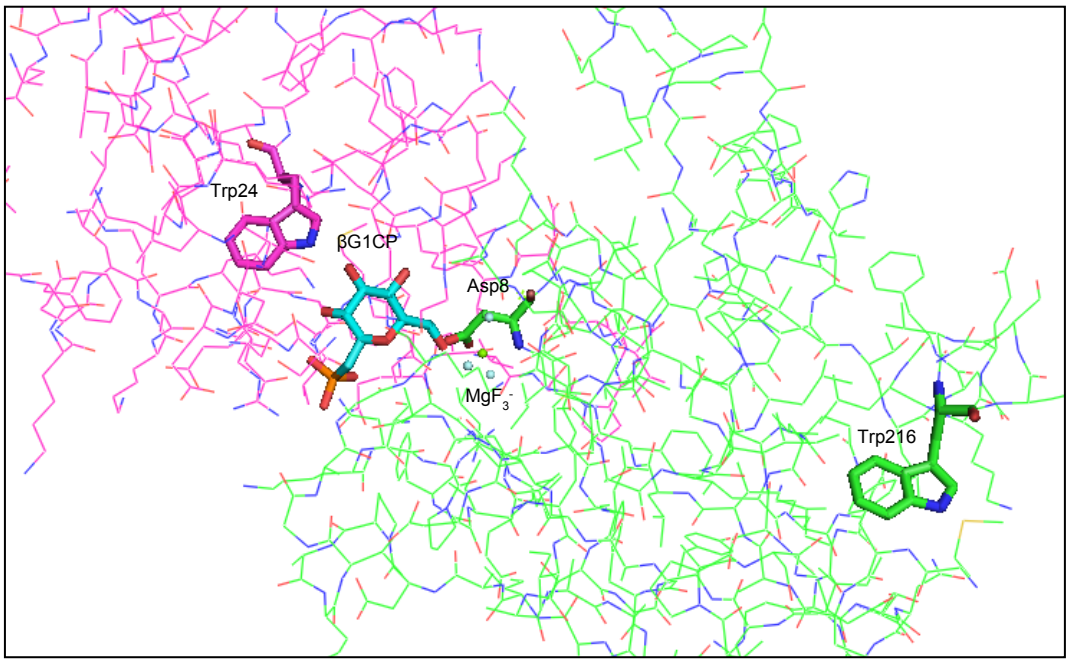

Figure 4. Crystal structure of the βPGM-MgF_3^--βG1CP TSA complex (4C4R).

The cap domain housing W24 is shown in magenta and the core domain housing W216 is shown in green. Both Trp residues are highlighted with sticks. Asp8 residue responsible for the phosphorylation of the substrate lies on the core domain and βG1CP ligand is positioned in the active site at the interface of both domains. MgF_3^- atoms are represented with spheres.

To substitute the natural tryptophan residues for ^{19}F-tryptophan, two different methods were explored. The first protocol was developed by Crowley and coworkers[38] who found that upon addition of 5-fluoroindole (Fig. 5A) to cell media, *E. coli* BL21 cells were able to incorporate the fluorinated indole into tryptophan (Method A). The second protocol involved the use of glyphosate to induce aromatic amino acid auxotrophy, followed by the addition of 5-fluorotryptophan (Fig. 5B), unlabeled phenylalanine, and unlabeled tyrosine (Method B).[38] Both methods did not show any major deleterious effect on protein overexpression or purification, however, the yields observed for the production of

5-fluorotryptophan βPGM (5FWβPGM) were ~47% for method A and ~85% for method B compared to the wild-type βPGM. Incorporation of ^{19}F-labeled amino acids are known to inhibit bacterial growth to different degrees.[8]

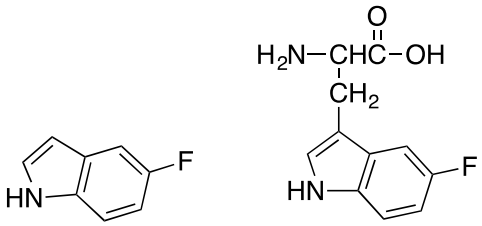

Figure 5. Chemical structures of 5-fluoroindole and 5-fluorotryptophan.

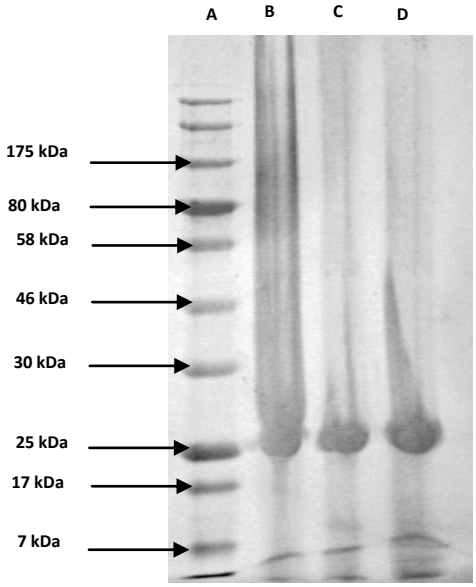

Figure 6. SDS-PAGE analysis of purified βPGM from *E. coli* BL21(DE3) expressed under three different conditions.

(A) NEB Biolabs broad range prestained protein marker (7-175 kDa); (B) unlabeled βPGM; (C) 5FWβPGM expressed with 5-fluoroindole (method A) (D) 5FWβPGM expressed with 5-fluorotryptophan (method B).

2.3 Efficacy of ^{19}F-labeling Methods

Literature precedent for ^{19}F protein labeling with methods A and B did not report on the percent of successful ^{19}F-labeled amino acid incorporated. Thus, to analyze the efficacy of labeling methods A and B for βPGM, ^{1}H-^{15}N HSQC and LC-MS/MS analysis were performed.

2.3.1 ^{1}H-^{15}N HSQC Analysis

Upon ^{15}N-labeling of 5FWβPGM produced by method A, we expected the ^{1}H-^{15}N HSQC of the labeled protein to show cross peaks for all nitrogen resonances except the two 5-fluoroindole tryptophan side chains. Therefore, comparing the integrations of the cross peaks from the tryptophan backbone and tryptophan side chain resonances would provide a quantitative analysis of 5-fluoroindole incorporation (Method A). ^{15}N-labeling of 5FWβPGM produced by method B would result in an unlabeled side chain and backbone nitrogen for 5FW residues, which would be absent from the ^{1}H-^{15}N HSQC. Comparing the integration of the tryptophan backbone cross peak to a backbone residue close in proximity in the enzyme structure would, therefore, provide a quantitative analysis of 5-fluorotryptophan incorporation. An HSQC spectra overlay of the wild-type ^{15}N-labeled βPGM and the ^{15}N-labeled βPGM from method A and B (Fig. 7) revealed that the incorporation of both ^{19}F-labeled tryptophan residues did not cause any structural perturbations in the enzyme tertiary structure, while suggesting a high efficacy for both methods. The HSQC spectra for both method A and B showed an absence of the distinct Trp side chain cross peaks as seen in the ^{15}N-labeled βPGM spectra which we interpreted as a high percent incorporation of ^{19}F-labeled tryptophan.

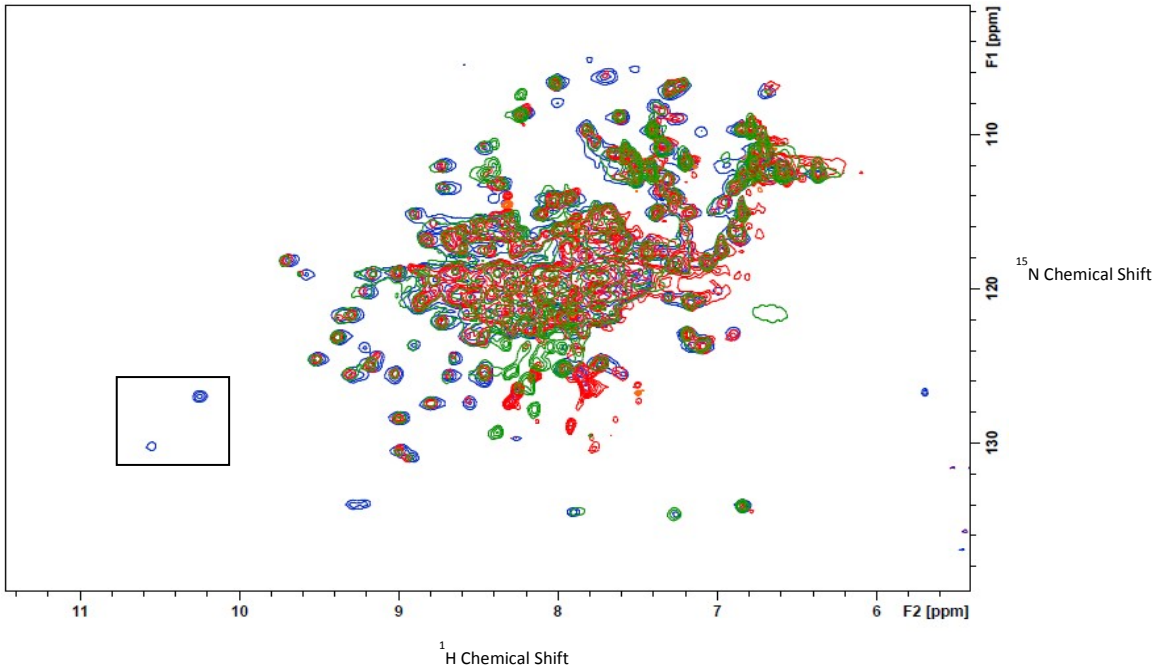

Figure 7. Overlaid ^{1}H-^{15}N HSQC spectra of βPGM.

^{15}N-labeled βPGM (500 μM) (blue), ^{15}N-labeled 5FWβPGM from method A (500 μM) (red) and method B (500 μM) (green). Both ^{15}N-labeled 5FWβPGM spectra (red and green) show the absence of cross peak resonances for the side chain Trp residues (black box).

2.3.2 LC-MS/MS Analysis

To more accurately quantify the effects of labeling, LC-MS/MS analysis of the peptides showed corresponding masses for fragments containing unfluorinated tryptophan (W24 and W216) and corresponding masses for fragments containing 5-fluorotryptophan (5FW24 and 5FW216). To generate peptides, endoproteinase Lys-C was used to digest βPGM. A ratio between the extracted ion count (XIC) of fragments containing 5FW24:W24 (Appendix 2A and 2C) and the extracted ion count (XIC) of fragments containing 5FW216:W216 provided a quantitative result for each method (Appendix 2B and 2D). Method A showed ~70% incorporation of 5-fluoroindole and method B showed ~85% incorporation of 5-fluorotryptophan. We, therefore, chose to use

method B to produce 5FWβPGM since both the levels of incorporation and quantity of protein production were highest.

2.4 NMR Analysis of 5FWβPGM

The incorporation of 5-fluorotryptophan was further analyzed by ^{19}F NMR spectroscopy. Two major unidentified ^{19}F resonances were observed at -120 and -123.5 ppm (Fig. 8A), along with the identified resonances for free F^- in solution at -119.5 ppm and MgF_x in solution at -155 ppm. The resonance seen at -123.5 ppm was noticeably broad showing the presence of a second species, indicative of an ongoing slow conformational exchange on the NMR time scale. The occurrence of a slow exchange is also presented by the minor resonance seen at -125 ppm, which may be a result of the previously reported minor conformation of βPGM that is in slow exchange with its major conformation.[33]

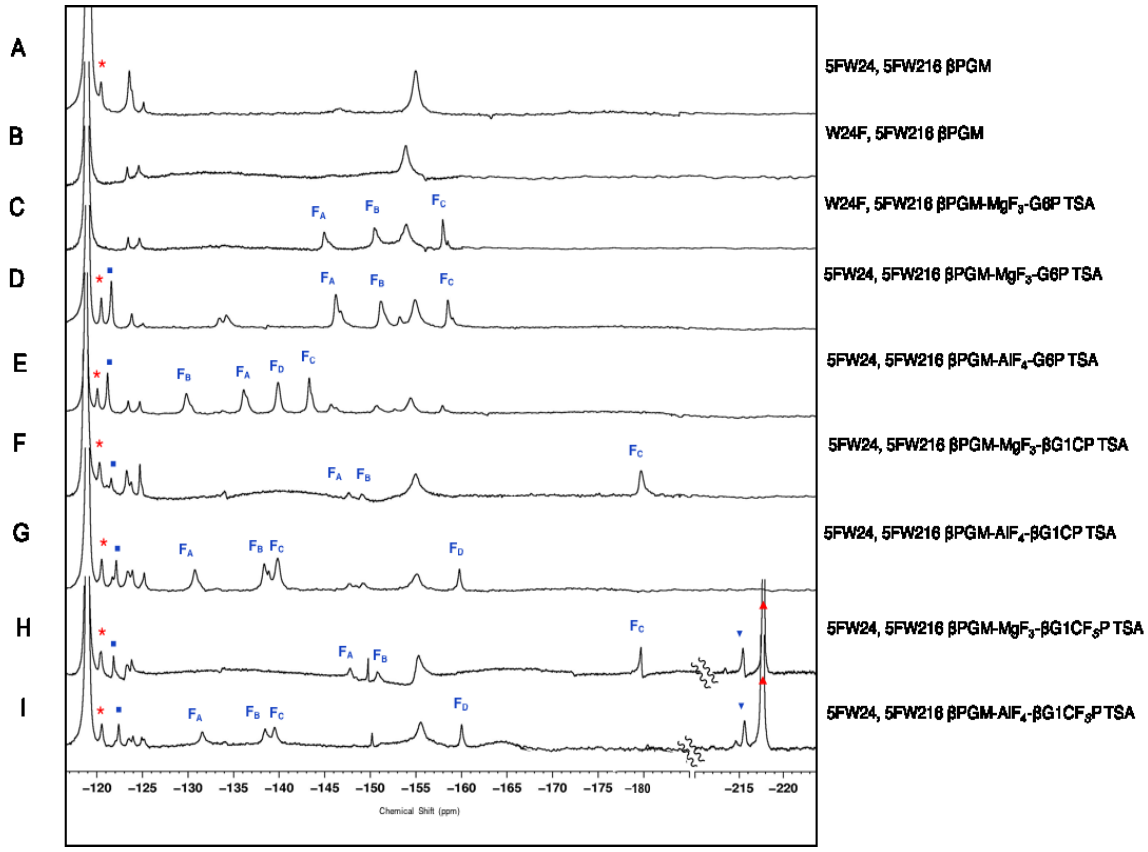

Figure 8. ^{19}F NMR spectra of step 1 and step 2 TSA complexes with ^{19}F- labeled wild-type and W24F mutant βPGM.

Blue boxes (■) are cap-closed 5FW24 resonances contributing to the complex formation, red asterisks (*) are apo-5FW24 resonances, blue inverse triangles (▼) are complex-bound ligand resonances, and red triangles (▲) are free ligand resonances. Resonances at -119 and -155 are from free F^- and MgF_x respectively. Assignment of MgF_3^- and AlF_4^- resonances were previously determined by chemical shift.[21,33] (A) 5FWβPGM; (B) W24F, 5FW216 5FWβPGM; (C) W24F, 5FW216 5FWβPGM-MgF_3-G6P TSA complex; (D) 5FWβPGM-MgF_3-G6P TSA complex; (E) 5FWβPGM-AlF_4-G6P TSA complex; (F) 5FWβPGM-MgF_3-βG1CP TSA complex; (G) 5FWβPGM-AlF_4-βG1CP TSA complex; (H) 5FWβPGM-MgF_3-βG1CF_SP TSA complex; (I) 5FWβPGM-AlF_4-βG1CF_SP TSA complex; Samples A and B contain 0.5 mM enzyme, 5 mM $MgCl_2$, 10 mM NH_4F, and 10% D_2O in 50 mM Hepes pH 7.2. Samples C-I contain 1 mM enzyme, 5 mM substrate, 5 mM $MgCl_2$, 10 mM NH_4F, and 10% D_2O in 50 mM Hepes pH 7.2. Samples E, G, and I also contain 1 mM of $AlCl_3$.

2.4.1 Assignment of ^{19}F-Trp NMR resonances

To determine the assignment of fluorine resonances observed in the ^{19}F NMR spectrum, a W24F mutant (W24F, 5FW216 5FWβPGM) was prepared using site-directed mutagenesis and confirmed by plasmid digestion with BglI and BstEII restriction

enzymes (Fig. 9). Protein expression was conducted using method B and yields were lower but comparable to those seen previously. The ^{19}F NMR spectrum for the W24F mutant showed two broader resonances at -123.5 ppm and -125 ppm (Fig. 8B). As a result, the ^{19}F resonance at -120 ppm, observed in the 5FWβPGM spectrum, was assigned to W24, the tryptophan close to the active site, due to its absence in the mutant spectrum. The two resonances observed in the mutant W24F spectrum, as well as the broad signal (-123.5 ppm) observed in the 5FWβPGM spectrum, and their different proportions to the wild-type 5FWβPGM, suggest that W216 on the core domain, exists in two different conformations that are in equilibria in the ground-state. In previously reported TSA complex crystal structures, W216 is consistently in an invariant environment, thus the two conformations of 5FW216 observed could result from a 5-fluoroindole ring flip, or a core domain conformation not observed crystallographically.[41,42]

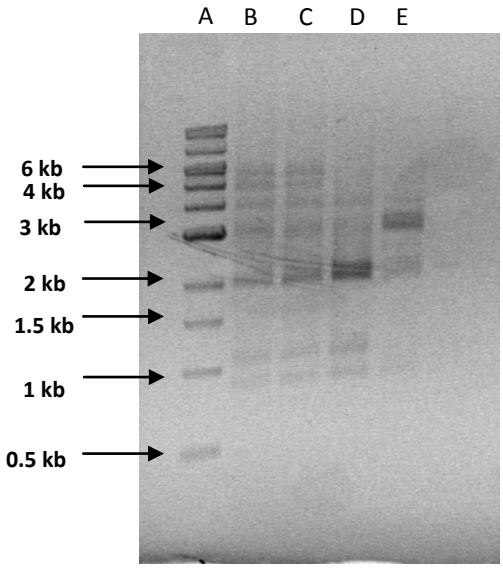

Figure 9. 1% agarose gel of pET-22b_*pgmB-His* and pET-22b_*pgmB*-His_W24F plasmid digested with restriction enzymes.

(A) 1 kb DNA ladder; (B), (C), (D) pET-22b_*pgmB*_His_W24F colonies digested with BglI and BstEII; (E) pET-22b_*pgmB* digested with *BglI* and *BstEII*.

2.4.2 Analysis of 5FW216 resonances

To investigate the cause of the two resonances observed for the 5FW216 residue, a W24F, 5FW216 βPGM-MgF_3^--G6P TSA complex was formed with the W24F mutant enzyme. Since W216 is ~22 Å from the active site, it was hypothesized that there would be little effect on W216 when substrate binding occurred. Upon addition of G6P to the apo-enzyme NMR solution, the chemical shift of the two resonances seen in the apo-W24F mutant spectrum remained unchanged and three new resonances at chemical shifts previously recorded for the βPGM-MgF_3^--G6P TSA complex were observed (Fig. 8B and 8C). The presence of the three new resonances were indicative of the formation of a W24F 5FW216 βPGM-MgF_3^--G6P TSA complex, indicating that complex formation is still feasible with the W24F substitution in the active site. The two 5FW216 resonances observed for the apo-W24F mutant were consistent in this TSA complex suggesting that the conformation of the enzyme core domain does not change as a result of TSA complexation, which is consistent with the proposed hinge model stating that the sole rotation of the cap domain is responsible for the exposure and closure of the active site.[7]

2.5 Formation of Step 1 and Step 2 Transition State Analog Complexes

^{19}F NMR experiments confirmed the formation of MgF_3^- and AlF_4^- complexes with 5FWβPGM (Fig. 8). In the presence of $MgCl_2$, NH_4F, and G6P, four new major resonances appeared in the ^{19}F NMR. Three were identified as the MgF_3^- resonances establishing the step 2 TSA complex, as previously reported for the non-fluorinated βPGM,[33] and one was located at -121.7 ppm, 1.2 ppm upfield ($\Delta\delta_F$) from the 5FW24 resonance seen in the apo-enzyme spectrum (Fig. 8D). The new resonance had the same

peak integral with the three MgF_3^- resonances and was identified as the 5FW24 "cap-closed" resonance. Addition of $AlCl_3$ (1 mM) resulted in the formation of the AlF_4^- complex which was verified by four fluorine resonances observed in the ^{19}F NMR, with chemical shifts as previously reported.[33] The same 5FW24 resonance was observed at -121.7 ppm, again 1.2 ppm upfield from the 5FW24 resonance in the apo-enzyme (Fig. 8E), which further confirmed the resonance assignment as the cap-closed conformation of 5FW24. Similar TSA complexation experiments were performed with βG1CP and βG1CF$_S$P (Fig. 8F-I). These two synthesized ligands were essential to the observation of the TSA complexes for the first phosphate transfer step (step 1).[21] In both instances, MgF_3^- and AlF_4^- complexes formed readily, with chemical shifts for each of the metal-coordinated fluoride ions as previously reported.[21]

2.6 Analysis of 5FW24 resonance in TSA complexes

Step 1 TSA complexes formed in the presence of either βG1CP or βG1CF$_S$P, $MgCl_2$, NH_4F, and 5FWβPGM. Chemical shift perturbations of the cap-closed 5FW24 resonance were observed. The apo and cap-closed resonance of 5FW24 revealed a different change in chemical shift ($\Delta\delta_F$) for the MgF_3^- complexes compared to the AlF_4^- complexes, whereas the G6P MgF_3^- and AlF_4^- TSA complexes (Table 1) had the same $\Delta\delta_F$. The $\Delta\delta_F$ of 5FW24 in the G6P-MgF_3^- and G6P-AlF_4^- complexes (step 2) were consistent (1.2 ppm) suggesting that ^{19}F NMR spectroscopy of 5-fluorotryptophan labeled βPGM provides new and additional insight into the enzyme TSA complexes. Different chemical shifts of the cap-closed 5FW24 resonance were also observed between G6P and βG1CP/βG1CF$_S$P MgF_3^- complexes as well as AlF_4^- complexes, which

can be attributed to the difference in orientation of sugar rings in the active site (Table 1). According to the previously published crystal structure of the step 1 TSA complexes,[21] the rotation of G6P in the active site relative to βG1CP results in a loss of coordination between W24 and the hydroxyl group on carbon 3. We hypothesize that this change in coordination is responsible for the different chemical shifts observed between the two complexes. Therefore, the effect that the difference in orientation of the hexose has on 5FW24 can be used as a method of binding analysis for βPGM ligands.

Table 1. ^{19}F chemical shifts of 5-fluorotryptophan labeled βPGM in apo and cap-closed enzyme conformations of step 1 and step 2 MgF_3^- and AlF_4^- complexes.

Fig. #	5FWβPGM TSA complex	5FW24 δ_{apo} (ppm)	5FW24 $\delta_{cap\text{-}closed}$ (ppm)	$\Delta\delta_F$ (ppm)
3D	G6P-MgF_3^-	-120.5	-121.7	1.2
3E	G6P-AlF_4^-	-120.5	-121.7	1.2
3F	βG1CP-MgF_3^-	-120.6	-121.8	1.2
3G	βG1CP-AlF_4^-	-120.6	-122.2	1.6
3H	βG1CF_SP-MgF_3^-	-120.6	-122.0	1.4
3I	βG1CF_SP-AlF_4^-	-120.6	-122.4	1.8

Comparison in integration between the 5FW24 resonances in the G6P complexes revealed a 2:1 ratio between the cap-closed and apo conformations. In an attempt to push the equilibrium towards sole formation of the TSA complexes, the concentration of G6P was increased up to 30 mM, however, integrations between the cap-closed and apo resonances remained constant. Integration of the cap-closed and apo 5FW24 resonance of step 1 analogs showed a 1:1 ratio, establishing that a reduced concentration of enzyme was bound in the βG1CP and βG1CF_SP complexes than in the G6P complex. These

results agree with the previously reported weaker binding affinity of βG1CP relative to G6P.[21]

2.7 Formation of Enzyme-Ligand Complex with βG16P analog

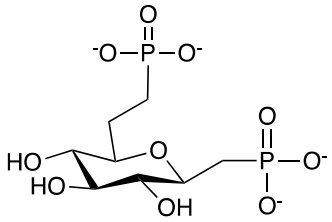

Figure 10. β-Glucose 1,6-bisphosphonate analog of βPGM intermediate.

β-Glucose 1,6-bisphosphonate (βG16CP) (Fig. 10) was synthesized as a βG16P analog by a previous member of the Jakeman lab.[39] Upon addition of 2.5 mM of βG16CP to 5FWβPGM in the presence of Mg^{2+}, a new resonance at -123.5 ppm appeared, 2.6 ppm upfield from 5FW24 of the apo-enzyme (Fig. 11B). This new resonance was assigned to 5FW24 of the ligand-bound enzyme, as it was similar to resonances seen for the cap-closed enzyme in TS1 and TS2 complexes. The observation of one separate resonance for the apo-enzyme and the ligand-bound enzyme suggested the formation of a slow-exchange complex between 5FWβPGM and βG16CP. This is consistent with the observation of slow-exchange complexes of TS1 and TS2 inhibitors of βPGM by ^{19}F NMR. In an attempt to push the equilibrium towards the ligand-bound enzyme conformation, increasing amounts of βG16CP were added. Upon doubling the concentration of ligand to 5 mM, integration of the 5FW24 apo enzyme resonance to its ligand-bound enzyme resonance revealed a slight increase towards the ligand-bound

enzyme resonance (Fig. 11C). However, an additional increase of βG16CP to 10 mM revealed no significant increase in the ligand-bound enzyme conformation suggesting that the enzyme had reached an equilibrium (Fig. 11D).

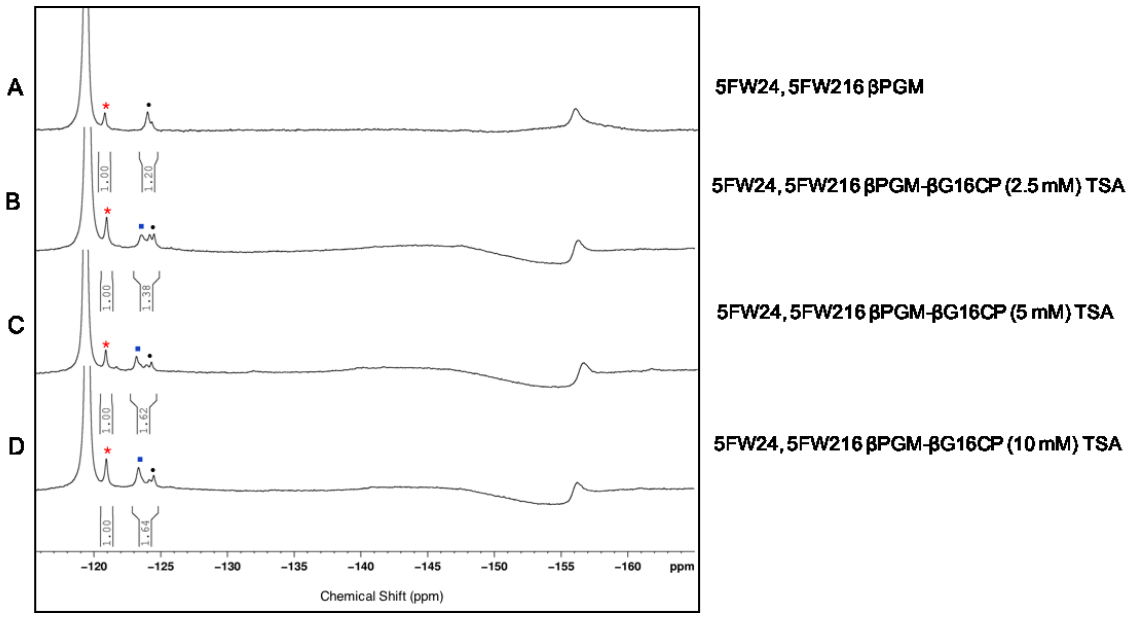

Figure 11. ^{19}F NMR spectra of 5FWβPGM-βG16CP TSA complex.

Red asterisks (*) are apo-5FW24 resonances, blue box (■) is the cap-closed 5FW24 resonances contributing to the complex formation, black circles (•) are the 5FW216 resonances. Resonances at -119.5 ppm and -155.5 ppm are a result of free F^- and MgF_x respectively. (A) 5FWβPGM apo-enzyme; (B) 5FWβPGM-βG16CP TSA complex with 2.5 mM βG16CP; (C) 5FWβPGM-βG16CP TSA complex with 5 mM βG16CP; (D) 5FWβPGM-βG16CP TSA complex with 10 mM βG16CP. Sample A contains 0.5 mM enzyme, 5 mM $MgCl_2$, 10 mM NH_4F, and 10% D_2O in 50 mM Hepes pH 7.2. Samples B, C, and D contain 1 mM enzyme, 5 mM $MgCl_2$, 10 mM NH_4F and 10% D_2O in 50 mM Hepes pH 7.2.

The $\Delta\delta_F$ of 5FW24 seen for this complex is different than those previously reported and observed by us for the TS1 and TS2 MgF_3^- and AlF_4^- complexes suggesting that the 5FWβPGM-βG16CP complex induces a different conformation than the metal fluoride complexes. The ^{19}F NMR result of a single slow exchange species is indicative of the

compound binding in one orientation. Although, the 1D ^{19}F NMR experiment did not provide insight into whether the C-1 or C-6 phosphonate functionality was bound adjacent to the catalytic nucleophile, Asp8, it did confirm that βG16CP binds to βPGM without the formation of metal fluoride complexes. Nonetheless, these observations emphasize the high sensitivity of 5FW, making it an effective probe for analyzing minor differences in enzyme conformation during ligand binding.

2.8 Attempted Formation of TSA Complexes with 2-Deoxy-2-Fluoro Analogs Of β-Phosphonates

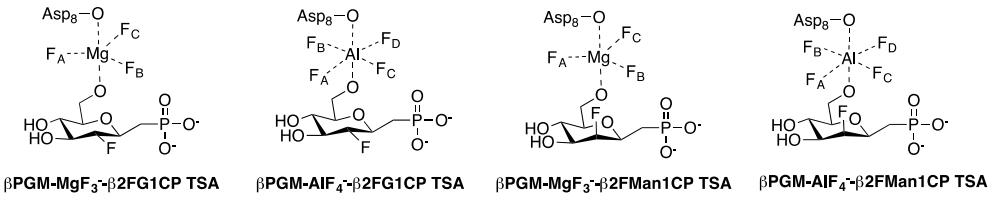

Figure 12. Potential metal fluoride TSA complexation products with 2-deoxy-2-fluoro analogs of β-glucose and β-mannose phosphonates.

β-2-deoxy-2-fluoro-glucose-1-*C*-phosphonate (β2FG1CP) and β-2-deoxy-2-fluoro-mannose-1-*C*-phosphonate (β2FMan1CP) compounds were synthesized by a member of the Jakeman group[40] and were tested as non-covalent inhibitors of βPGM.

2.8.1 Attempts at β2FG1CP Complexation

In an attempt to form the MgF_3^- TSA complex with β2FG1CP, 5FWβPGM was treated with the fluorinated ligand in the presence of $MgCl_2$ and NH_4F. The ^{19}F NMR resonances for two out of three fluoride ions bound to magnesium at -148 and -180 ppm were observed in very low intensity (blue arrows in Fig. 13B), however, the cap-closed 5FW24

resonance seen in the previous ligand-bound complexes was absent from the spectrum (Fig. 13B). A resonance 0.8 ppm upfield from the free β2FG1CP resonance was also observed, however, it was of greater intensity than the MgF_3^- resonances observed, suggesting β2FG1CP binds to the enzyme but not as a metal fluoride complex.

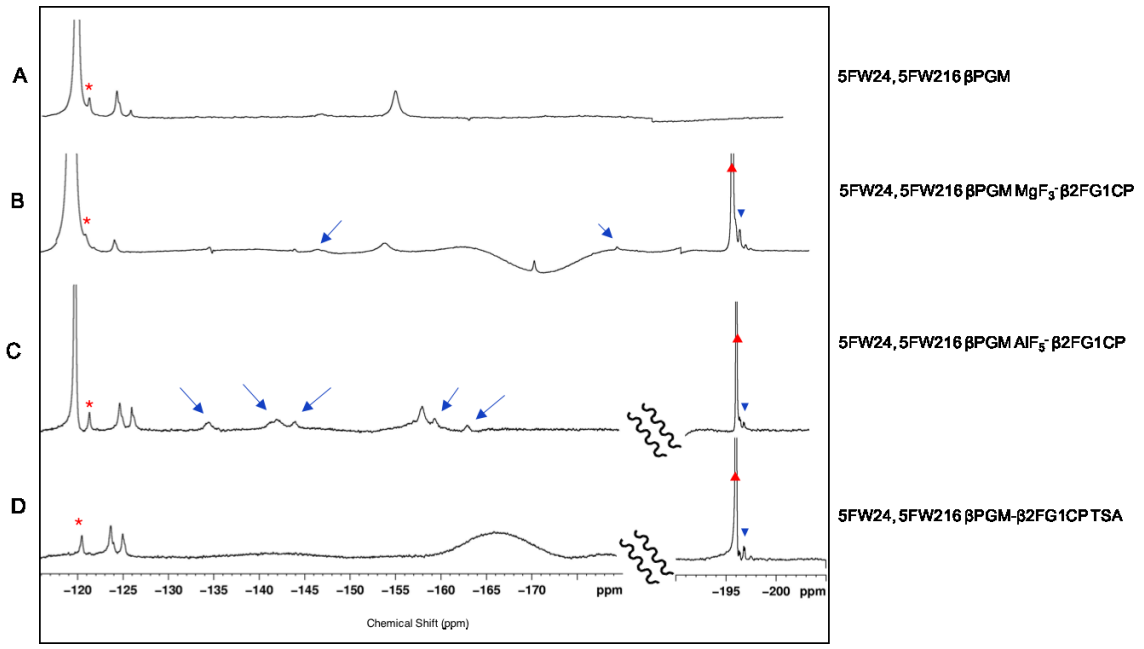

Figure 13. ^{19}F NMR spectra of 5FWβPGM with β2FG1CP and metal fluorides.

Red asterisks (*) are apo-5FW24 resonances, blue inverse triangles (▼) are complex-bound β2FG1CP resonances, and red triangles (▲) are free β2FG1CP resonances. Resonances at -119 and -155 are from free F^- and MgF_x respectively. (A) apo-5FWβPGM; (B) 5FWβPGM-MgF_3-β2FG1CP TSA complex; (C) anticipated 5FWβPGM-AlF_4-β2FG1CP TSA complex; (D) 5FWβPGM-β2FG1CP complex; Sample A contain 0.5 mM enzyme, 5 mM $MgCl_2$, 10 mM NH_4F, and 10% D_2O in 50 mM Hepes pH 7.2. Samples B and C contain 1 mM enzyme, 5 mM β2FG1CP, 5 mM $MgCl_2$, 10 mM NH_4F, and 10% D_2O in 50 mM Hepes pH 7.2. Samples C also contains 1 mM of $AlCl_3$. Sample D contains 1 mM enzyme, 5 mM β2FG1CP, 5 mM $MgCl_2$, and 10% D_2O in 50 mM Hepes pH 7.2.

It has been reported that the AlF_4^- TSA complex forms more readily than the MgF_3^- TSA complex at neutral pH,[20] thus, $AlCl_3$ was added to the β2FG1CP NMR enzyme solution as a source of Al^{3+}. ^{19}F NMR showed five new resonances (blue arrows in Fig. 13C) of

weak intensity and a resonance of higher intensity 0.8 ppm upfield from the free β2FG1CP; however, a second 5FW24 resonance was not observed (Fig. 13C). Four out of the five new resonances observed resembled the chemical shifts for the four fluoride resonances of AlF_4^-, however, they were shifted upfield in comparison with TSA complexes in the presence of effective ligands. The low intensity of MgF_3^- resonances and the five new aluminum fluoride resonances questions the formation of a TSA complex, however, the presence of a second resonance for β2FG1CP suggests that β2FG1CP binds to 5FWβPGM without the formation of metal fluoride complexes. To confirm the above hypothesis, 5FWβPGM was treated with β2FG1CP in the absence of fluoride (Fig. 13D). As expected, a resonance was observed 0.8 ppm upfield from free β2FG1CP, however, a second resonance for 5FW24 was still absent. Overall, these observations not only question the source of the five aluminum fluoride resonances observed in the spectra but also suggest the binding of β2FG1CP in an orientation that does not affect 5FW24.

2.8.2 Attempts at β2FMan1CP Complexation

Similar to the glucose analog, the ability of the enzyme to form MgF_3^- and AlF_4^- TSA complexes was also examined with β2FMan1CP. β2FMan1CP did not form a stable complex in the presence of MgF_3^- as the three complexed fluoride resonances along with a second resonance for cap-closed 5FW24 were not observed in the spectrum (Fig. 14B). An additional resonance for β2Man1CP was also absent from the spectrum, suggesting that the ligand has a very weak binding affinity for 5FWβPGM, contrary to that seen for the glucose analog, β2FG1CP. Upon addition of $AlCl_3$ (1 mM), five new resonances

(blue arrows in Fig. 14C) were observed in the spectrum, however, an additional resonance for the cap-closed 5FW24 was not oberved along with an additional resonance for β2FMan1CP (Fig. 14C). The five new resonances observed were similar to that seen in the aluminum fluoride β2FG1CP spectrum. Since there is no indicaiton of β2FMan1CP binding to the enzyme, we hypothesized that the five fluoride resoances could be a result of various hydrolyzed aluminum fluoride species in solution as previously reported,[64] or an aluminum fluoride complex formng in the active site with the replacement of the ligand hydroxyl group with a fluoride ion, resulting in a stable enzyme-AlF_5 complex. To determine which of the two was occuring, $AlCl_3$ (1 mM) and NH_4F (10 mM) were added to 5FWβGM in the absence of a ligand (Fig. 14D). ^{19}F NMR showed the same five resonances that were observed in Fig. 14C, confirming that the fluoride resonances observed are independent of ligand binding. To determine if the aluminum fluoride resonances were a result of hydrolyzed aluminum fluoride species, $AlCl_3$ (1 mM) was added to NH_4F (10 mM) in the absence of 5FWβPGM and ligand (Fig. 14E). Only the resonance at -154 ppm assigned to an AlF_x species was present, confirming our hypothesis that a stable enzyme-AlF_5^- complex is forming in the active site of 5FWβPGM in the absence of a ligand (Fig. 15).

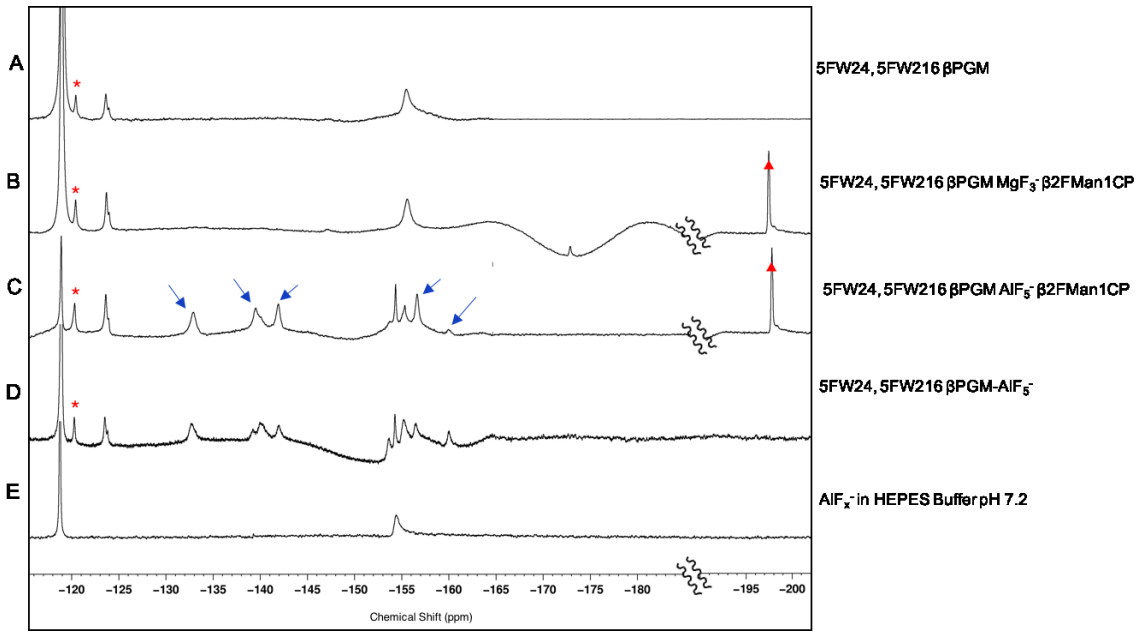

Figure 14. ^{19}F NMR spectra of 5FWβPGM with β2FMan1CP and metal fluorides.

Red asterisks (*) are apo-5FW24 resonances, and red triangles (▲) are free β2FMan1CP resonances. (A) apo-5FWβPGM; (B) anticipated 5FWβPGM-MgF_3-β2FMan1CP TSA complex; (C) anticipated 5FWβPGM-AlF_4-β2FMan1CP TSA complex; (D) apo-5FWβPGM with $AlCl_3$ and NH_4F; (E) $AlCl_3$ and NH_4F in HEPES pH 7.2 . Sample A contain 0.5 mM enzyme, 5 mM $MgCl_2$, 10 mM NH_4F, and 10% D_2O in 50 mM Hepes pH 7.2. Samples B and C contain 1 mM enzyme, 5 mM β2FG1CP, 5 mM $MgCl_2$, 10 mM NH_4F, and 10% D_2O in 50 mM Hepes pH 7.2. Samples C also contains 1 mM of $AlCl_3$. Resonances at -119, -154, and -155 are from free F^-, AlF_x and MgF_x respectively.

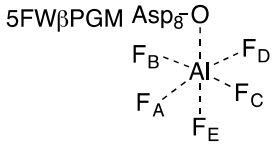

Figure 15. Proposed 5FWβPGM-AlF_5^- complex.

2.9 Conclusions

Overall, the incorporation of 5FW in βPGM provided a sensitive spectroscopic probe to monitor ligand binding. 5FWβPGM was successful in metal fluoride complexation proving that incorporation of two 5FW residues, 5FW24, which is 3 Å from the active site and 5FW216, which is 22 Å from the active site, did not affect the formation of previously reported transition state analog complexes. ^{19}F NMR resonances for both 5FW residues were assigned based on results from site-directed mutagenesis that revealed that 5FW216 exists in two different conformations, providing two different ^{19}F resonances that are independent of ligand binding. 5FW24 showed sensitivity toward the formation of MgF_3^- and AlF_4^- TSA complexes of different ligands as separate ^{19}F resonances were observed for the apo-enzyme and for the cap-closed enzyme. A ^{19}F NMR spectra of 5FWβPGM also reported successful complexation with βG16CP in a conformation different than that seen for the metal fluoride TS1 and TS2 complexes. The ability of the enzyme to form metal fluoride complexes with β2FG1CP and β2FMan1CP was also examined; however, stable complexes were not observed by ^{19}F NMR spectroscopy. The ^{19}F NMR spectra of β2FMan1CP revealed no evidence of binding, but the ^{19}F NMR spectra of β2FG1CP and 5FWβPGM in the absence of fluoride provided evidence that β2FG1CP binds to the enzyme in an orientation that prevents metal fluoride complexation and does not affect 5FW24. Thus ^{19}F NMR analysis of 5FWβPGM provides an effective method to monitor the binding of ligands and potential inhibitors of βPGM.

CHAPTER 3. RESULTS AND DISCUSSION: SYNTHESIS

3.1 Introduction

The synthesis of non-covalent inhibitors and mechanism-based inactivators of βPGM were attempted. Non-covalent inhibitors were expected to inhibit phospho-βPGM and mechanism-based inactivators were expected to form a covalent bond with the dephosphorylated enzyme resulting in time-dependent inhibition.

3.1.1 Non-covalent Inhibitors of βPGM

To design a non-covalent inhibitor, we decided to mimic the phosphate bond of βG1P with a phosphonate linkage. Studies have shown that replacing the bridging oxygen atom with a carbon atom provides a suitable mimic while introducing a non-hydrolyzable bond.[43] The use of phosphonates as phosphate analogs has been explored in many different applications,[44-49] presenting phosphonates as inhibitors of enzymes with phosphate hydrolase activity. Previous work by Allen and coworkers reported α-galactose 1*C*-phosphonate as a competitive inhibitor for βPGM with a K_i value in the micromolar range,[50] and work by Waltho and coworkers report β-glucose 1*C*-phosphonates (βG1CP and βG1CF$_S$P) as ligands that form stable metal fluoride TSA complexes with βPGM.[21] Although βG1CP has been evaluated with metal fluorides as a TSA, the inhibition constant of βG1CP in the absence of metal fluorides has not yet been reported, thus we decided to synthesize βG1CP as a non-covalent inhibitor for βPGM.

3.1.2 Mechanism-based Inactivators of βPGM

To design mechanism-based inactivators for βPGM, we attempted to synthesize 1,6-bisphosphate mimics (**8** and **12**) by the derivatization of the C-6 hydroxyl group on βG1CP with various electrophilic groups. βPGM has been shown to have a high affinity for its intermediate, β-glucose 1,6-biosphosphate (βG16P), compared to its biological substrate, β-glucose 1-phosphate (βG1P). Kinetic studies reveal that βG16P binds 20 times more tightly than βG1P;[22] therefore the development of inhibitors to mimic βG16P should allow for binding at low inhibitor concentrations. The synthesis of phosphofluoridate compounds (**16** and **21**) were also explored as mechanism-based inactivators. Phosphofluoridates have been shown to strongly inhibit various serine proteases;[58-61] however, an attempt to inhibit α-phosphoglucomutase (αPGM) with glucose 6-phosphofluoridate and 2-fluoroglucose 1-phosphofluoridate resulted in a lack of inactivation and competitive K_i values in the millimolar range.[62] In order for the phosphofluoridates to inhibit αPGM, the active site serine must be dephosphorylated to allow for the serine hydroxyl group to attack the ligand phosphofluoridate group via a nucleophilic substitution, breaking the P-F bond. Thus, it was hypothesized that its poor inhibition was due to the phosphofluoridates being poor phosphate acceptors, leaving the enzyme in its phosphorylated state. We predicted that this issue would not be seen with βPGM, as its phosphorylated aspartic acid residue is more labile than the phosphorylated serine residue in αPGM.

We decided to design four mechanism-based inactivators (Scheme 3). Compound **8** has a bromoacetyl functionality installed on the C-6 hydroxyl of βG1CP. Literature precedence reports the use of bromoketone *C*-glycosides as inactivators of glycosidases through the

formation of a covalent bond.[53] We hypothesized that we would see an analogous mechanism-based inactivation between the bromoacetyl group and βPGM. Additionally, compound **12** has an epoxide installed on the C-6 hydroxyl of βG1CP whilst compounds **16** and **21** are phosphofluoridate derivatives. It was anticipated that the electrophilic group on compounds **8**, **12**, **16**, and **21** would react with the nucleophilic carboxylate present in the βPGM active site, as shown in Scheme 3.

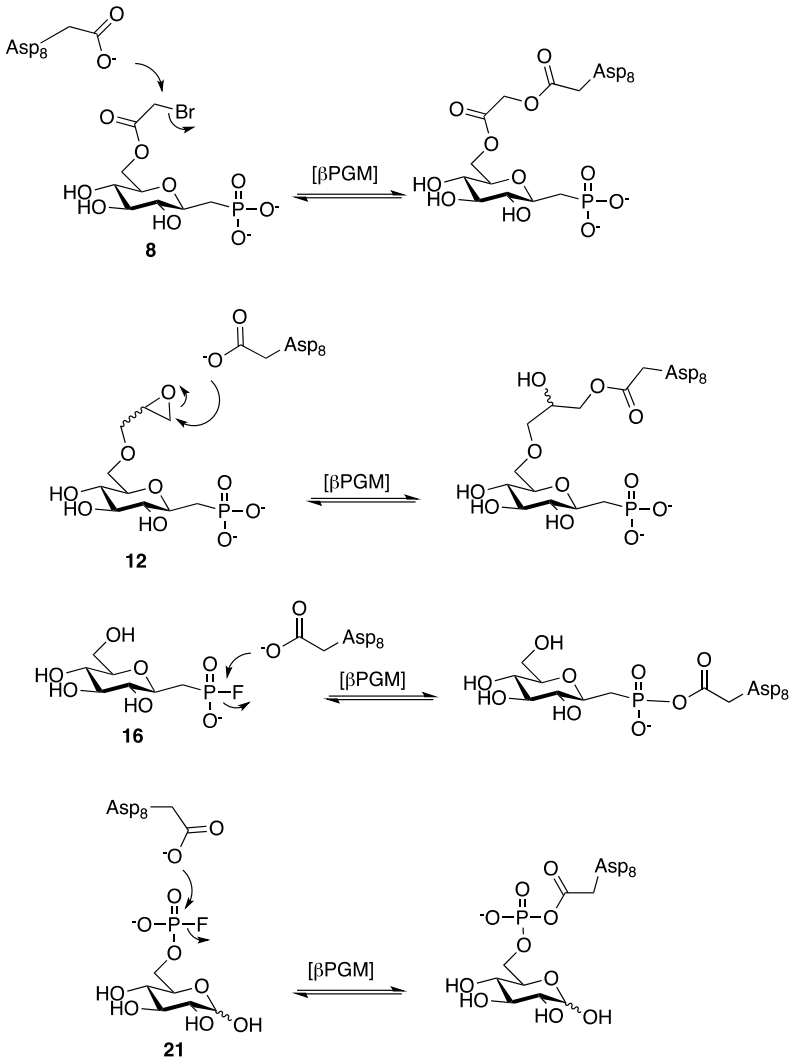

Scheme 3. Proposed mechanism of inactivation of βPGM with mechanism-based inactivators.

In addition, a phosphate group was installed at C-6 of βG1CP (**10**) as a potential non-covalent inhibitor and a βG16P mimic. We were curious to see if the addition of a phosphate group at C-6 of βG1CP would alter its binding affinity. We hypothesized that this βG16P mimic would either lead to activation of the enzyme by transfer of its C-6 phosphate group, or inhibition of the enzyme as a result of its product βG1CP (Scheme 4).

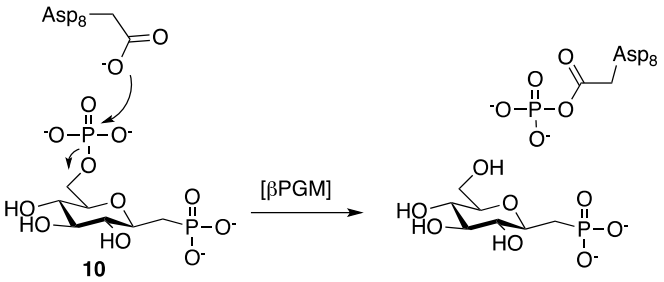

Scheme 4. Proposed mechanism of action of βPGM with **10**.

3.2 The Synthesis of β-Glucose-1*C*-Phosphonate (βG1CP)

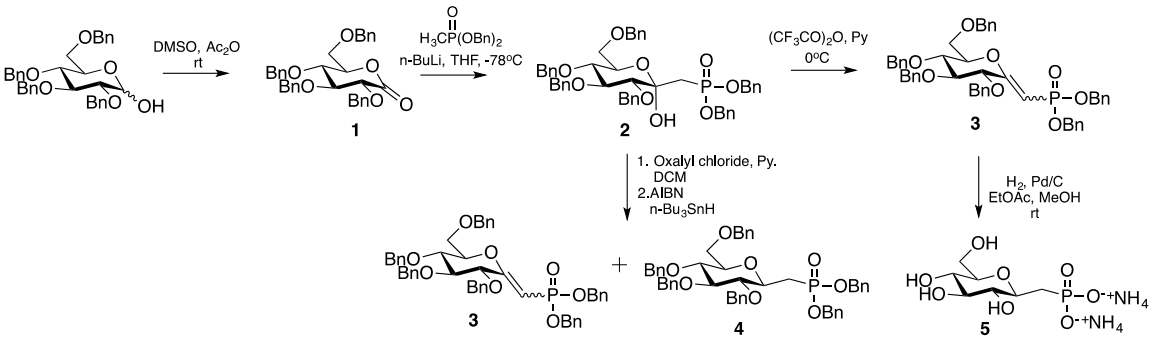

Scheme 5. Synthesis of βG1P phosphonate analog.

The synthesis of the glucose 1-phosphate analog was accomplished by following literature methods[49] as outlined in Scheme 5. The synthesis began with the treatment of commercially available 2,3,4,6-tetra-*O*-benzyl-D-glucopyranose under Albright-Goldman oxidation conditions[66] to afford **1** in good yield (86%). Freshly prepared dibenzyl methyl phosphonate, synthesized from dibenzyl phosphite and methyl iodide, was treated with n-butyllithium in THF before reacting with lactone **1** at -78°C, producing the protected α-hydroxy ketose phosphonate **2** in 76% yield. To generate **3**, two methods were evaluated. The first method involved conversion of the α-hydroxy into a reactive oxalyl ester followed by its decomposition with AIBN and tributyltin hydride via the Barton-McCombie deoxygenation. Two major products with similar R_f values were detected by TLC, ^{31}P NMR, and LC-MS/MS and were assigned to the deoxygenated product **3** (30%) and the *exo*-glycal product **4** (70%) after characterization, with an overall yield of 60%. To avoid a mixture of products, the second approach involved the deoxygenation of **2** via an elimination reaction using trifluoroacetic anhydride,[51] to afford exclusively the *exo*-glycal product **3** in 54% yield. The *exo*-glycal was then converted to **5** under hydrogenation conditions at atmospheric pressure to yield **5**.

3.3 Attempted C-6 Derivatization of β-Glucose-1*C*-Phosphonate

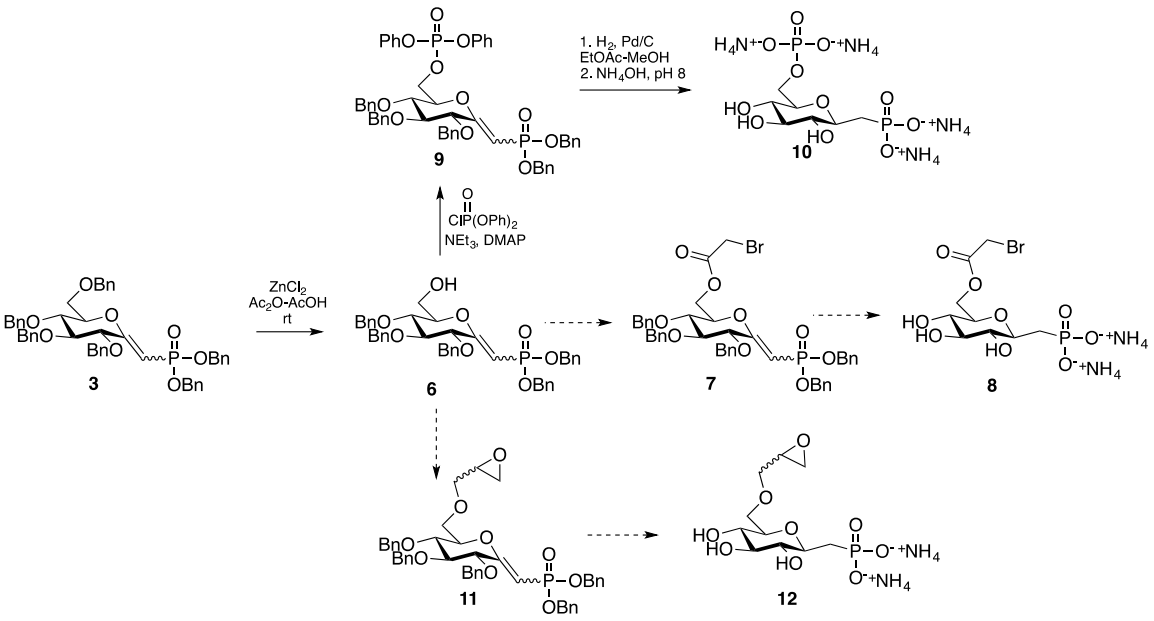

Scheme 6. Proposed synthesis of various βG16P analogs.

The synthesis of transition state analogs was initiated by substitution of the primary benzyl protecting group at C-6 to an acetyl group using zinc chloride and acetic anhydride.[54] Subsequent deprotection of the crude product with potassium carbonate afforded **6** in 46% yield.

Our first attempt to install an electrophilic handle onto C-6 of βG1CP was via the bromoacetylation of **6** (Scheme 6), which was difficult to achieve under various reaction conditions. A uronium-based coupling reaction was tested with bromoacetic acid under literature conditions[52] (Method A) but the bromoester product **7** was not observed by TLC or LC-MS/MS (Fig. 16A). Different conditions were explored by altering the literature conditions as outlined in Table 2, and product formation was monitored by TLC

and LC-MS/MS. A slight increase in the equivalencies of acid and TBTU had no effect on the reaction after 4 hours, so the reaction was subjected to an increase in temperature to 50°C (Method B). Both changes resulted in no improvement in product formation. Changing the base to a slightly more basic amine (Method C), also had no effect on the reaction (Fig. 16B). To determine the cause for the lack of product formation, the reaction was performed with the literature reactants, α-D-methyl glycoside and benzoic acid (Method D). After 4 h, a new spot was evident by TLC and the formation of product was confirmed by LC-MS/MS (Fig. 16C). The same reaction was performed using the literature alcohol, however bromoacetic acid was used (Method E). After 20 h, no product was observed by LC-MS/MS (Fig. 16D). These observations confirmed that the substitution of benzoic acid for bromoacetic acid resulted in the lack of product formation. Therefore, bromoacetic acid is too acidic and an insufficient nucleophile for this reaction.

Table 2. Uronium-based coupling reaction conditions explored

Method	**Alcohol**	**Acid**	**Acid equiv.**	**TBTU equiv.**	**Base**	**Base equiv.**	**Time** (h)	**Temp** (°C)
A	**6**	Bromoacetic acid	1.0	1.0	DIPEA	2.0	4	rt
B	**6**	Bromoacetic acid	1.2	1.5	DIPEA	2.0	8	50
C	**6**	Bromoacetic acid	1.2	1.5	DBU	2.0	8	50
D	α-D-methyl glycoside	Benzoic acid	1.0	1.0	DIPEA	2.0	4	rt
E	α-D-methyl glycoside	Bromoacetic acid	1.0	1.0	DIPEA	2.0	20	rt

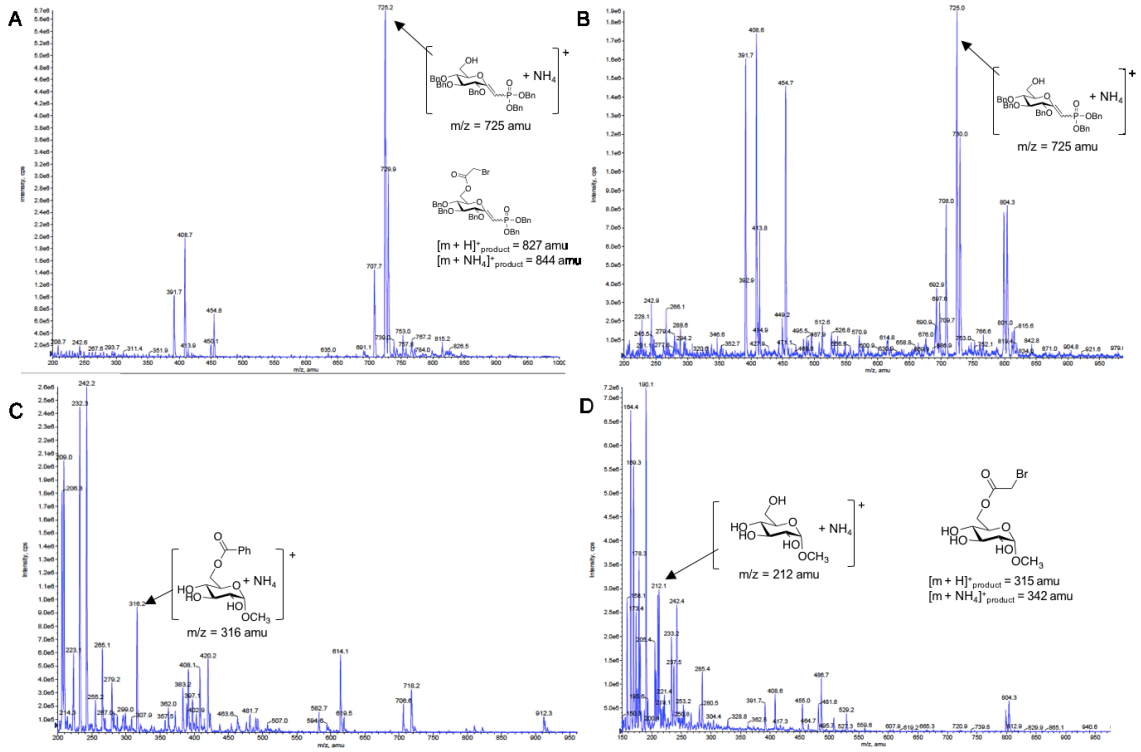

Figure 16. LC-MS/MS positive Q1 spectra of bromoacetic acid coupling reaction.

Spectra of m/z of compounds present during Method A (A), Method C (B), Method D (C), and Method E (D) reaction conditions.

In another attempt to synthesize a mechanism-based inactivator, we performed several nucleophilic substitution reactions with epichlorohydrin, which would result in an epoxide at C-6 (Scheme 7). Various reaction conditions (Table 3) were attempted but all resulted in little to no product formation. Initially, **6** was reacted using literature conditions[55] and monitored over 22 h (Method A). As the reaction progressed, TLC showed the formation of several products; however, the starting material was not fully consumed. LC-MS/MS confirmed that the product mixture did not contain the desired product, **11**, but rather many forms of the hydrolyzed phosphate product (Fig. 17A). Optimization of the reaction was performed with α-D-methyl glycoside. To prevent

hydrolysis of the phosphate group, a selection of non-nucleophilic bases was examined. First, an excess of triethylamine with DMAP as the catalyst was tested and monitored for 24 h (Method B). Product formation was not evident by TLC after the indicated time, so the temperature was increased to 50°C; however, the desired product mass was not observed by LC-MS/MS after a few hours (Fig. 17B). Changing the base to DIPEA and DBU (Method C and D) also had no effect on product formation (Fig. 17C). Lastly, we tried conditions used in the literature for the substitution of an epoxide via epibromohydrin (Method E).[56] Using NaH as a base showed a higher consumption of starting material comparatively by TLC, however, it still provided a low product yield (Fig. 17D). Therefore, further screening must be done to optimize this reaction.

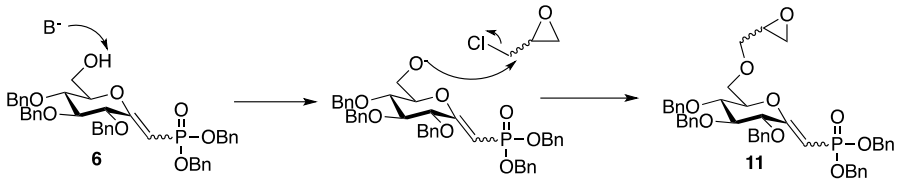

Scheme 7. The substitution reaction of **6** with epichlorohydrin under basic conditions.

Table 3. Epoxide-substitution reaction conditions explored

Method	**Glucose derivative**	**Base**	**Base equiv.**	**Catalyst**	**Solvent**	**Time** (h)	**Temp** (°C)
A	**6**	50% NaOH	32.5	TBAB	THF	22	rt
B	α-D-methyl glycoside	Triethylamine	22.0	DMAP	THF	24	rt – 50
C	α-D-methyl glycoside	DIPEA	1.3	TBAB	THF	24	rt
D	α-D-methyl glycoside	DBU	1.3	TBAB	THF	24	rt
E	α-D-methyl glycoside	NaH	1.3	TBAB	DMF	24	rt

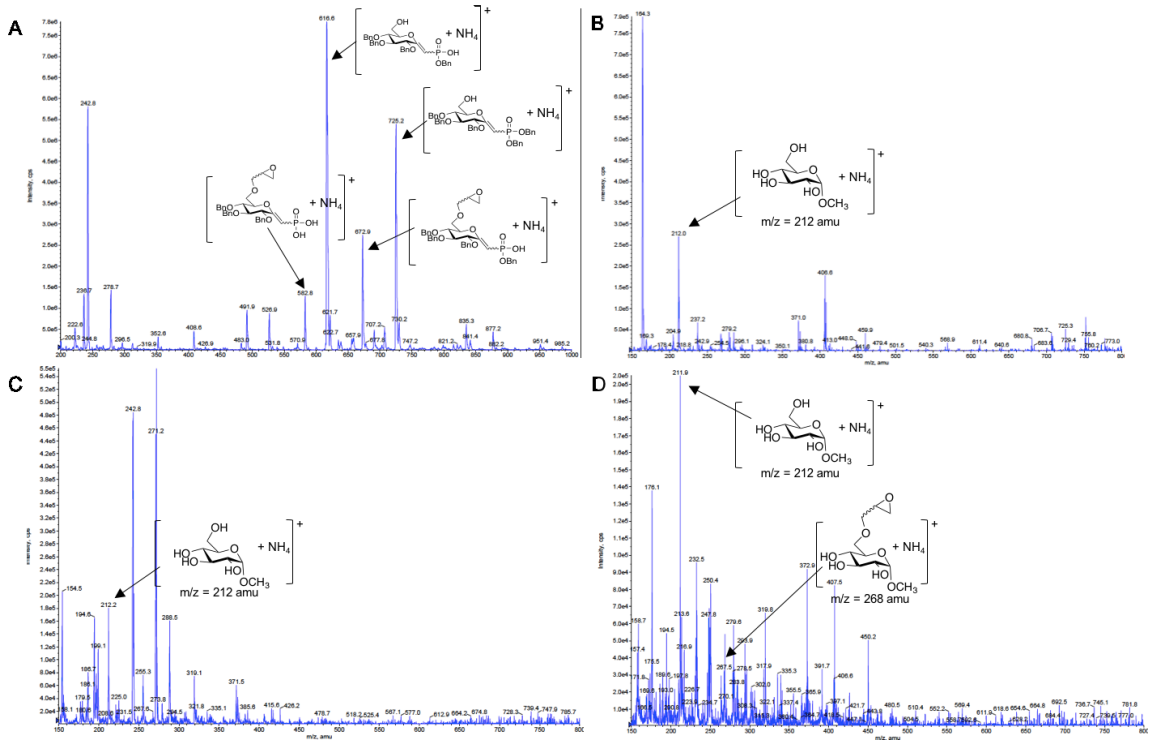

Figure 17. LC-MS/MS positive Q1 spectra for oxirane substitution reaction.

Spectra of m/z of compounds present during Method A (A), Method B (B), Method D (C), and Method E (D) reaction conditions.

As previously mentioned, βG1CP is an acceptable mimic for βG1P and causes inhibition of βPGM due to its non-hydrolyzable C-P bonds. However, since the enzyme intermediate, βG16P has a lower binding constant than βG1P, substituting a phosphate group onto C-6 of βG1CP (**10**) could increase its binding affinity. To synthesize compound **10**, compound **6** was phosphorylated using conditions that have been successfully employed for the formation of glycosyl phosphates in the Jakeman lab.[57] Compound **6** was treated with diphenyl chlorophosphate in the presence of triethylamine and DMAP and after 6 h, **9** was produced in a 90% yield. The product was confirmed by ^{31}P-^{1}H 2D HMBC experiment which showed a correlation between the diphenyl

phosphate and H-6 protons and a correlation between the dibenzyl phosphonate and the H-1' proton (Fig. 18). Global deprotection of **9** via hydrogenation afforded impure **10**. Product purification via a reversed-phase C18 column (MeOH/ddH_2O gradient) was not successful (Fig. 19).

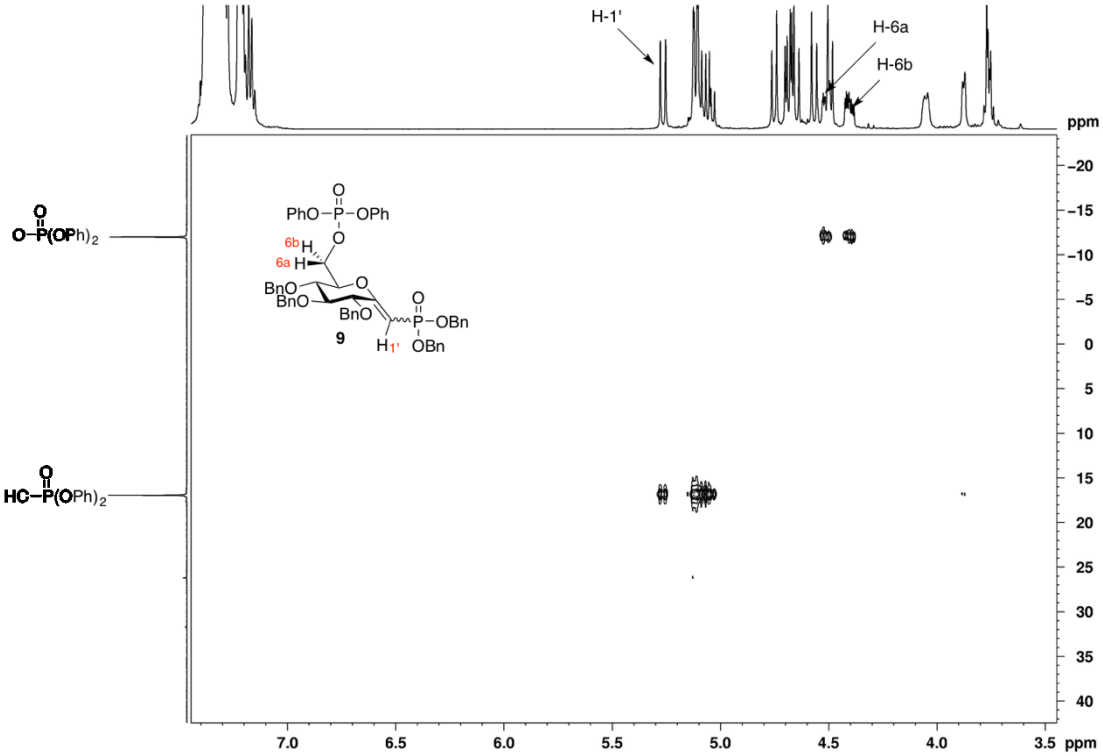

Figure 18. 2D ^{31}P-^{1}H HMBC spectra of **9** (500 MHz, $CDCl_3$).

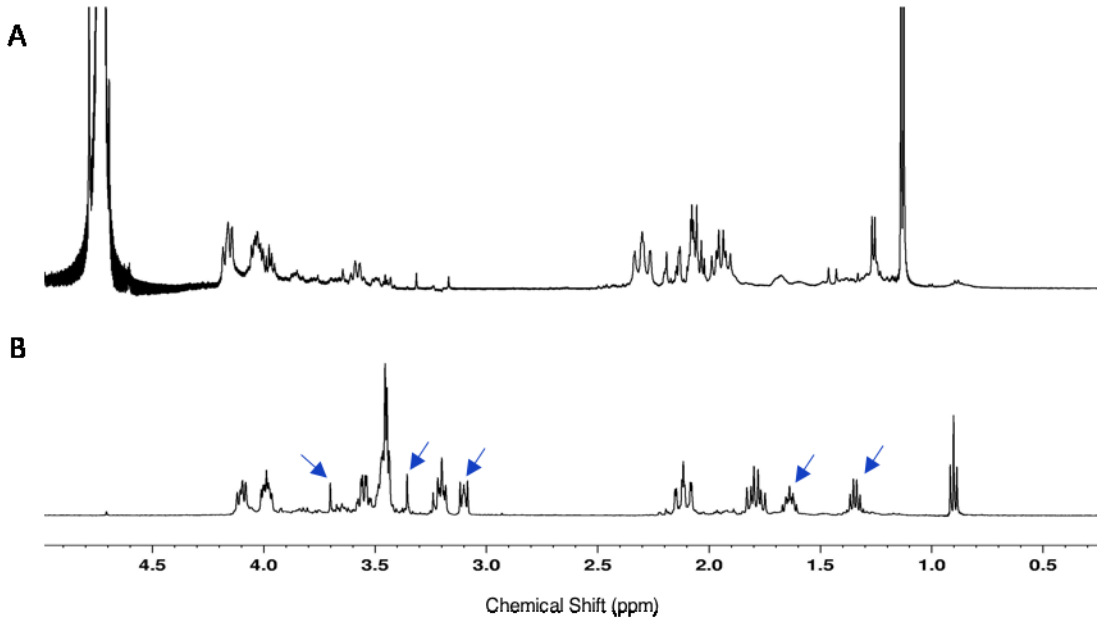

Figure 19. ^{1}H NMR of **10** before (A) and after (B) purification by a C18 column.
Blue arrows represent the unidentified impurities.

3.4 Attempted Synthesis of Phosphofluoridates with βG1CP

Literature precedence includes the synthesis of glucose 6-phosphofluoridate and the attempted synthesis of α-D-glucopyranosyl phosphofluoridate which resulted in the 1,2-cyclic phosphate product due to the lability of the phosphorus-fluorine bond.[62] It was proposed that the phosphofluoridate product of βG1CP would not form the 1,2-cyclic product as easily as the α-anomer due to the unfavourable bond angle of the β-anomer. Thus, we performed the reaction with **13** under literature conditions[62] using 2,4-dinitrofluorobenzene and tributylamine to generate **14**, but it turned out that the product was a mixture with the β-1,2-cyclic G1CP **15** (Scheme 8).

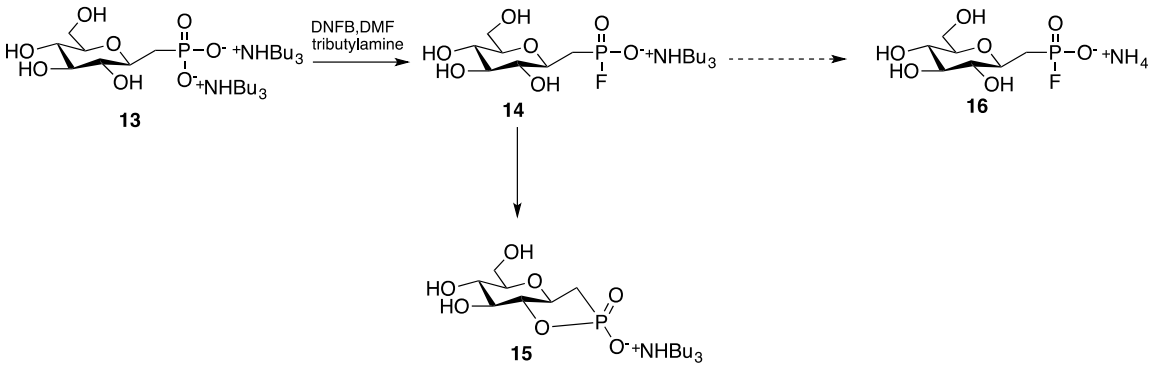

Scheme 8. Synthetic scheme of the βG1CP phosphofluoridate products.

The reaction proceeds through a 2,4-dinitrophenyl intermediate before the subsequent nucleophilic attack of fluoride (Scheme 9). As the reaction proceeded, ^{31}P NMR spectroscopy showed the disappearance of a peak at 35 ppm, which was presumed to be the 2,4-dinitrophenyl intermediate, and the appearance of a doublet at 22 ppm with a coupling constant of 980 Hz which is observed in other sugar phosphofluoridates (Fig. 20).[62] The ^{19}F NMR spectrum also showed the appearance of doublet with a coupling constant of 980 Hz, confirming the formation of the phosphofluoridate product.

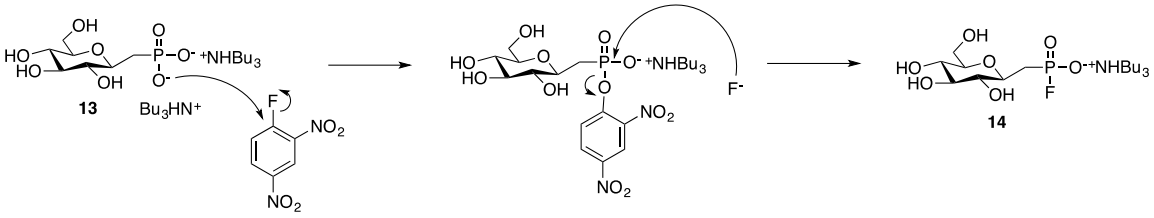

Scheme 9. The phosphofluoridation reaction mechanism of **14**.

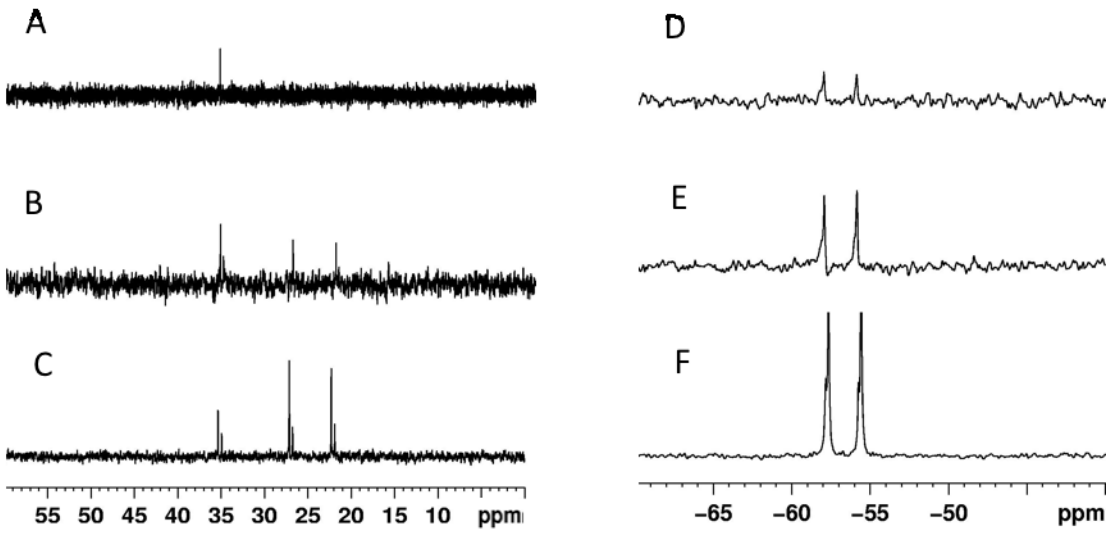

Figure 20. ^{31}P NMR and ^{19}F NMR spectra of phosphofluoridation reaction with βG1CP.
A-C are recorded ^{31}P NMR spectra and D-F are recorded ^{19}F NMR spectra. (A) and (D) were recorded after a reaction time of 5 h; (B) and (E) were recorded after a reaction time of 20 h; (C) and (F) were recorded after 48 h and work-up.

After work-up, a second product was also observed by ^{31}P NMR at 34.5 ppm (Fig. 20C) and was partially isolated using a Sephadex LH20 column. The product was characterized by 2D COSY correlations and ^{13}C NMR chemical shifts. ^{1}H NMR reported the chemical shifts for H-1, H-2, and H-3 protons had shifted downfield in comparison to the starting material (Fig. 21) and ^{13}C NMR exhibited splitting of C-3 with a coupling constant of 9.4 Hz, which is not observed in the ^{13}C NMR of the starting material. Thus, we identified the product as β-glucose 1,2-cyclic phosphonate, **15**, since coupling constants observed were similar to those reported for 1,2-cyclic phosphates.[63] The R_f values of **14** and **15** were very similar (Fig. 22), thus, the phosphofluoridate product, **14**, was not successfully isolated by the Sephadex LH20 column and was unstable toward reversed-phase column conditions. Using a coupled assay to glucose 6-phosphate dehydrogenase (Section 4.1), a mixture of **14** and **15** were screened as inhibitors of

βPGM. No significant inhibition was seen up to 2 mM, (Fig. 23) therefore the optimization of this reaction was not pursued any further.

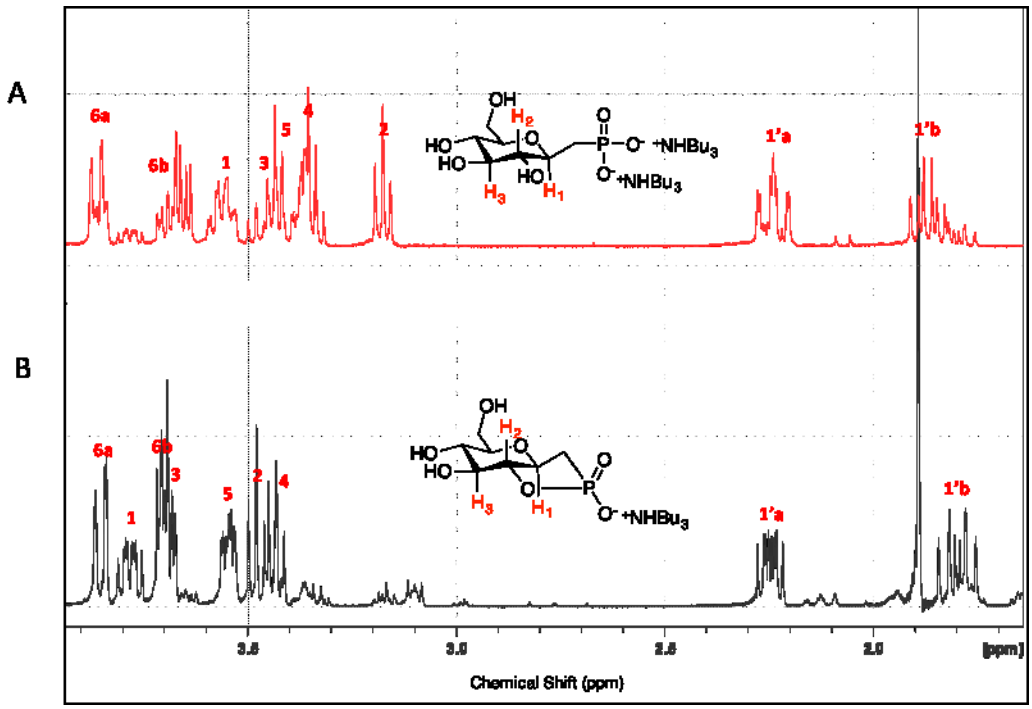

Figure 21. ^{1}H NMR spectra of **13** (A) and **15** (B).

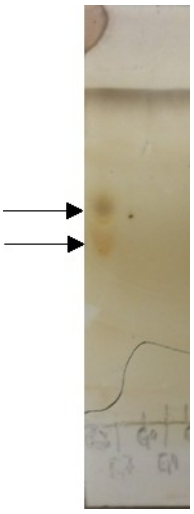

Figure 22. TLC on silica of **14** and **15**. Mixture was eluted in 7:2:1 isopropanol:water:ammonium hydroxide.

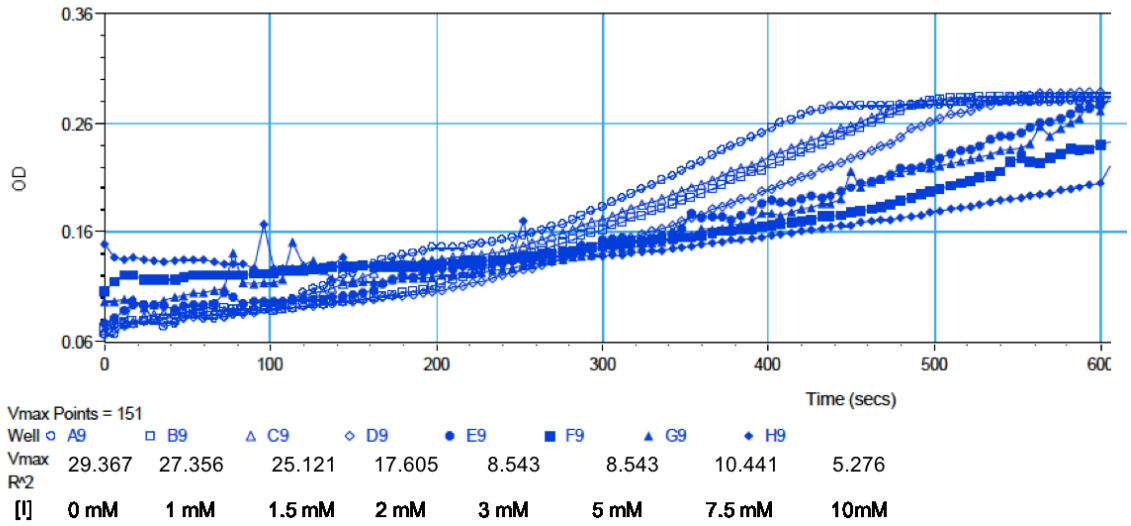

Figure 23. Change in A_{340} vs. time plot monitoring the inhibition assay of βPGM with **14** and **15.** Vmax values are the slopes for the linear portions of each curve and [I] is the concentration of a mixture containing **14** and **15**.

3.5 Attempted Synthesis of Phosphofluoridates with G6P

Due to the formation of the cyclized product and the difficulty in purification of **14** and **15**, the use of protecting groups was explored to generate the glucose 6-phosphofluoridate product, **21** (Scheme 10). The synthesis began with 1,2,3,4-tetra-*O*-acetyl-α-D-glucopyranose (**17**) which was generated via an enzymatic reaction with *Candida rugosa* lipase and α-D-glucose pentacetate.[65] **17** was treated with diphenyl chlorophosphate in pyridine and after 6 h, the starting material was completely consumed as judged using TLC, affording **18** in a 98% yield. The phosphate protecting groups were removed via hydrogenolysis to afford **19**. Addition of excess tributylamine converted **19** to its tributylamine salt before being treated with 2,4-dinitrofluorobenzene to generate **20** in a 56% yield. In order to remove the acetyl ester protecting groups to afford **21,** two deprotection methods were evaluated. Initially, **20** was added to potassium carbonate in

methanol, since it had been effective in the deprotection of the primary acetate to afford **6.** The reaction was monitored by TLC and after 3 h the starting material was fully consumed, however, the ^{19}F NMR and ^{31}P NMR spectra (Fig. 24) showed product breakdown. The ^{19}F NMR spectra (Fig. 24C) of the reaction mixture reported a minor doublet at -78 ppm for the phosphofluoridate product and a strong singlet at -122 ppm, the chemical shift for free fluoride (F^-). The ^{31}P NMR spectra (Fig. 24D) of the reaction mixture reported a breakdown of the phosphofluoridate product, as the doublet at -10 ppm had disappeared, and a mixture of unidentified products. A second attempt to deprotect **20** was attempted with a mixture of triethylamine, water, and methanol. Similarly, the reaction was monitored by TLC, and when the starting material was consumed, the ^{19}F NMR and ^{19}P NMR spectra were similar to that observed in Fig. 24C and 24D, reporting breakdown of the phosphofluoridate and a mixture of unidentified products. Thus, the P-F bond of the phosphofluoridate is not stable to aqueous basic conditions and a different protecting group method should be attempted.

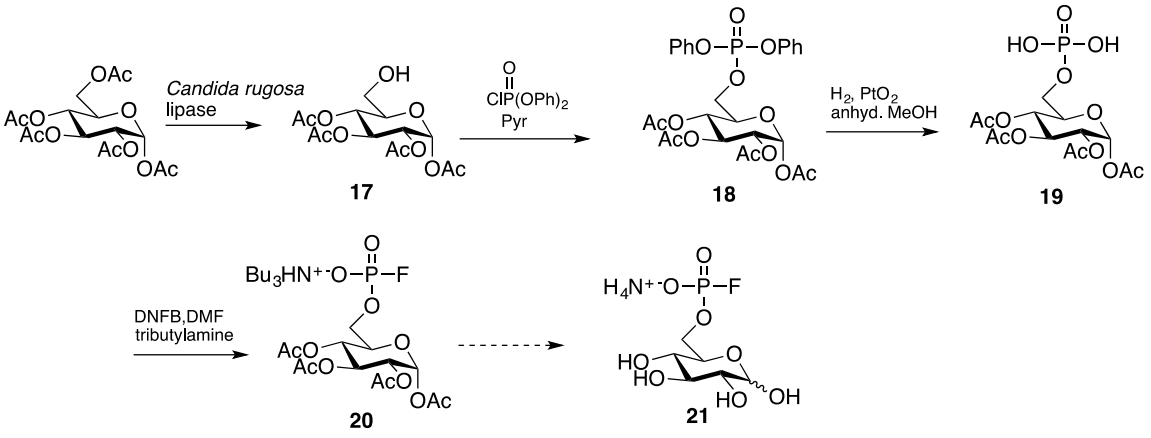

Scheme 10. Synthetic scheme of acetyl-protected G6P phosphofluoridate reactions.

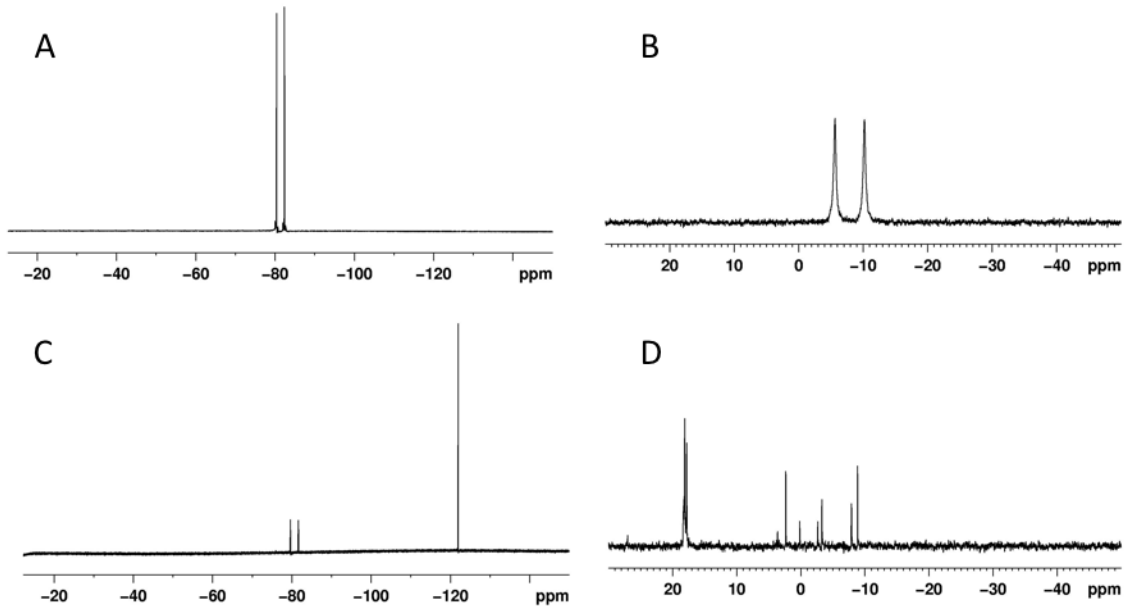

Figure 24. ^{19}F NMR (A and C) and ^{31}P NMR (B and D) spectra of **20** and its deprotection reaction.

A and B are spectra of purified **20** and C and D are crude reaction mixture of **20** treated with K_2CO_3 in MeOH.

CHAPTER 4. RESULTS AND DISCUSSION: KINETIC EVALUATION AND INHIBITION STUDIES OF βPGM

Excerpts of this section were taken from Ampaw, A.; Bhattasali, D.; Cohen, A.; Jakeman, D. L. *Submitted to Chem. Sci.* **2016.**

4.1 Introduction

To perform kinetic analysis on βPGM, a coupled assay with glucose 6-phosphate dehydrogenase (G6PDH) was used.[5,22] As βPGM converts βG1P to G6P, G6PDH oxidizes the βPGM enzyme product to 6-phosphogluconolatcone via the reduction of $NADP^+$ to NADPH (Scheme 11). This reaction can be monitored spectrophotometrically by the accumulation of NADPH (A_{340}).

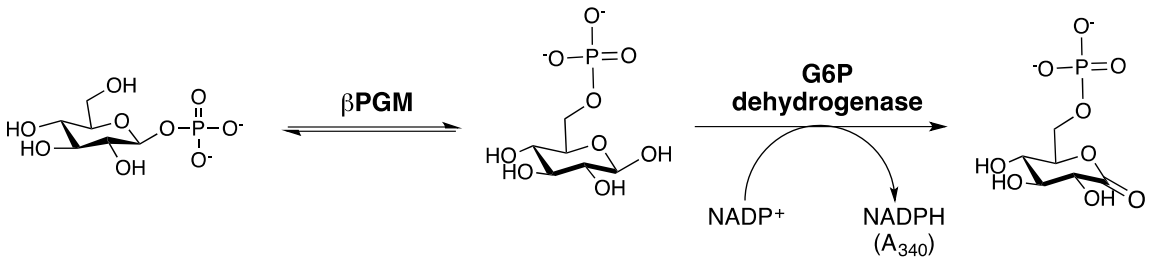

Scheme 11. Mechanistic scheme of βPGM-G6PDH coupled assay.

Extensive kinetic studies on βPGM reveal that freshly purified and isolated enzyme exists in its dephosphorylated form and thus a phosphorylating agent is needed to gain optimal activity.[5,33] The enzyme substrate, βG1P, is not sufficient to perform initial phosphorylation of βPGM due to its low affinity for the dephosphorylated enzyme.[5] Thus, the enzyme intermediate βG16P or a similar analog must be used to activate the enzyme. βG16P, αG16P, and α-fructose-1,6-bisphosphate (αF16BP) have all been

reported as phosphorylating agents for βPGM via their C-6 phosphate group,[5] hence the reason for βG1P being a poor activator. For the purpose of our kinetic studies, αF16BP was used as an activator to measure steady-state kinetics and inhibition.

4.2 Kinetic Evaluation of 5FWβPGM

Table 4. Kinetic parameters for wild-type and 5-fluorotryptophan βPGM (5FWβPGM) with βG1P.

	Wild-type βPGM	**5FWβPGM**
K_m (μM)	9.0 ± 0.7	10.1 ± 2.1
k_{cat} (s^{-1})	7.7 ± 0.1	3.8 ± 0.1
Specific activity (Umg^{-1})	15.4	5.1

Kinetic studies were performed for both wild-type and 5FWβPGM (Table 4) to confirm kinetic competence of the fluorinated enzyme. αF16BP was used as an activator[5] and a Michaelis-Menten equation was fitted to the steady-state velocity data to generate K_m and k_{cat} values (Fig. 25). The K_m of βG1P was 10.1 μM, which was comparable to previously recorded results (14.7 μM)[22] for the wild-type enzyme. This suggests that the incorporation of two 5FW amino acid residues into the enzyme structure, one adjacent to the active site and one distal to the active site, did not have an effect on the binding affinity of the native substrate, which agrees with the previous observation of the TSA complexes by ^{19}F NMR. The k_{cat} value of the wild-type and ^{19}F-labeled enzyme was

slightly lower than reported (17 s^{-1})[22] which could be a result of the incorporation of a His_6-tag at the C-terminus of the enzyme sequence.

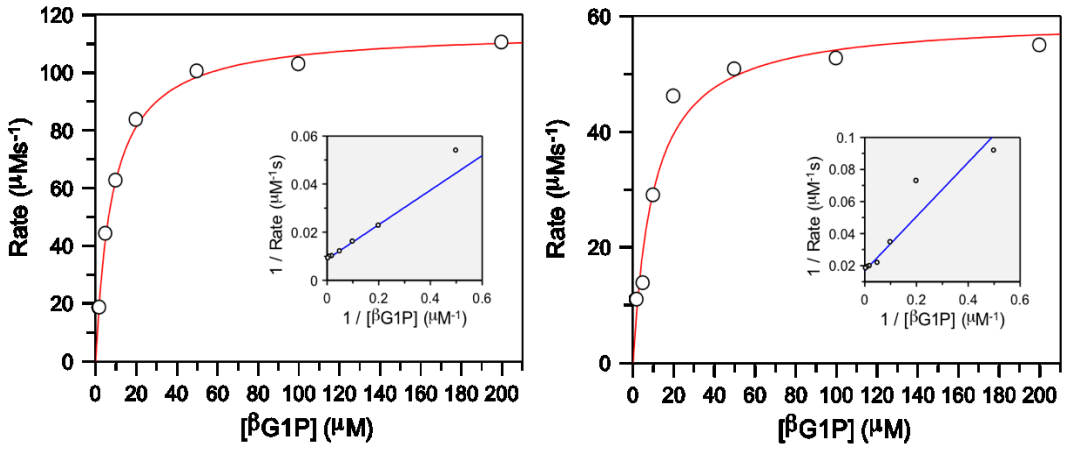

Figure 25. Michaelis-Menten and double-reciprocal plots of 50 nM wild-type unlabeled βPGM (A) and 50 nM 5FWβPGM (B).

Assays included 2 mM $MgCl_2$, 0.5 mM $NADP^+$, 5 U/mL G6PDH, 150 μM αF16BP, and βG1P in 50 mM Hepes pH 7.2

4.3 Inhibition Studies of 5FWβPGM with Phosphonate Analogs

Table 5. Measured inhibition constants for phosphonate analogs with 5FWβPGM.

Inhibitor	IC_{50} (μM)	$K_{i(comp)}$ (μM)
βG1CP	13 ± 5 (5FWβPGM) 18 ± 3 (wild-type βPGM)	4.67 ± 0.04
βG1CF_SP	11 ± 2 (5FWβPGM) 15 ± 2 (wild-type βPGM)	4.03 ± 0.03
β2FG1CP	19 ± 6	2.68 ± 0.04
β2FMan1CP	>1000	Not determined
βG16CP	186 ± 73	Not determined

4.3.1 βG1CP and βG1CF$_S$P IC_{50} and K_i Determination

Although the formation of βG1CP and βG1CF$_S$P TSA complexes have been extensively studied,[20,21,33] the kinetic analysis of gluco-configured phosphonates as non-covalent inhibitors for βPGM has not been reported. Inhibition studies were performed without NH_4F, as fluorine inhibition has already been reported in the low milimolar range.[22,33] IC_{50} measurements of both ligands were performed with wild-type and 5FWβPGM; however, there was no significant differences in values between the two enzymes (Table 5). For 5FWβPGM, βG1CP and βG1CF$_S$P both show IC_{50} values in the micromolar range (13 ± 5 μM and 11 ± 2 μM respectively) (Fig. 26). βG1CP and βG1CF$_S$P did not show any sign of inhibition toward G6PDH up to a ligand concentration of 1 mM. To evaluate if enzyme inhibition was time-dependent, assays containing 50 nM 5FWβPGM, 2 mM $MgCl_2$, 0.5 mM $NADP^+$, 5 U/mL G6PDH, and 150 μM αF16BP in 50 mM Hepes pH 7.2 were pre-incubated at 5 min, 10 min, and 20 min time points before dilution with βG1P. The extent to which βG1CP and βG1CF$_S$P inhibited 5FWβPGM was not affected by various pre-incubation times.

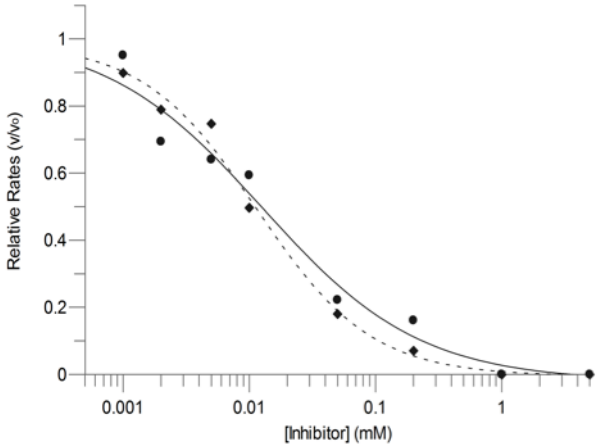

Figure 26. IC_{50} plots of methylene phosphonate (βG1CP) and fluoromethylene phosphonate ($\beta G1CF_SP$) compounds.

βG1CP (circle and solid line) and $\beta G1CF_SP$ (diamond and dashed line) show non-time dependent inhibition of 5FWβPGM. Assays included 50 nM 5FWβPGM, 2 mM $MgCl_2$, 0.5 mM $NADP^+$, 5 U/mL G6PDH, 150 μM αF16BP, and 10 μM βG1P in 50 mM Hepes pH 7.2.

The mode of inhibition of these inhibitors was determined from double-reciprocal plots (Fig. 27) that showed both analogs as competitive inhibitors with K_i values of 4.67 ± 0.04 μM for βG1CP and 4.03 ± 0.03 μM for $\beta G1CF_SP$. These values suggest that phosphonate compounds bind 5-6 times less strongly than the enzyme intermediate, βG16BP (K_m = 0.72 ± 0.04 μM),[22] whereas they show a slightly stronger binding affinity than the native substrate, βG1P.[22] Nonetheless, these data are measured without fluorine in the solution and so it is not representative of the inhibition, or formation constant, of the MgF_3^- or AlF_4^- complexes with these compounds.

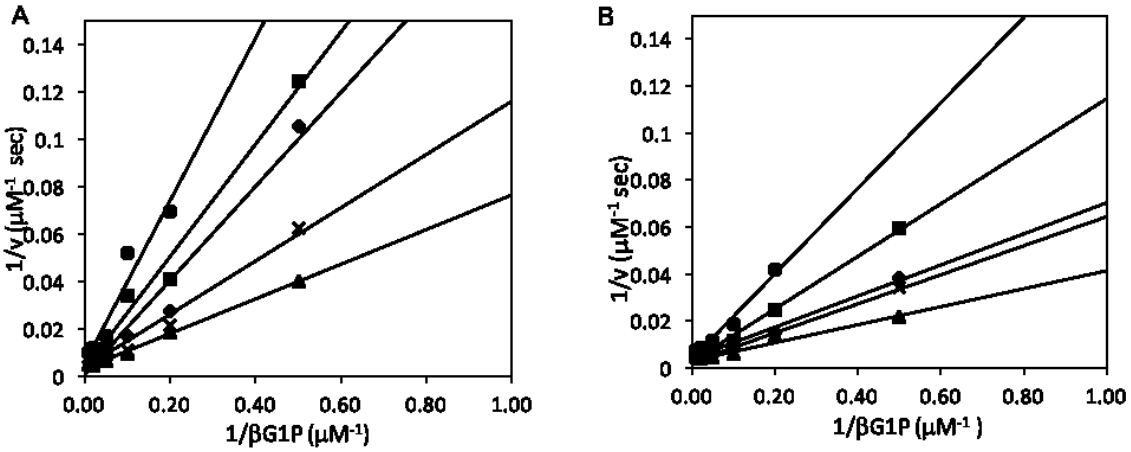

Figure 27. Double-reciprocal plots for the inhibition of βPGM with phosphonate compounds.

Varying concentration of βG1CP (A) and $\beta G1CF_SP$ (B) show competitive inhibition. Assays contain 2 mM $MgCl_2$, 0.5 mM $NADP^+$, 5 U/mL G6PDH, 150 μM αF16BP, and βG1P in 50 mM Hepes pH 7.2. ▲ 0 μM, ✕ 2 μM, ◆ 5 μM, ■ 10 μM, ● 20 μM.

4.3.2 β2FG1CP and β2FMan1CP IC_{50} and K_i Determination

An IC_{50} of 19 ± 6 μM was measured for the inhibition of 5FWβPGM with β2FG1CP, and similar to βG1CP and $\beta G1CF_SP$, time-dependent inhibition was not observed. β2FG1CP did not report any sign of inhibition toward G6PDH up to a ligand concentration of 1 mM. Double reciprocal plots displayed that β2FG1CP showed competitive inhibition of βPGM (Fig. 28) (K_i = 2.68 ± 0.04 μM). This result is in agreement with our earlier hypothesis stating that β2FG1CP binds to 5FWβPGM by observation of a second ligand resonance in the ^{19}F NMR spectra. Similar to the other phosphonates, β2FG1CP has a stronger binding affinity than the enzyme native substrate but a weaker binding affinity than the enzyme intermediate. β2FMan1CP showed only slight signs of inhibition up to 1 mM concentrations, which also agrees with the lack of metal fluoride complexation seen by ^{19}F NMR.

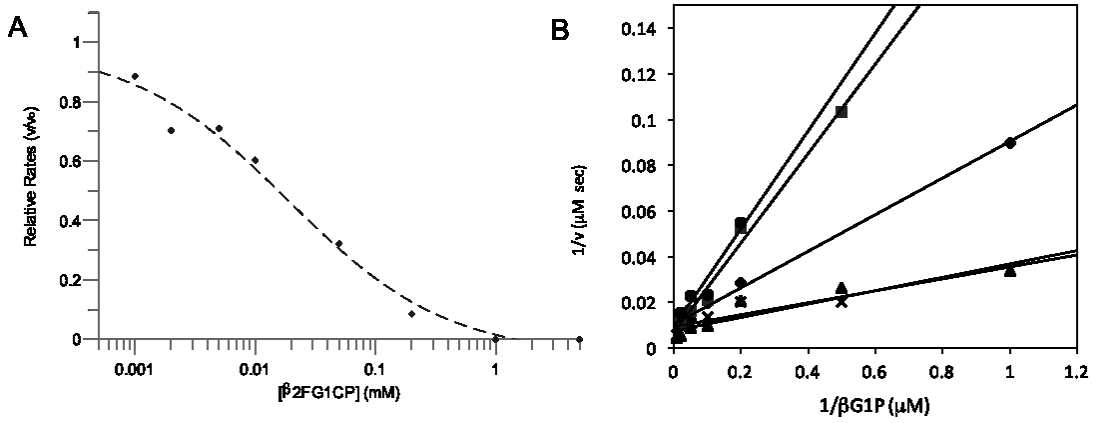

Figure 28. IC_{50} (A) and double-reciprocal plot (B) for the inhibition of 50 nM βPGM with β2FG1CP.

Assays contain 2 mM $MgCl_2$, 0.5 mM $NADP^+$, 5 U/mL G6PDH, 150 μM αF16BP, and βG1P in 50 mM Hepes pH 7.2. ▲ 0 μM, ✕ 2 μM, ◆ 5 μM, ■ 10 μM, ● 20 μM.

4.3.3 βG16CP IC_{50} Determination

To determine the degree of inhibition of βG16CP towards 5FWβPGM, a similar inhibition assay was performed. We observed an IC_{50} value for βG16CP of 186 ± 73 μM without the observation of time-dependent inhibition (Fig. 29). The requirement of αF16BP as an activator may compete with the inhibitor for the βPGM active site to phosphorylate βPGM. It was previously reported that high concentrations of activating agents inhibit the formation of βPGM-MgF_3^- complexation;[33] thus, βG16CP complexation with βPGM may have also been inhibited due to the activator. For this reason, we attempted to incubate βG16CP with 5FWβPGM before the addition of αF16BP, however results remained consistent. We also attempted to lower the activator concentration, however this resulted in a very low enzyme activity, preventing accurate IC_{50} values from being obtained. βG16CP did not report any sign of inhibition toward G6PDH up to a ligand concentration of 1 mM.

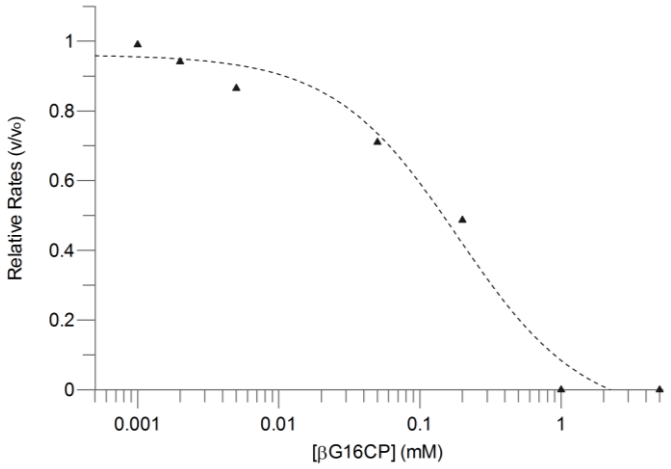

Figure 29. IC_{50} plot of βG16CP as an inhibitor of βPGM.

Assay includes 50 nM βPGM, 2 mM $MgCl_2$, 0.5 mM $NADP^+$, 5 U/mL G6PDH, 150 μM αF16BP, and 10 μM βG1P in 50 mM Hepes pH 7.2.

CHAPTER 5. EXPERIMENTAL

5.1 General Methods

5.1.1 General Synthetic Methods

All reactions were performed under a nitrogen atmosphere with oven-dried glassware. Thin-layer chromatography was used to monitor reactions unless otherwise stated. Glass Silicycle^{TM} coated silica gel plates were used and visualized either by ultraviolet light (λ = 254 nm), a potassium permanganate dip (3.0 g potassium permanganate, 20.0 g potassium carbonate, 5.0 mL 5% aqueous sodium hydroxide, 300 mL distilled water), or a *p*-anisaldehyde dip (*p*-anisaldehyde 3.4%, sulfuric acid 2.2%, and acetic acid 1.1% in ethanol). Compounds were concentrated either by a rotary evaporator, or an EZ-Bio Genevac. Compounds were lyophilized with a Heto PowerDry freeze dryer. Purifications were performed using a bench-top glass column unless otherwise stated.

NMR spectra for synthetic compounds were acquired using Bruker AV-300 and AV-500 spectrometers at Dalhousie University NMR[3].

5.1.2 General procedure for plasmid transformation into *E. coli* cells

Chemically competent *E. coli* cells (NEB 5α, NEB 10β, BL21 DE3) were thawed on ice in 20 μL aliquots. A diluted plasmid (2 μL) (1:10) was added and the cells were incubated on ice for 30 min. The reaction was heat shocked at 42°C for 30 s, then incubated on ice for 2 min. SOC media (200 μL) was added to the reaction mixture and the cells were incubated at 37°C for 1 h with agitation. The cells were plated in 20 μL

and 200 μL aliquots on LB agar supplemented with 100 μg/mL ampicillin and grown at 37°C overnight.

5.1.3 General procedure for plasmid isolation using the Bio Basic Inc. EZ-10 Spin Column MiniPrep Kit

The overnight bacteria culture (2 mL) was transferred into a 2 mL microcentrifuge tube and centrifuged at 15 231 x g for 2 min. The supernatant was decanted and the cell pellet was resuspended in 100 μL of solution I containing 10 mg/mL of RNase. The resuspended cell pellet was gently mixed and incubated at room temperature for 1 min. VisualLyse (1 μL) was added followed by 200 μL of Solution II. The components were gently mixed and incubated at room temperature for 1 min. 350 μL of Solution III was added, and the components were gently mixed and incubated at room temperature for 1 min. The DNA mixture was centrifuged at 15 231 x g for 5 min and the supernatant was transferred to an EZ-10 column. The column was centrifuged at 12 692 x g for 2 min and the flow-through was discarded. The Wash Solution (750 μL) was added to the column and the column was centrifuged at 12 692 x g for 2 min. The flow-through was discarded and the wash step was repeated. The flow-through was discarded and the column was centrifuged at 12 692 x g for 1 min. The column was transferred to a clean 1.5 mL microcentrifuge tube and the elution buffer (50 μL) was added to the center of the column. The column was incubated at room temperature for 2 min then centrifuged at 12 692 x g for 2 min. The extracted pure DNA was stored at -20°C.

5.1.4 General procedure for cell lysis

Overnight bacteria cultures were centrifuged at 2 993 x g for 5 min at 4°C. The cell pellet was resuspended in lysis buffer (16 mL of 25 mM imidazole buffer, 3 mL glycerol, 1 mL of 10% Triton X, 0.5 mg/mL lysozyme, and 1 μg/mL DNAase) and agitated on ice for 30 min. The cell lysate was sonicated at 50% amplitude for a total of 25 s (5 s pulses with 5 s rests). The cell lysate was centrifuged at 15 231 x g for 10 min at 4°C in 2 mL aliquots. The supernatant was pooled and kept for purification by column chromatography, while cell pellets were stored at -70°C.

5.1.5 General procedure for 1% agarose gel electrophoresis

A 1% agarose gel was made by adding 0.30 g of agarose to ddH_2O (30 mL). The agarose solution was poured into a gel plate (Bio-Rad) and allowed to solidify. The gel loading buffer (2 μL) was added to 10 μL DNA samples before the samples were loaded onto the gel. The gel was immersed in 1X Tris/Acetate/EDTA (TAE) buffer (Section 5.8) stained with ethidium bromide (0.75 μg/mL) and a voltage of 120 V was applied for 30 min.

5.1.6 General procedure for sodium dodecyl sulfate polyacrylamide gel electrophoresis (SDS-PAGE)

SDS-PAGE (10%) gels were made with two different solutions. A 10% resolving solution containing 1.24 mL ddH_2O, 1.37 mL resolving buffer (1.5 M Tris-HCl pH 8.8), 2.75 mL acrylamide solution (30% acrylamide, 0.8% bisacrylamide), 27.5 μL 20% SDS, 110 μL 10% ammonium persulfate (APS), and 6 μL tetramethylethylenediamine (TEMED) was allowed to solidify in a glass gel plate (Bio-Rad) before adding a 5% stacking solution. The stacking solution was composed of 1.11 mL ddH_2O, 500 μL

stacking buffer (1.5 M Tris-HCl pH 6.8), 340 μL acrylamide solution, 10 μL 20% SDS, 60 μL 10% APS, and 6 μL TEMED. SDS-PAGE loading dye (1 μL) (Section 5.8) was added to 5-10 μL protein samples and the samples were heated at 95°C for 10 min before they were loaded onto the gel. Gels were immersed in a 1X SDS-PAGE running buffer (Section 5.8) and a voltage of 150 V was applied for 45 min. Proteins were visualized by staining with Protein Stain (Sci-Med. Inc Bridgewater NS.) as directed by manufacturer.

5.2 Expression and Isolation of βPGM

5.2.1 *E. coli* NEB 5α pET-22b(+)_*pgmB* transformation and isolation

The gene encoding βPGM (*pgmB*) cloned in the pET-22b(+) expression vector was received as a gift from Waltho and Blackburn at the University of Sheffield. The plasmid was quantified using spectrophotometry. The quantified plasmid (39 ng/μL) was transformed into chemically competent *E. coli* NEB 5α cells according to the general procedure described above. Three colonies were used to inoculate 25 mL LB media containing 0.1 mg/mL ampicillin (LB_{Amp}) and were incubated at 37°C with shaking (250 rpm) overnight. Plasmid isolation of pET-22b(+)_*pgmB* from *E. coli* NEB 5α was performed using the Bio Basic Inc. EZ-10 Spin Column MiniPrep Kit following the manufacturers instructions.

5.2.2 pET-22b(+) and *pgmB* digestion

pET-22b(+)_*pgmB* was isolated from *E. coli* NEB 5α according to general procedure (Section 5.1.3) and was confirmed by a plasmid digestion with the restriction enzymes NdeI and XhoI. The reaction mixture consisted of the following:

Component	Volume (μL)	Source
NdeI (2000 U/mL)	1	NEB
XhoI (10 U/μL)	1	MBI
pET-22b(+)_*pgmB*	5	
CutSmart Buffer (10X)	1	NEB
Sterile ddH_2O	2	

The reaction mixture was incubated at 37°C for 1 h. The digestion product was analyzed via agarose gel electrophoresis according to the general procedure described above (Fig. 30).

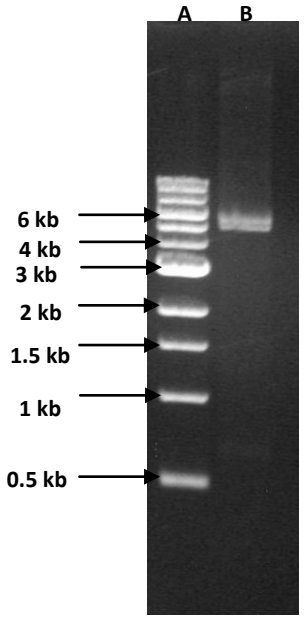

Figure 30. 1% agarose gel of pET-22b_*pgmB* plasmid digested with NdeI and XhoI.
(A) 1 kb DNA ladder; (B) pET-22b_*pgmB* plasmid.

5.2.3 Overexpression and purification of βPGM

pET-22b(+)_*pgmB* (39 ng/μL) was transformed into chemically competent *E. coli* BL21(DE3) (New England Biolabs) according to general procedure. The transformants

were used to inoculate LB_{Amp} media (25 mL) and grown overnight with shaking (250 rpm) at 37°C. 3.3 mL of the overnight culture was used to inoculate 3 x 330 mL of LB_{Amp} in 1 L flasks. Aliquots of the remaining inoculum were combined with one half volume of (1:1) sterile glycerol and stored at -70°C. The cultures were grown at 37°C with shaking (250 rpm) for 2-3 h until an OD_{600} of ~0.6-0.8 was reached. IPTG was added to a final concentration of 1 mM to each bacterial culture and incubated at 17°C overnight. Protein overexpression was confirmed via SDS-PAGE analysis through the comparison of culture samples before and after the addition of IPTG. The overnight cultures were centrifuged at 4°C for 1 h at 2993 x g and the supernatant was discarded. The cell pellet was lysed according to the general procedure described above. The lysate was then loaded onto a DEAE Sephadex A-25 column for purification by Fast Protein Liquid Chromatography (FPLC) (AKTA Purifier 10) at 4°C. The protein was eluted using a linear gradient of 0-0.5 M NaCl in 50 mM HEPES buffer and monitored by UV absorbance 280 nm. Eluent was collected in 1 mL fractions and the fractions were analyzed by SDS-PAGE. The fractions containing pure βPGM were pooled and concentrated to 2.5 mL by ultrafiltration (5 000 x g at 4°C in 10 000 MWCO centrifical filters). The concentrated protein was desalted using a PD-10 desalting column (GE Healthcare) to remove all imidazole and NaCl contamination following manufacturers instructions. The desalting column was equilibrated with 5 x 4 mL of HEPES buffer before the concentrated protein was loaded onto the column. The desalted protein was eluted with 3.5 mL of HEPES buffer and collected, providing 30.6 mg/L of pure protein. Enzyme concentrations were determined using spectrophotometric analysis (ε_{280} = 19 940 M^{-1} cm^{-1}). The extinction coefficient was obtained by entering the βPGM amino acid

sequence into the ProtParam tool on the ExPASy database. The protein concentration was calculated using the Beer-Lambert Law (Equation 1).

5.2.4 Overexpression and purification of ^{15}N-βPGM

E. coli BL21(DE3) pET-22b(+)*_pgmB* glycerol stock (25 μL) was used to inoculate 25 mL LB_{Amp} and was incubated at 37°C with shaking (250 rpm) overnight. The overnight culture (3.3 mL) was used to inoculate 3 x 330 mL of LB_{Amp} in 1 L flasks. Bacterial cultures were grown at 37°C with shaking (250 rpm) for 2-3 h until an OD_{600} of ~0.6-0.8 was reached. The cultures were centrifuged at 2993 x g for 5 min and the supernatant was discarded. The cell pellet was resuspended in 6 mL of minimal growth media (12 g/L NaH_2PO_4, 6 g/L K_2HPO_4, 1 g/L $^{15}NH_4Cl$, 2 g/L D-glucose, 4 mL/L 1M $MgSO_4$, and 1.8 mL/L 1mM $FeSO_4$) and distributed evenly between 3 x 330 mL minimal media in 1 L flasks. IPTG was added to 1 mM and bacterial cultures were incubated at 17°C overnight, 250 rpm. Cell lysis was performed according to general procedure. Protein purification and concentration was performed similar to the procedure previously described for βPGM, providing 27.8 mg/L of pure ^{15}N-labeled protein.

5.2.5 Overexpression and purification of ^{15}N-5FWβPGM using 5-fluoro-D/L-tryptophan and 5-fluoroindole

Growth conditions for ^{19}F-labeled βPGM were taken from a procedure described by Crowley and associates with the following modifications.[38] LB_{Amp} (25 mL) was inoculated with 25 μL *E. coli* BL21(DE3) pET-22b(+)*_pgmB* glycerol stock and incubated at 37°C with shaking (250 rpm) overnight. The overnight culture (3.3 mL) was used to inoculate 6 x 330 mL of LB_{Amp} in 1 L flasks. Bacterial cultures were grown at

37°C with shaking (250 rpm) for 2-3 h until an OD_{600} of ~0.6-0.8 was reached. The bacterial cultures were centrifuged at 2993 x g for 5 min and the supernatant was discarded. The cell pellet was resuspended in 12 mL of minimal growth media (12 g/L NaH_2PO_4, 6 g/L K_2HPO_4, 1 g/L $^{15}NH_4Cl$, 2 g/L D-glucose, 4 mL/L 1 M $MgSO_4$, and 1.8 mL/L 1 mM $FeSO_4$) and distributed evenly between 6 x 330 mL minimal media in 1 L flasks. Bacterial cultures were incubated at 37°C with shaking (250 rpm) for 30 min. 3 x 330 mL bacterial cultures were supplemented with 1 mL of sterile L-phenylalanine, L-tyrosine, 5-fluoro-D/L-tryptophan, and glyphosate solutions for final concentrations of 60 mg/L, 60 mg/L, 120 mg/L, and 1 g/L respectively, and 3 x 330 mL bacterial cultures were supplemented with 1 mL solution of 5-fluoroindole in DMSO for a final concentration of 60 mg/L. IPTG was added to 1 mM in all 6 x 330 mL bacterial cultures and cultures were incubated at 17°C overnight, 250 rpm. Cell lysis was performed according to the general procedure. Protein purification and concentration was performed similar to the procedure previously described for βPGM, providing 13.0 mg/L of 5FWβPGM (using 5-fluoroindole) and 23.5 mg/L of 5FWβPGM (using 5-fluorotryptophan).

5.3 Expression and Isolation of βPGM-His

5.3.1 pET-22b(+)_*pgmB*-His mutagenesis

pET-22b(+)_*pgmB* was mutated using the QuikChange Lightning Site-Directed Mutagenesis Kit (Agilent Technologies) according to the manufacturers instructions and the following primers: pgmB_hisF 5'-GAA AGA AGT TTG GCT TCA AAA GCA AAA AGA GCT CGA GCA CCA CCA C-3' and pgmB_hisR 5'-GTG GTG GTG CTC

GAG CTC TTT TTG CTT TTG AAG CCA AAC TTC TTT C-3'. These primers converted a TAA stop codon to a SacI restriction site (underlined) to allow for expression of a His_6-tag. The mutagenesis reaction mixture was composed of the following:

Components	**Volume (μL)**	**Source**
reaction buffer (10X)	5	Agilent Technologies
pET-22b(+)_*pgmB*	5	
100 ng/μL pgmB_hisF	1.25	IDT
100 ng/μL pgmB_hisR	1.25	IDT
dNTP mix	1	Agilent Technologies
QuikSolution Reagent	1.5	Agilent Technologies
HF DNA polymerase	1	Agilent Technologies
Sterile ddH_2O	34	

The reaction was subjected to 20 cycles using a thermal cycler (Biometra) with the following parameters:

Segment	**Cycles**	**Temperature**	**Time**
Initial Denaturation	1	95°C	2 min
	18		
Denaturation		95°C	20 s
Annealing		60°C	10 s
Extension		68°C	3 min
Final Extension	1	68°C	5 min

The mutated plasmid was transformed into chemically competent *E. coli* NEB 10β (New England Biolabs) according to the general procedure mentioned above. Six colonies were used to inoculate 6 x 25 mL LB_{Amp} and incubated at 37°C overnight, 250 rpm. pET-22b(+)_*pgmB*-His was isolated using the general procedure. The six isolated plasmids were digested with the restriction enzyme SacI. The reaction mixture contained the following:

Component	**Volume (μL)**	**Source**
SacI (10 U/μL)	1	MBI
pET-22b(+)_*pgmB*-His	5	
Buffer ECI136II (10X)	1	MBI
Sterile ddH_2O	3	

The reaction mixture was incubated at 37°C for 1 h and the digestion product was analyzed by agarose gel electrophoresis. The plasmids showing the correct restriction digest pattern were stored at -20°C and used for protein expression.

pET-22b(+)_*pgmB*-His was quantified using spectrophotometry. The quantified plasmid (40 ng/μL) was transformed into chemically competent *E. coli* BL21(DE3) according to the general procedure mentioned above. A colony was used to inoculate LB_{Amp} (25mL) and bacterial culture was incubated at 37°C overnight, 250 rpm. pET-22b(+)_*pgmB*-His was isolated using the general procedure. The isolated plasmid was digested with the restriction enzymes PstI and SacI (Fig. 3). The digestion mixtures contained the following:

Component	Volume (μL)	Source
SacI (10 U/μL)	1	MBI
PstI (10 U/μL)	1	MBI
pET-22b(+)_*pgmB*-His	5	
Y^+ Tango Buffer (10X)	1	MBI
Sterile ddH_2O	1	

5.3.2 Overexpression and purification of ^{15}N- and ^{15}N-5FW βPGM-His

^{15}N- and^{15}N-5FW βPGM-His were overexpressed using the same procedure as for ^{15}N- and ^{15}N-5FWβPGM using 5-fluoro-D/L-tryptophan and 5-fluoroindole. Protein overexpression was confirmed via SDS-PAGE analysis through the comparison of culture samples before and after the addition of IPTG. The cell pellets were lysed according to the general procedure. The cell lysate was loaded onto a HiTrap 5 mL Chelating HP NTA-Ni^{2+} affinity column for purification by FPLC at 4°C. Protein was eluted at a flow rate of 2.5 mL/min using a step-wise gradient of 250 mM imidazole buffer in 25 mM imidazole buffer (Section 5.8) as shown in table below:

Step	250 mM imidazole buffer (%)	volume (mL)
1	1	25
2	10	25
3	20	75
4	50	60
5	100	40
6	2	50

Eluent was collected in 1 mL fractions and monitored by UV absorbance 280 nm. The fractions were analyzed by SDS-PAGE. The fractions containing pure βPGM were pooled and concentrated to 2.5 mL by ultrafiltration (5 000 x g at 4°C in Amicon Ultra-15 (EMD Millipore) 10 000 MWCO centrifugal filters). The concentrated protein was desalted using a PD-10 desalting column and eluted with 50 mM HEPES pH 7.2. Protein concentrations were determined using spectrophotometric analysis (ε_{280} = 19 940 M^{-1} cm^{-1}), and protein amounts were similar to those of the same method.

5.4 Expression and Isolation of W24F 5FWβPGM mutant

5.4.1 pET-22b(+)_*pgmB*-His W24F mutagenesis

pET-22b(+)_*pgmB*-His was mutated using the QuikChange Lightning Site-Directed Mutagenesis Kit (Agilent Technologies) according to manufacturers instructions and the following primers: pgmB_His_W24F_F 5'- ATT AAT GCC AAT TTC TTC AGC CAA AGC CTT **AAA** GGC TCT AAA ATG ATA CTC TGC GGT ATC -3' and pgmB_His_W24F_R 5'- GAT ACC GCA GAG TAT CAT TTT AGA GCC **TTT** AAG GCT TTG GCT GAA GAA ATT GGC ATT AAT -3'. These primers converted Trp24 to Phe24 (bold) and incorporated a BglI restriction site (underlined). The mutagenesis reaction mixture was composed of the following:

Components	Volume (μL)	Source
reaction buffer (10X)	5	Agilent Technologies
pET-22b(+)_*pgmB*-His	5	
pgmB_His_W24F_F	1.25	IDT
pgmB_His_W24F_R	1.25	IDT
dNTP mix	1	Agilent Technologies
QuikSolution Reagent	1.5	Agilent Technologies
HF DNA polymerase	1	Agilent Technologies
Sterile ddH_2O	34	

The mutagenesis reaction was subjected to 20 cycles using a thermal cycler with similar parameters used for pET-22b(+)_*pgmB*-His mutagenesis. The mutated plasmid was transformed into chemically competent *E. coli* NEB 5α according to the general procedure. Three colonies were used to inoculate 25 mL of LB_{Amp} in 125 mL flasks at 37°C overnight, 250 rpm. pET-22b(+)_*pgmB*-His_W24F was isolated according to the general procedure. pET-22b(+)_*pgmB*-His_W24F was digested with the restriction enzymes BglI and BstEII. The digestion mixture consisted of the following:

Component	Volume (μL)	Source
BglI (10 000 U/mL)	4	NEB
BstEII (10 000 U/mL)	4	MBI
pET-22b(+)_*pgmB*-His_W24F	20	
Buffer 3.1 (10X)	3	NEB

The digestion mixture was incubated at 37°C for 1 h and the digestion products were analyzed by agarose gel electrophoresis (Fig. 7). The plasmids showing the correct restriction digest pattern were stored at -20°C and used for protein expression.

pET-22b(+)_*pgmB*-His_W24F was quantified using spectrophotometry. The quantified plasmid (36 ng/μL) was transformed into chemically competent *E. coli* BL21(DE3) according to the general procedure. A colony was used to inoculate 25 mL LB_{Amp} and bacterial culture was incubated at 37°C overnight, 250 rpm. pET-22b(+)_*pgmB*-His_W24F was isolated using the general procedure. The isolated plasmid was digested with the restriction enzymes BglI and BstEII using the same volumes stated above. The digestion mixture was incubated at 37°C for 1 h and the digestion products were analyzed by agarose gel electrophoresis.

5.4.2 Overexpression and purification of W24F 5FWβPGM-His

W24F 5FWβPGM-His was overexpressed using the same procedure as for ^{15}N-5FWβPGM using 5-fluoro-D/L-tryptophan. Protein overexpression was confirmed via SDS-PAGE analysis through the comparison of culture samples before and after the addition of IPTG. The cell pellets were lysed according to the general procedure. The cell lysate was loaded onto a HiTrap 5 mL Chelating HP NTA-Ni^{2+} affinity column for purification by FPLC at 4°C. Protein was eluted using the same method as for ^{15}N-5FWβPGM. The fractions containing pure βPGM were pooled and concentrated to 2.5 mL by ultrafiltration (5 000 x g at 4°C in Amicon Ultra-15 (EMD Millipore) 10 000 MWCO centrifugal filters). The concentrated protein was desalted using a PD-10 desalting column and eluted with 50 mM HEPES pH 7.2. Protein concentrations were

determined using spectrophotometric analysis (ε_{280} = 19 940 M^{-1} cm^{-1}), providing 18.5 mg/L of W24F 5FWβPGM. The extinction coefficient was not altered to account for mutation.

5.5 Enzyme NMR Methods

All 1D ^{19}F NMR spectra were recorded at 5°C with a *zgflqn* pulse program and acquired over 3000-6000 transients with a sweep width of 160 ppm on a Bruker Avance 500 MHz spectrometer equipped with a 5 mm Smart probe, operating at 470 MHz for fluorine. 5FWβPGM NMR samples were prepared with 0.5 mM 5FWβPGM, 1 mM dithiothreitol (DTT), 5 mM $MgCl_2$, and 10% D_2O in 50 mM HEPES pH 7.2. 5FWβPGM MgF_3-TSA complexes were prepared with 1 mM unlabeled or 5FWβPGM, 1 mM DTT, 5 mM $MgCl_2$, 10 mM NH_4F, 5 mM substrate and 10% D_2O in 50 mM HEPES pH 7.2 unless otherwise stated. 5FWβPGM AlF_4-TSA complexes were prepared as previous with the addition of 1 mM $AlCl_3$. All ^{19}F NMR were referenced with NH_4F (-119.5 ppm). 2D ^{1}H-^{15}N HSQC spectra were recorded at 27°C with a *hsqcetgpsi* pulse program and acquired over 128 scans. 1 mM DSS was used to reference ^{1}H NMR shifts. Samples contained 500 μM 5FW or unlabeled ^{15}N βPGM, 5 mM $MgCl_2$ and 10% D_2O in 50 mM HEPES pH 7.2.

5.6 Protein LC-MS/MS Methods

Liquid chromatography-tandem mass spectrometry (LC-MS/MS) analysis of ^{19}F-labeled βPGM was performed for method A (5-fluoroindole incorporation) and method B (5-fluorotryptophan incorporation) βPGM. Gel bands from SDS-PAGE containing ^{19}F-βPGM were excised from the gel and rinsed with deionized water. Excised gel bands

were processed using Investigator ProGest automated system (Genomic Solutions). Samples were reduced using 100 uL of 10 mM dithiothreitol (DTT), alkylated with 100 uL of 55 mM iodoacetamide and finally digested with Lys-C. The peptides were extracted from the gel pieces by three 20 min incubations with a solution (30 μL) containing acetonitrile (50%) and formic acid (5%) in LC−MS-grade water with gentle agitation. The extracts were pooled and dried using a vacuum concentrator (Speed Vac Concentrator, SPD 111 V-230, Thermo Electron Corp.) and finally resuspended in LC−MS-grade water (15 μL) containing acetonitrile (3%) and formic acid (0.5%). LC-MS/MS was performed using a nano flow liquid chromatography system (Ultimate3000RSLCnanno, ThermoScientific) interfaced to a hybrid ion trap-orbitrap high resolution tandem mass spectrometer (VelosPro, ThermoScientific) operated in data-dependent acquisition (DDA) mode. 1 μl of each sample was injected onto a capillary column (50cm × 75um PicoTip/PicoFrit Self packed column with Jupiter C18 4u chromatographic media, Phenomenex) at a flow rate of 300 nl min−1. Samples electro-sprayed at 1.2 kV using a dynamic nanospray probe. Chromatographic separation was carried out using 90 min linear gradients (Mobile Phase A: 0.1% formic acid in MS-grade water, mobile phase B: 0.1% formic acid in MS-grade acetonitrile,) from 3% B to 35% B over 60 min, then increasing to 95% B over 5 min. MS/MS spectra were acquired using both collision induced dissociation (CID) and higher-energy collisional dissociation (HCD) for the top 15 peaks in the survey 30 000 resolution MS scan. The raw files were acquired (Xcalibur, ThermoFisher) and exported to Proteome Discoverer 2.0 (ThermoFisher) software for peptide and protein identification using SequestHT search algorithm. Extracted ion chromatographs (XICs) were obtained using XCalibur software

(ThemoFisher) by screening for specific peptide masses using 50 ppm extraction windows. The intensity of the XIC of peptide fragments containing W24 and 5FW24 (AVLFDLDGVITDTAEYHFRA**W**K) were quantitatively compared, as well as the peptide fragments containing W216 and 5FW216 (EV**W**LQK).

5.7 βPGM Kinetic Assay Methods

Kinetic data of βPGM were obtained using a SpectraMax Plus UV/vis spectrophotometer. All assays were carried out in 100 L total volumes at 25°C in 50 mM HEPES pH 7.2. The turnover of βG1P to G6P was monitored over a 10 min period through a coupled reaction to glucose 6-phosphate dehydrogenase (G6PDH) (*Leuconostoc mesenteroides*). The release of NADPH (ε_{340} = 6.22 $mM^{-1}cm^{-1}$) by G6PDH allowed for the measurement of reaction rates. Kinetic assays for unlabeled βPGM and 5FWβPGM contained 2 mM $MgCl_2$, 0.5 mM $NADP^+$, 5 U/mL G6PDH, 150 mM α-fructose 1,6-bisphosphate, 50 nM unlabeled βPGM or 150 nM 5FWβPGM, and 0 – 200 μM βG1P unless otherwise stated. Reactions were initiated with the addition of substrate and steady state rates were obtained from the linear portions of time vs. A_{340} plots. Using GraFit 5.0.4, a Michaelis-Menten curve was fit to the data according to the following equation:

$$v = \frac{V_{max} \cdot [S]}{K_m + [S]}$$

where v represents the steady state rate of reaction, V_{max} is the maximum rate the enzyme can achieve, K_m is the substrate concentration needed to reach ½ V_{max} and [S] is the

substrate concentration. k_{cat} values were calculated from the above equation. Calculated errors are a result of standard errors.

Specific activity of each enzyme was measured using similar conditions and was calculated according to the following equation:

$$specific\ activity = \left(0.001 \times \frac{(\Delta A_{340}/t)}{\varepsilon_{340}} \times v_T\right) \times \left(\frac{1}{c} \times 1000\right) \times \frac{1}{v_E \cdot d}$$

A_{340} represents the absorbance recorded at 340 nm, ε_{340} is the extinction coefficient of NADPH at 340 nm ($mM^{-1}cm^{-1}$), t is the time elapsed over the change in absorbance (min), v_T is the total assay volume (μL), c is the enzyme concentration (mg/mL), v_E is the amount of enzyme added to the reaction (μL), and d is the dilution factor.

5.8 βPGM Inhibition Assay Methods

Evaluation of inhibitors were performed using a SpectraMax Plus UV/vis spectrophotometer. All assays were carried out in 100 μL total volumes at 25°C in 50 mM HEPES pH 7.2. The turnover of βG1P to G6P was monitored through a coupled reaction to glucose 6-phosphate dehydrogenase (G6PDH). The release of NADPH (ε_{340} = 6.22 $mM^{-1}cm^{-1}$) by G6PDH allowed for the measurement of reaction rates. IC_{50} assays contained 2 mM $MgCl_2$, 0.5 mM $NADP^+$, 5 U/mL G6PDH, 150 mM α-fructose 1,6-bisphosphate, 10 μM βG1P, 50 nM unlabeled or 5FWβPGM and 0 – 10 mM inhibitor. Reactions were initiated by addition of βG1P and were monitored over a period of 20 min. The linear portions of A_{340} over time progress curves were plotted on a relative rate

vs. inhibitor concentration plot using GraFit 5.0.4. A logarithmic curve was fitted to the data points using the following equation:

$$y = \frac{Range}{1 + \left(\frac{x}{IC_{50}}\right)^{s}} + Background$$

where y is the relative rate of reaction, x is the inhibitor concentration, range is the fitted uninhibited value minus the background, s is the slope factor, and the background is the minimum value multiplied by 0.95.

The inhibitor binding constant (K_i) was measured using similar conditions. Assays containing 2 mM $MgCl_2$, 0.5 mM $NADP^+$, 5 U/mL G6PDH, 150 mM α-fructose 1,6-bisphosphate, 50 nM unlabeled or 5FWβPGM, and 0 – 200 μM βG1P were evaluated for different inhibitor concentrations (0 – 50 μM). The rate of reaction from the linear portions of A_{340} over time progress curves were plotted and K_i values were determined from the following competitive inhibition equation:

$$v_i = \frac{v_{max}[S]}{K_s\left(1 + \frac{[I]}{K_I}\right) + [S]}$$

5.9 Buffers and Media

LB Media

10 g/L tryptone

5 g/L yeast extract

10 g/L NaCl

pH 7.5

LB-Agar Media

10 g/L tryptone

5 g/L yeast extract

10 g/L NaCl

15 g/L agar

pH 7.5

25 mM Imidazole buffer

300mM NaCl

20mM Tris•HCl,

25 mM imidazole; pH= 8.0

250 mM Imidazole buffer

300 mM NaCl

20 mM Tris•HCl,

250 mM imidazole; pH= 8.0

TAE buffer

40 mM Tris-acetate

1 mM EDTA, pH 8.2

2X SDS-PAGE loading dye

0.1 mL/mL Tris-HCl pH 6.8

0.3 mL/mL glycerol

0.15 mL/mL β-mercaptoethanol

0.018 g/mL bromophenol blue

100 mL ddH_2O

10X SDS-PAGE running buffer

10 g/L SDS

30 g/L Tris

144.1 g/L glycine

5.10 Equations

Equation 1 – Beer-Lambert Equation

$$\boldsymbol{A_{280} = \varepsilon_{280} \times c \times l}$$

A_{280} = absorbance at 280 nm

ε_{280} = extinction coefficient at 280 nm

c = concentration

l = path length

5.11 Compound Preparation and Characterization Data

2,3,4,6-Tetra-*O*-benzyl-D-gluconolactone (1)

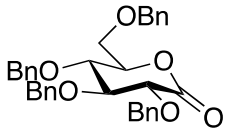

1

To a solution of 2,3,4,6-tetra-*O*-benzyl-D-glucopyranose (8.1 g, 15 mmol) in anhydrous dimethyl sulfoxide (38.7 mL), acetic anhydride (31.0 mL) was added and the mixture was stirred at room temperature for 12 h. After completion, the reaction mixture was diluted with water (30 mL) and the aqueous layer was extracted with diethyl ether (5 x 40 mL). The organic layers were combined and dried with Na_2SO_4, filtered, and concentrated under reduced pressure. Purification was performed by silica chromatography (4:1 *n*-hexane/ ethyl acetate) to obtain pure **1** as a colourless oil (6.95 g, 12.9 mmol) in 86%

yield. ^{1}H NMR (500 MHz, $CDCl_3$) δ = 7.24-7.46 (m, 20H, 4 Ph), 5.06 (d, *J* = 11.5 Hz, 1H, CHPh), 4.79 (t, *J* = 11.5 Hz, 2H, 2 x CHPh), 4.62-4.72 (m, 3H, CH_2Ph), 4.52-4.60 (m, 3H, CH_2Ph and H-5), 4.20 (d, *J* = 6.6 Hz, 1H, H-2), 4.02 (t, *J* = 6.9 Hz, 1H, H-4), 4.00 (t, *J* = 6.7 Hz, 1H, H-3), 3.79 (dd, *J* = 2.4 Hz, 11.0 Hz, 1H, H-6a), 3.75 (dd, *J* = 3.4 Hz, 11.0 Hz, 1H, H-6b); ^{13}C NMR (125 MHz, $CDCl_3$) δ = 169.2 (C-1), 137.6, 137.5 (2C), 136.9 (4 x quaternary aromatic C), 127.8-128.4 (20 x aromatic CH), 80.9 (C-3), 78.1 (C-5), 77.4 (C-2), 76.0 (C-4), 73.8 (CH_2Ph), 73.7 (2 x CH_2Ph), 73.5 (CH_2Ph), 68.2 (C-6). Spectroscopic data was consistent with literature.[66]

2,3,4,6-Tetra-*O*-benzyl-C-(1'-dibenzylphosphonomethyl)-α-D-glucopyranoside (2)

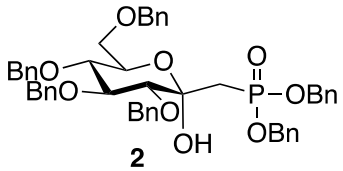

2

A stirred solution of dibenzyl methyl phosphonate (7.25 g, 26.2 mmol) in anhydrous THF (76 mL) was cooled to -78°C. *N*-butyllithium (10.49 mL, 26.2 mmol of a 2.5 M solution in hexanes) was slowly added and reaction was stirred for 30 min. A solution of lactone **1** (4.71 g, 87.4 mmol) in anhydrous THF (30 mL) was added to mixture, cold bath was removed and stirring continued for 2 h. The mixture was quenched by addition of saturated NH_4Cl (50 mL) and the organic layer was separated. Organic layer was washed with water and the combined aqueous layers were extracted with CH_2Cl_2 (3 x 50 mL). The combined organic layers were dried with anhydrous Na_2SO_4, filtered and

concentrated. Purification was performed by silica chromatography (2:1 *n*-hexane/ethyl acetate) to obtain pure **2** as a white solid (5.43 g, 6.67 mmol) in 76% yield. ^{1}H NMR (500 MHz, $CDCl_3$) δ = 7.23-7.42 (m, 30H, 6 Ph), 5.89 (s, 1H, anomeric OH), 5.15 (d, J = 7.8 Hz, 2H, CH_2Ph), 4.98-5.02 (m, 4H, CH_2Ph), 4.89-4.91 (m, 2H, CH_2Ph), 4.69 (d, J = 11.6 Hz, 1H, CHPh), 4.61 (d, J = 10.9 Hz, 1H, CHPh), 4.48 (d, J = 12.1 Hz, 1H, CHPh), 4.36 (d, J = 12.1 Hz, 1H, CHPh), 4.19 (t, J = 9.3 Hz, 1H, H-3) 4.18 (m, 1H H-5), 3.81 (dd, J = 3.7 Hz, 10.9, 1H, H-6a), 3.76 (t, J = 9.6 Hz, 1H, H-4), 3.66 (dd, J = 1.5 Hz, 10.9 Hz, 1H, H-6b), 3.34 (dd, J = 1.4 Hz, 9.5 Hz, 1H, H-2), 2.45 (dd, J = 15.3 Hz $^{2}J_{H\text{-}P}$ = 17.7 Hz, 1H, H-1'a), 1.88 (dd, J = 15.3 Hz, $^{2}J_{H\text{-}P}$ = 19, 1H, H-1'b); ^{13}C NMR (125 MHz, $CDCl_3$) δ = 138.8, 138.5, 138.1 (2C), 136.6 (d, $^{3}J_{C\text{-}P}$ = 6.8 Hz), 136.0 (d, $^{3}J_{C\text{-}P}$ = 6.7 Hz) (6 x quaternary aromatic C), 127.1-128.8 (30 x aromatic CH), 97.1 (d, $^{2}J_{C\text{-}P}$ = 8.1 Hz, C-1), 83.4 (d, $^{4}J_{C\text{-}P}$ = 3.7 Hz C-3), 82.9 (d, $^{3}J_{C\text{-}P}$ = 13.5 Hz, C-2), 78.6 (C-4), 75.8, 75.4, 75.1, 73.5 (4 x CH_2Ph), 71.4 (C-5), 69.0 (C-6), 68.3 (d, $^{2}J_{C\text{-}P}$ = 5.3 Hz, P-O-CH_2Ph), 67.1 (d, $^{2}J_{C\text{-}P}$ = 6.1 Hz, P-O-CH_2Ph), 34.0 (d, J = 136.3 Hz, C-1'); $^{31}P\{^{1}H\}$ NMR (202 MHz, $CDCl_3$) δ = 29.5 (s, 1P). LRMS (ESI, positive mode): found 833.5 $(M + NH_4)^+$. $C_{49}H_{51}O_9P$ requires $(M + NH_4)^+$ 833.3. Spectroscopic data was consistent with literature.[49]

Dibenzyl (*E/Z*)-*C*-(1-deoxy-2,3,4,6-tetra-*O*-benzyl-D-glucopyranosyl-2-ylidene) methanephosphonate (3)

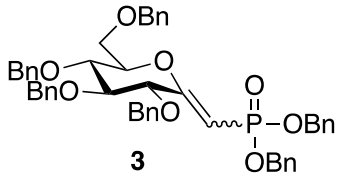

3

Pyridine (6.88 mL, 85.4 mmol) and trifluoroacetic anhydride (6.02 mL, 42.7 mmol) were successively added to a solution of lactol **2** (4.61 g, 5.66 mmol) in anhydrous THF (65 mL) at 0°C. The resulting solution was stirred and allowed to reach room temperature over 1.5 h. Solution was concentrated under reduced pressure and CH_2Cl_2 (50 mL) was added. Organic mixture was extracted with a saturated solution of $NaHCO_3$, dried with anhydrous $MgSO_4$, filtered and concentrated. Purification was performed by silica chromatography (2:1 *n*-hexane/ethyl acetate) to obtain pure **3** as a light yellow oil (2.45 g, 3.08 mmol) in 54% yield. ^{1}H NMR (500 MHz, $CDCl_3$) δ = 7.20-7.35 (m, 30H, 6 Ph), 5.21 (d, *J* = 12.7 Hz, 1H, H-1'), 5.06-5.10 (m, 4H, CH_2Ph), 4.75 (d, *J* = 11.6 Hz, 1H, CHPh), 4.73 (d, *J* = 11.6 Hz, 1H, CHPh), 4.69 (d, *J* = 11.4 Hz, 1H, CHPh), 4.67 (d, *J* = 11.4 Hz, 1H, CHPh), 4.59 (d, *J* = 11.7 Hz, 1H, CHPh), 4.57 (d, *J* = 11.4 Hz, 1H, CHPh), 4.56 (d, *J* = 12.0 Hz, 1H, CHPh), 4.47 (d, *J* = 12.0 Hz, 1H, CHPh), 4.02 (dt, *J* = 2.7 Hz, 9.9 Hz,1H, H-5), 3.97 (d, *J* = 6.3 Hz, 1H, H-2), 3.89 (dd, *J* = 6.8 Hz, 9.9 Hz, 1H, H-4), 3.79 (t, *J* = 6.3 Hz, 1H, H-3), 3.70 (m, 2H, H-6a and H-6b); ^{13}C NMR (125 MHz, $CDCl_3$) δ = 165.9 (C-1), 138.2, 138.1, 138.01, 137.34, 137.01 (d, $^3J_{C\text{-}P}$ = 6.8 Hz), 137.90 (d, $^3J_{C\text{-}P}$ = 6.3 Hz) (6 x quaternary aromatic C), 128.7-127.8 (30 x aromatic CH), 94.4 (d, $^1J_{C\text{-}P}$ = 191.4 Hz, C-1'), 83.5 (C-3), 78.8 (C-2), 78.7 (C-5), 77.1 (C-4), 74.2, 74.1, 73.7, 72.9 (4 x

CH_2Ph), 68.3 (C-6), 67.4 (d, $^2J_{C\text{-}P}$ = 5.1 Hz, P-O-CH_2Ph), 67.1(d, $^2J_{C\text{-}P}$ = 5.1 Hz, P-O-CH_2Ph); $^{31}P\{^1H\}$ NMR (202 MHz, $CDCl_3$) δ = 17.7 (s, 1P). LRMS (ESI, positive mode): found 815.2 $(M + NH_4)^+$. $C_{49}H_{49}O_8P$ requires $(M + NH_4)^+$ 815.3. Spectroscopic data was consistent with literature.[49]

Ammonium *C*-(1-deoxy-β-D-glucopyranosyl) methane phosphonate (5)

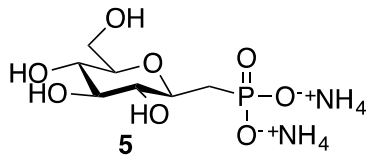

5

A stirring mixture of **3** (625 mg, 0.785 mmol) 10% palladium on carbon (174 mg, 1.64 mmol), ethyl acetate (26 mL) and methanol (26 mL) was degassed under vacuum and saturated with hydrogen gas under 1 atm pressure. Suspension was stirred at room temperature for 12 h, filtered through a pad of celite and concentrated to give the free phosphonic acid as a colorless oil. The oil was then dissolved in water (1 mL), and adjusted to pH 8 with 2 M NH_4OH, then lyophilized to obtain **5** as an off-white foam (199 mg, 0.772 mmol) in 98% yield. ^1H NMR (500 MHz, D_2O) δ = 3.92 (dd, *J* = 2.2 Hz, 12.4 Hz, 1H, H-6a), 3.67 (dd, *J* = 6.4 Hz, 12.4 Hz, 1H, H-6b), 3.61-3.65 (m, 1H, H-1), 3.52 (t, *J* = 9.0 Hz, 1H, H-3), 3.45 (td, *J* = 2.2 Hz, 6.4 Hz, 9.7 Hz, 1H, H-5), 3.37 (t, *J* = 9.4 Hz, 1H, H-4), 3.32 (t, *J* = 9.1 Hz, 1H, H-2), 1.87-2.01 (m, 2H, H-1'a, H-1'b); ^{13}C NMR (125 MHz, D_2O) δ = 79.4 (C-5), 77.4 (C-3), 76.5 (C-1), 75.4 (d, $^3J_{C\text{-}P}$ = 6.2 Hz, C-2), 70.0 (C-4), 61.2 (C-6), 33.6 (d, $^1J_{C\text{-}P}$ = 127.1 Hz, C-1'); $^{31}P\{^1H\}$ NMR (202 MHz, D_2O) δ = 20.4 (s, 1P). LRMS (ESI, negative mode): found 257.4 $(M - H)^-$. $C_7H_{15}O_8P$ (M

- H)$^-$ 257.0. requires Spectroscopic data was consistent with literature.[49]

Dibenzyl (*E/Z*)-*C*-(1-deoxy-2,3,4-tri-*O*-benzyl-D-glucopyranosyl-2-ylidene) methanephosphonate (6)

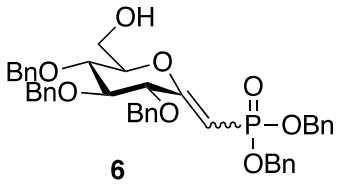

6

To a freshly fused (under vacuum) $ZnCl_2$ (0.726 g, 5.33 mmol), 1:2 AcOH-Ac_2O (2.84 mL) was added and stirred until the salt dissolved. The solution was then cooled to 0°C and a solution of **3** (0.283 g, 0.355 mmol) in 1:2 AcOH-Ac_2O (2.84 mL) was added drop wise. The reaction mixture was stirred at room temperature for 2.5 h and quenched by the addition of water (10 mL). CH_2Cl_2 (15 mL) was added and aqueous layer was separated. The organic layer was extracted with conc. $NaHCO_3$ (3 x 10 mL), water (10 mL), and brine (5 mL), dried with anhydrous Na_2SO_4, filtered and concentrated under reduced pressure. Crude material was dried further under vacuum overnight and directly used in next step. To the crude material in anhydrous MeOH (5.6 mL), potassium carbonate (14.7 mg) was added and mixture was stirred for 4 h. A concentrated solution of NH_4Cl (5 mL) was added and quenched mixture was extracted with EtOAc (5 x 10 mL). Organic layers were combined, washed with brine (5 mL), dried over $MgSO_4$, filtered and concentrated under reduced pressure. Purification was performed by silica chromatography (2:1 *n*-hexane/ethyl acetate) to obtain pure **6** as a light yellow oil (0.108 g, 0.153 mmol) in an overall yield of 46%. ^{1}H NMR (500 MHz, $CDCl_3$) δ = 7.30-7.43 (m, 25H, 5 Ph), 5.07-5.14 (m, 5H, CH_2Ph, H-1'), 4.80 (d, *J*=12.7 Hz, 1H, CHPh) 4.72 (d, *J* = 11.2 Hz, 1H,

CHPh) 4.61-4.67 (m, 3H, 3 x CHPh), 4.42 (d, J = 11.8 Hz, 1H, CHPh), 4.14 (m, 1H, H-5), 3.95-4.00 (m, 2H, H-6a, H-2), 3.88-3.92 (m, 2H, H-3, H-4), 3.80 (dd, J = 3.1 Hz, 12.5 Hz, 1H, H-6b); ^{13}C NMR (126 MHz, $CDCl_3$) δ = 165.9 (C-1), 138.1, 137.8, 137.1, 136.6 (d, $^3J_{C\text{-}P}$ = 6.5 Hz), 136.4 (d, $^3J_{C\text{-}P}$ = 6.3 Hz) (5 x quaternary aromatic C), 128.7-127.9 (25 x aromatic CH), 95.4 (d, $^1J_{C\text{-}P}$ = 189.9 Hz, C-1'), 84.0 (C-3), 79.2 (C-5), 78.6 (d, $^3J_{C\text{-}P}$ = 14.9 Hz, C-2), 76.5 (C-4), 74.5, 73.0, 71.6 (3 x CH_2Ph), 67.5 (d, $^2J_{C\text{-}P}$ = 5.0 Hz, P-O-CH_2Ph), 67.2 (d, $^2J_{C\text{-}P}$ = 5.0 Hz, P-O-CH_2Ph), 61.1 (C-6); $^{31}P\{^1H\}$ NMR (202 MHz, $CDCl_3$) δ = 18.4 (s, 1P). LRMS (ESI, positive mode): found 725.0 $(M + NH_4)^+$. $C_{42}H_{43}O_8P$ requires $(M + NH_4)^+$ 725.3.

Dibenzyl (*E/Z*)-*C*-(1-deoxy-2,3,4-tetra-*O*-benzyl-6-*O*-diphenylphosphate-D-glucopyranosyl-2-ylidene) methanephosphonate (9)

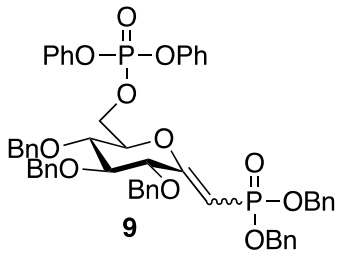

9

To a solution of **(6)** (0.108 g, 0.153 mmol) in anhydrous dichloromethane (1 mL), triethylamine (0.03 mL, 0.184 mmol), DMAP (cat. amount), and diphenyl chlorophosphate (0.04 mL, 0.184 mmol) were added and mixture was stirred at room temperature for 6 h. MeOH (3 mL) was added and stirred for 15 min before all solvents were evaporated under reduced pressure. The crude residue was purified by silica gel

column chromatography (6:4 *n*-hexane/acetone) to obtain pure **9** as an oil (0.129 g, 0.138 mmol) in 90% yield. ^{1}H NMR (500 MHz, $CDCl_3$) δ = 7.15-7.39 (m, 35H, 7 Ph), 5.25 (d, *J* = 12.5 Hz, H-1'), 5.09-5.12 (m, 4H, CH_2Ph), 4.74 (d, *J* = 11.3 Hz, 1H, CHPh), 4.68 (d, *J* = 11.5 Hz, 1H, CHPh), 4.67 (d, *J* = 11.1 Hz, 1H, CHPh), 4.64 (*J* = 11.3 Hz, 1H, CHPh), 4.56 (d, *J* = 11.5 Hz, 1H, CHPh), 4.49 (ddd, *J* = 1.9 Hz, 5.1 Hz, 6.9 Hz, 1H, H-6a), 4.48 (d, *J* = 11.1 Hz, CHPh), 4.38 (ddd, *J* = 3.3 Hz, 6.3 Hz, 9.6 Hz, 1H, H-6b), 4.04 (dt, *J* = 2.9 Hz, 6.5 Hz, 1H, H-5), 3.87 (d, *J* = 5.1 Hz 1H, H-2), 3.74-3.78 (m, 2H, H-3, H-4); ^{13}C NMR (125 MHz, $CDCl_3$) δ =164.9 (C-1),150.6 (d, $^{2}J_{C\text{-}P}$ = 7.4 Hz), 150.6 (d, $^{2}J_{C\text{-}P}$ = 7.4 Hz) (2 x quaternary P-O-Ph), 137.8, 137.7, 137.1, 136.9 (d, $^{3}J_{C\text{-}P}$ = 6.1 Hz), 136.8 (d, $^{3}J_{C\text{-}P}$ = 6.1 Hz) (5 x quaternary aromatic C), 125.6.0-130.0 (31 x aromatic CH), 120.3 (t, $^{3}J_{C\text{-}P}$ = 5.4 Hz, 4 x aromatic CH), 95.8 (d, $^{1}J_{C\text{-}P}$ = 191.3 Hz, C-1'), 83.2 (C-3), 78.4 (d, $^{3}J_{C\text{-}P}$ = 14.3 Hz, C-2), 77.1 (d, $^{3}J_{C\text{-}P}$ = 8.3 Hz, C-5), 76.4 (C-4), 74.2, 74.1, 72.9 (3 x CH_2Ph), 67.6 (d, $^{2}J_{C\text{-}P}$ = 5.4 Hz, P-O-CH_2Ph), 67.2 (d, $^{2}J_{C\text{-}P}$ = 5.4 Hz, P-O-CH_2Ph), 66.7 (d, $^{2}J_{C\text{-}P}$ = 5.2 Hz, C-6); $^{31}P\{^{1}H\}$ NMR (202 MHz, $CDCl_3$) δ = 16.9 (s, 1P), -12.0 (s, 1P). LRMS (ESI, positive mode): found 957.3 $(M + NH_4)^+$. $C_{54}H_{52}O_{11}P_2$ requires $(M + NH_4)^+$ 957.3.

1,2,3,4-Tetra-*O*-acetyl-α-D-glucopyranose (17)

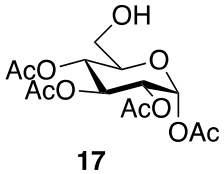

17

1,2,3,4,6-Penta-*O*-acetyl-α-D-glucopyranose (1.0 g) was dissolved in a mixture of *Candida rugosa* lipase (0.5 g) and 25 mM phosphate buffer pH 4 containing 20% of 1,4-dioxane (120 mL). The mixture was stirred (250 rpm) at 30°C and monitored by TLC

over 48 h. The suspension was filtered through Celite and washed with 1,4-dioxane and EtOAc, followed by an extraction with EtOAc. The crude product was concentrated under vacuum and the residue was purified by crystallization in diethyl ether/*n*-hexane (4:1) to give pure **17** as a white solid (0.813 g, 2.33 mmol) in 92% yield. ^{1}H NMR (500 MHz, $CDCl_3$) δ = 6.37 (d, *J* = 3.7 Hz, 1H, H-1), 5.54 (t, *J* = 10.0 Hz, 1H, H-3), 5.12 (t, *J* = 10.0 Hz, 1H, H-4), 5.09 (dd, *J* = 3.7 Hz, 10.2 Hz, 1H, H-2), 3.94 (dq, *J* = 2.4 Hz, 3.9 Hz, 6.3 Hz, 10.4 Hz, 1H, H-5), 3.74 (ddd, *J* = 2.2 Hz, 8.0 Hz, 10.2 Hz, 1H, H-6a), 3.60 (ddd, *J* = 4.2 Hz, 6.1 Hz, 10.4 Hz, 1H, H-6b), 2.21 (s, 3H, $C(O)CH_3$), 2.11 (s, 3H, $C(O)CH_3$), 2.07 (s, 3H, $C(O)CH_3$), 2.05 (s, 3H, $C(O)CH_3$); ^{13}C NMR (125 MHz, $CDCl_3$) δ =170.5, 170.4, 169.9, 168.9 (4 x C=O), 89.4 (C-1), 72.3 (C-5), 69.8 (C-3), 69.6 (C-2), 68.5 (C-4), 61.1 (C-6), 21.1, 20.9, 20.8, 20.6 (4 x C(O)**CH_3**). Spectroscopic data was consistent with the literature.[65]

1,2,3,4-Tetra-*O*-acetyl-α-D-glucopyranosyl-6-diphenylphosphate (18)

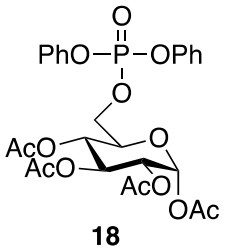

18

Diphenyl chlorophosphate (0.35 mL, 1.72 mmol), triethylamine (0.25 mL, 1.72 mmol), and a catalytic amount of 4-dimethylaminopyridine were added to a solution of **17** (0.500 g, 1.44 mmol) in anhydrous dichloromethane (9 mL). Reaction mixture was stirred at room temperature for 6 h. MeOH was added and after 15 min of stirring, solvents were evaporated under vacuum. Residue was purified by silica chromatography (1:1 *n*-hexane/

ethyl acetate) to afford pure **18** as a white solid (0.829 g, 1.43 mmol) in 98% yield. ^{1}H NMR (500 MHz, $CDCl_3$) δ = 7.41-7.23 (m, 10H, 2 Ph), 6.30 (d, *J* = 3.7 Hz, 1H, H-1), 5.46 (t, *J* = 9.8 Hz, 1H, H-3), 5.10 (t, *J* = 9.8 Hz, 1H, H-4), 5.01 (dd, *J* = 10.2 Hz, 3.7 Hz, 1H, H-2), 4.36 (ddd, *J* = 2.3 Hz, 6.8 Hz, 9.2 Hz 1H, H-6a), 4.26 (ddd, *J* = 4.7 Hz, 8.3 Hz, 11.7 Hz, 1H, H-6b), 4.17-4.21 (dt, *J* = 2.4 Hz, 10.3 Hz, 1H, H-5), 2.16 (s, 3H, C(O)CH_3), 2.06 (s, 6H, 2 x C(O)CH_3), 2.04 (s, 3H, C(O)CH_3); ^{13}C NMR (125 MHz, $CDCl_3$) δ = 170.5, 169.8, 169.3, 168.8 (4 x C=O) 150.0 (2 x quaternary aromatic C), 130.0, 125.7, 120.3 (10 x aromatic CH), 89.1 (C-1), 70.6 (C-5), 70.5 (C-3), 70.0 (C-2), 69.3 (C-4), 68.2 (C-6), 21.0, 20.9, 20.8, 20.6 (4 x C(O)**CH_3**); ^{31}P{^{1}H} NMR (202 MHz, $CDCl_3$) δ = -12.1 (s, 1P). Spectroscopic data was consistent with literature.[65]

1,2,3,4-Tetra-*O*-acetyl-α-D-glucopyranosyl-6-phosphate (19)

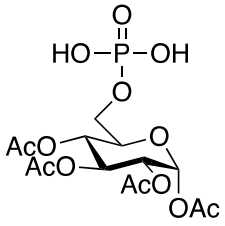

19

A solution of anhydrous methanol (8.2 mL) was added to a round-bottom flask containing **18** and platinum (IV) oxide (0.161 g, 0.71 mmol) and was stirred under hydrogen gas for 16 h at room temperature. The mixture was filtered through celite and concentrated to give **19** as a white solid (0.534 g, 1.25 mmol) in 87% yield. ^{1}H NMR (500 MHz, $CDCl_3$) δ = 6.34 (d, *J* = 3.7 Hz, 1H, H-1), 5.46 (t, *J* = 9.7 Hz, 1H, H-3), 5.16 (t, *J* = 9.7 Hz, 1H, H-4), 5.07 (dd, *J* = 3.9 Hz, 10.3 Hz, 1H, H-2), 4.21-4.23 (d, *J* = 9.3 Hz, 1H, H-5), 4.05-4.09 (m, 2H, H-6a & H-6b), 2.21 (s, 3H, C(O)CH_3), 2.07 (s, 3H, C(O)CH_3),

2.03 (s, 3H, C(O)CH_3), 2.02 (s, 3H, C(O)CH_3) ppm; ; ^{13}C NMR (125 MHz, $CDCl_3$) δ = 171.9, 171.4, 171.2, 170.7 (4 x C=O), 90.3 (C-1), 72.1 (d, $^3J_{C\text{-}P}$ = 8.1 Hz, C-5), 71.5 (C-3), 70.9 (C-2), 69.6 (C-4), 65.8 (d, $^2J_{C\text{-}P}$ = 4.6 Hz, C-6), 20.8, 20.7, 20.4 (4 x ``C(O)**CH_3**); ^{31}P{^{1}H} NMR (202 MHz, $CDCl_3$) δ = -0.19 (s, 1P). LRMS (ESI, negative mode): found 427.4 $(M - H)^-$. $C_{14}H_{21}O_{13}P$ requires $(M - H)^-$ 427.1. Spectroscopic data was consistent with literature.[65]

1,2,3,4-Tetra-*O*-acetyl-α-D-glucopyranosyl 6-[Tri-*n*-butylammonium phosphofluoridate] (20)

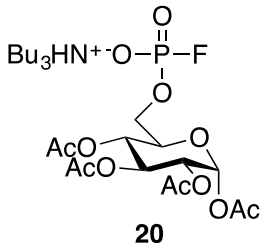

20

19 (0.432 g, 1.00 mmol) was converted into a tributylamine salt by treatment with excess *n*-tributylamine. The solvent was evaporated and the material was further dried under vacuum overnight. The gum was dissolved in DMF (3.5 mL) containing *n*-tributylamine (0.74 mL, 3 mmol) and dinitrofluorobenzene (0.316 g, 1.7 mmol) and stirred for 48 h while protected from moisture using a $CaCl_2$ guard tube. Water (5 mL) was added to quench the solution and mixture was extracted several times with diethyl ether (8 mL) until aqueous layer was no longer yellow in colour. Aqueous layer was concentrated under reduced pressure. Crude product was purified by silica chromatography (9:1 acetone/methanol) to obtain pure **20** as a yellow solid (0.423 g, 0.688 mmol) in 69%

yield. ^{1}H NMR (500 MHz, MeOD) δ = 6.37 (d, *J* = 3.3 Hz, 1H, H-1), 5.46 (t, *J* = 9.9 Hz, 1H, H-3), 5.16 (t, *J* = 9.9 Hz, 1H, H-4), 5.05 (dd, 3.6 Hz, 9.9 Hz 1H, H-2), 4.18-4.20 (d, *J* = 10.3 Hz, 1H, H-5) 4.01-4.10 (m, 2H, H-6a, H-6b), 3.14 (t, *J* = 8.3 Hz, 4H, 2 x $NH_3^+\mathbf{CH_2}$), 2.21 (s, 3H, $C(O)CH_3$), 2.08 (s, 3H, $C(O)CH_3$), 2.03 (s, 6H, 2 x $C(O)CH_3$), 1.70-1.76 (m, 4H, 2 x $NH_3^+CH_2\mathbf{CH_2}$), 1.43-1.50 (m, 4H, 2 x $NH_3^+CH_2\ CH_2\mathbf{CH_2}$), 1.03 (t, *J* = 7.4 Hz, 6H, 2 x $NH_3^+(CH_2)_3\mathbf{CH_3}$); ^{13}C NMR (125 MHz, MeOD) δ = 171.9, 171.5, 171.3, 170.7 (4 x C=O), 90.3 (C-1), 72.3 (d, $^{3}J_{C\text{-}P}$ = 8.3 Hz, C-5), 71.5 (C-3), 70.9 (C-2), 69.6 (C-4), 65.9 (d, $^{2}J_{C\text{-}P}$ = 4.8 Hz, C-6), 54.1 ($NH_3^+\mathbf{CH_2}$), 26.9 ($NH_3^+CH_2\mathbf{CH_2}$ and $NH_3^+CH_2\ CH_2\mathbf{CH_2}$), 21.1, 20.8, 20.7, 20.4 (4 x $C(O)\mathbf{CH_3}$), 14.1 ($NH_3^+(CH_2)_3\mathbf{CH_3}$); ^{31}P{^{1}H} NMR (202 MHz, MeOD) δ = -10.2 (d, *J* = 925 Hz, 1P); ^{19}F{^{1}H} NMR (470 MHz, MeOD) δ =-82.3 (d, *J* = 925 Hz, 1F). HRMS (ESI, negative mode): found 429.1 $(M - H)^-$. $C_{14}H_{20}FO_{12}P$ requires $(M - H)^-$ 429.1.

CHAPTER 6. CONCLUSIONS

^{19}F-Labeled β-phosphoglucomutase was successfully expressed with the incorporation of two 5-fluorotryptophan amino acid residues, 5FW24 and 5FW216. Two methods of incorporating fluorinated amino acid were evaluated and a quantitative analysis via LC-MS/MS confirmed that using 5-fluoro-D/L-tryptophan (method B), provided a greater incorporation of 5FW in βPGM. Site-directed mutagenesis revealed that 5FW216, located on the core domain, exists in two different conformations in its ground state which were not affected by ligand binding. On the other hand, 5FW24, located on the cap domain, exists in a different conformation upon ligand binding, providing a resonance with a different chemical shift. The chemical shift of the cap-closed 5FW24 resonance varied among the metal fluoride complexes with TS1 analogs, βG1CP and βG1CF$_S$P, TS2 analogs, G6P, and among complexation with βG16CP, emphasizing that 5FW24 is a sensitive probe to monitor ligand binding. 2-Deoxy-2-fluoro glucose and mannose phosphonate compounds did not form metal fluoride complexes, however the ^{19}F NMR spectra of β2FG1CP with 5FWβPGM revealed that β2FG1CP bound to 5FWβPGM in the absence of metal fluorides, which was further confirmed by inhibition studies. Kinetic analysis of 5FWβPGM revealed that the incorporation of two fluorotryptophan residues, 5FW24 and 5FW216, did not affect the kinetic ability of the enzyme compared to the wild-type βPGM. Compounds βG1CP, βG1CF$_S$P, and β2FG1CP, were confirmed as competitive inhibitors towards 5FWβPGM with respect to βG1P with K_i values of 4.67 ± 0.04 μM, 4.03 ± 0.03 μM, and 2.68 ± 0.04 μM respectively. βG16CP exhibited inhibition towards 5FWβPGM; however, compared to the other phosphonate compounds, a larger

IC_{50} value was observed (186 ± 73 μM). We hypothesized that the activator, αF16BP, may compete with βG16CP for the active site, resulting in its large IC_{50} value.

The synthesis of mechanism-based inactivators of 5FWβPGM were also explored. Several attempts were made to introduce a bromoacetyl and epoxide electrophilic handle at C-6 of βG1CP; however, all attempts were unsuccessful. Phosphofluoridate analogs of βG1CP and G6P were also attempted. Phosphofluoridation of βG1CP resulted in an inseparable mixture with the phosphofluoridate analog of βG1CP (**14**) and the 1,2-cyclic phosphonate analog (**15**), while deprotection of the acetyl-protected glucose 6-phosphofluoridate (**20**) resulted in decomposition of the phosphorus-fluorine bond. Therefore, alternate protocols must be explored to synthesize mechanism-based inactivators of 5FWβPGM.

REFERENCES

(1) Lad, C.; Williams, N. H.; Wolfenden, R. *Proc. Natl. Acad. Sci* **2003**, 100, 5607-5610.

(2) Allen, K. N.; Dunaway-Mariano, D. *Trends Biochem. Sci.* **2004**, *29*, 495-503.

(3) Burroughs, A. M.; Allen, K. N.; Dunaway-Mariano, D.; Aravind, L. *J. Mol. Biol.* **2006**, *361*, 1003-1034.

(4) Lahiri, S.; Zhang, G.; Dunaway-Mariano, D.; Allen, K. *Biochemistry* **2002**, *41*, 8351-8359.

(5) Zhang, G.; Dai, J.; Wang, L.; Dunaway-Mariano, D. *Biochemistry* **2005**, *44*, 9404-9416.

(6) Ramos, A.; Boels, I. C.; de Vos, W. M.; and Santos, H. *Appl. Environ. Microbiol.* **2001**, *67*, 33-41.

(7) Dai, J.; Finci, L.; Zhang, C.; Lahiri, S.; Zhang, G.; Peisach, E.; Allen, K. N.; Dunaway-Mariano, D. *Biochemistry* **2009**, *48*, 1984-1995.

(8) Frieden, C.; Hoeltzli, S. D.; Ban, J. G. *Methods Enzymol.* **2004**, *380*, 400-415.

(9) Sarker, M.; Orrell, K. E.; Xu, L.; Tremblay, M.; Bak, J. J.; Liu, X.; Rainey, J. K. *Biochemistry* **2016**, *55*, 3048-3059.

(10) Matei, E.; Gronenborn, A. M. *Angew. Chem. Int. Ed.* **2016**, *55*, 150-154.

(11) Gee, C. T.; Koleski, E. J.; Pomerantz, W. C. *Angew. Chem. Int. Ed.* **2015**, *54*, 3735-3739.

(12) Yang, F.; Yu, X.; Liu, C.; Qu, C. X.; Gong, Z.; Liu, H. D.; Li, F. H.; Wang, H. M.; He, D. F.; Yi, F. *Nat. Commun.* **2015**, *6*, 8202.

(13) Leung, E. W.; Yagi, H.; Harjani, J. R.; Mulcair, M. D.; Scanlon, M. J.; Baell, J. B.; Norton, R. S. *Chem. Biol. Drug Des.* **2014**, *84*, 616-625.

(14) Curtis-Maroma, R.; Doko, D.; Rowe, M. L.; Richards, K. L.; Williamson, R. A.; Howard, M. J. *Org. Biomol. Chem.* **2014**, *12*, 3808-3812.

(15) Mishra, N. K.; Urick, A. K.; Ember, S. W. J.; Schonbrunn, E.; Pomerantz, W. C. *ACS Chem. Biol.* **2014**, *9*, 2755-2760.

(16) Suarez, J.; Haapalainen, A.; Cahill, S. M.; Ho, M. C.; Yan, F. N.; Almo, S. C.; Schramm, V. L. *Chem. Biol.* **2013**, *20*, 212-222.

(17) Liu, J. J.; Horst, R.; Katritch, V.; Stevens, R.C.; Wüthrich, K. *Science* **2012**, *335*, 1106-1110.

(18) Kitevski-LeBlanc, J. L.; Prosser, R. S. *Prog. Nucl. Magn. Reson. Spectrosc.* **2012**, *62*, 1-33.

(19) Visser, N. V.; Westphal, A. H.; Nabuurs, S. M.; van Hoek, A.; van Mierlo, C. P. M.; Visser, A. J. W. G.; Broos, J.; van Amerongen, H. *FEBS Lett.* **2009**, *583*, 2785-2788.

(20) Baxter, N. J.; Blackburn, G. M.; Marston, J. P.; Hounslow, A. M.; Cliff, M. J.; Bermel, W.; Williams, N. H.; Hollfelder, F.; Wemmer, D. E.; Waltho, J. P. *J. Am. Chem. Soc.* **2008**, *130*, 3952-3958.

(21) Jin, Y.; Bhattasali, D.; Pellegrinia, E.; Forget, S.; Baxtera, N. J.; Cliff, M. J.; Bowler, M. W.; Jakeman, D. L.; Blackburn, M.; Waltho, J. P. *Prod. Nat. Acad. Sci* **2014**, *111*, 12384-12389.

(22) Baxter, N. J.; Hounslow, A. M.; Bowler, M. W.; Williams, N. H.; Blackburn, G. M.; Waltho, J. P. *J. Am. Chem. Soc.* **2009**, *131*, 16334-16335

(23) Cliff, M. J.; Bowler, M. W.; Varga, A.; Marston, J. P.; Szabo, J.; Hounslow, A. M.; Baxter, N. J.; Blackburn, G. M.; Vas, M.; Waltho, J. P. *J. Am. Chem. Soc.* **2010**, *132*, 6507-6516.

(24) Graham, D. L.; Lowe, P. N.; Grime, G. W.; Marsh, M.; Rittinger, K.; Smerdon, S. J.; Gamblin, S. J.; Eccleston, J. F. *Chem. Biol.* **2002**, *9*, 375-381.

(25) Wolfenden, R. *Chem. Rev.* **2006**, *106*, 3379-3396.

(26) Schramm, V. L. *Curr. Opin. Struct. Biol.* **2005**, *15*, 604-613.

(27) Clausen, J. D.; Bublitz, M.; Arnou, B.; Olesen, C.; Andersen, J. P.; Møller, J. V.; Nissen, P. *Structure* **2016**, *24*, 617-623.

(28) Johannes, M.; Oberbillig, T.; Hoffmann-Roder, A. *Org. Biomol. Chem.* **2011**, *9*, 5541-5546.

(29) Namanja-Magliano, H. A.; Stratton, C. F.; Schramm, V. L. *Chem. Biol.* **2016**, *11*, 1669-1676.

(30) Peck, A.; Sunden, F.; Andrews, L. D.; Pande, V. S.; Herschlag, D. *J. Mol. Biol.* **2016**, *428*, 2758-2768.

(31) Ray, W. J.; Puvathingal, J. M. *Biochemistry* **1990**, *29*, 2790-2801.

(32) Griffin, J. L.; Bowler, M. W.; Baxter, N. J.; Leigh, K. N.; Dannatt, H. R. W.; Hounslow, A. M.; Blackburn, G. M.; Webster, C. E.; Cliff, M. J.; Waltho, J. P. *Proc. Natl. Acad. Sci. U. S. A.* **2012**, *109*, 6910-6915.

(33) Baxter, N. J.; Olguin, L. F.; Golicnik, M.; Feng, G.; Hounslow, A. M.; Bermel, W.; Blackburn, G. M.; Hollfelder, F.; Waltho, J. P.; Williams, N. H. *Proc. Natl. Acad. Sci. U. S. A.* **2006**, *103*, 14732-14737.

(34) Lu, P.; Jarema, M.; Mosser, K.; Daniel, W. E. *Proc Natl Acad Sci U S A* **1976**, *73*, 3471-3475.

(35) Khan, F.; Kuprov, I.; CraggHore, P. J.; Jackson, S. E. *J. Am. Chem. Soc.* **2006**, *128*, 10729-10737.

(36) Kranz, J.; Lu, J.; Hall, K. *Protein Sci.* **1996**, *5*, 1567-1583.

(37) Campos-Olivas, R.; Aziz, R.; Helms, G. L.; Evans, J. N. S.; Gronenborn, A. M. *FEBS Lett.* **2002**, *517*, 55-60.

(38) Crowley, P. B.; Kyne, C.; Monteith, W. B. *Chem. Commun.* **2012**, *48*, 10681-10683.

(39) Ghosh, R.; and Jakeman, D.L.; *manuscript in preparation* **2016**.

(40) Zhu, J.S.; and Jakeman, D.L.; *manuscript in preparation* **2016**.

(41) Sorensen, M. D.; Kristensen, S. M.; Bjorn, S.; Noris, K.; Olsen, O.; Led, J. J. *J. Biol. NMR* **1996**, *8*, 391-403.

(42) Hansson, H.; Mattson, P. T.; Allard, P.; Haapaniemi, P.; Vihinen, M.; Smith, C. I. E.; Hard, T. *Biochemistry* **1998**, *37*, 2912-2924.

(43) Engel, R. *Chem. Rev.* **1977**, *77*, 349-367.

(44) K. Moonen, I. Laureyn and C. Stevens, *Chem. Rev*., **2004**, *104*, 6177-6216.

(45) L. Han, J. Hiratake, A. Kamiyama and K. Sakata, *Biochemistry*, **2007**, 46, 1432-1447.

(46) Forget, S. M.; Jee, A.; Smithen, D. A.; Jagdhane, R.; Anjum, S.; Beaton, S. A.; Palmer, D. R.; Syvitski, R. T.; Jakeman, D. L. *Org. Biomol. Chem.* **2015**, *13*, 866-875.

(47) Beaton, S. A.; Jiang, P. M.; Melong, J. C.; Loranger, M. W.; Mohamady, S.; Veinot, T. I.; Jakeman, D. L. *Org. Biomol. Chem.* **2013**, *11*, 5473-5480.

(48) Loranger, M. W.; Forget, S. M.; McCormick, N. E.; Syvitski, R. T.; Jakeman, D. L. *J. Org. Chem.* **2013**, *78*, 9822-9833.

(49) Forget, S. M.; Bhattasali, D.; Hart, V. C.; Cameron, T. S.; Syvitski, R. T.; Jakeman, D. L. *Chem. Sci.* **2012**, *3*, 1866-1878.

(50) Tremblay, L. W.; Zhang, G.; Dai, J.; Dunaway-Mariano, D.; Allen, K. N. *J. Am. Chem. Soc.* **2005**, *127*, 5298-5299.

(51) Caravano, A.; Vincent, S. P. *Eur. J. Org. Chem.* **2009**, *2009*, 1771-1780.

(52) Twibanire, J. K.; Grindley, T. B. *Org. Lett.* **2011**, *13*, 2988.

(53) Howard, S.; Withers, S. G. *J. Am. Chem. Soc.* **1998**, *120*, 10326-10331.

(54) Lu, W.; Navidpour, L.; Taylor, S. D. *Carbohydr. Res.* **2005**, *340*, 1213-1217.

(55) Tewari, N.; Tiwari, W. K.; Tripathi, R. P.; Chaturvedi, V.; Srivastava, A.; Srivastava, R.; Shukla, P. K.; Chaturvedi, A. K.; Gaikwad, A.; Sinha, S.; Srivastava, B. S. *Biorg. Med. Chem* **2004**, *14*, 329-332.

(56) Kumar, P.; Shustov, G.; Liang, H.; Khlebnikov, V.; Zheng, W.; Yang, X.; Cheeseman, C.; Wiebe, L. I. *J. Med. Chem.* **2012**, *55*, 6033-6046.

(57) Forget, S. M.; Jee, A.; Smithen, D. A.; Jagdhane, R.; Anjum, S.; Beaton, S. A.; Palmer, D. R.; Syvitski, R. T.; Jakeman, D. L. *Org. Biomol. Chem.* **2015**, *13*, 866-875.

(58) Noda, K.; Koyanagi, M.; Kamiya, C. *J. Food Sci.* **1994**, *59*, 585-587.

(59) Levine, A. E.; Walsh, K. A.; Fodor, E. J. B. *Dev. Biol.* **1978**, *63*, 299-306.

(60) Sugumaran, M.; Saul, S. J.; Ramesh, N. *Biochem. Biophys. Res. Commun.* **1985**, *132*, 1124-1129.

(61) Saul, S. J.; Sugumaran, M. *FEBS Lett.* **1986**, *208*, 113-116.

(62) Percival, M. D.; Withers, S. G. *J. Org. Chem.* **1992**, *57*, 811-817.

(63) O'Conner, J. V.; Nunez, H. A.; Barker, R. *Biochemistry* **1979**, *18*, 500-507.

(64) Martin, R. B. *Coord. Chem. Rev.* **1996**, *149*, 23-32.

(65) Rodriguez-Perez, T.; Lavandera, I.; Fernandez, S.; Shanghai, Y. S.; Ferrero, M.; Gotor, V. *Eur. J. Org. Chem.* **2007**, 2769-2778.

(66) Albright, J.; Goldman, L. *J. Am. Chem. Soc.* **1967**, *89*, 2416-2423.

APPENDIX 1. NMR SPECTRA

^{1}H NMR. 2,3,4,6-Tetra-*O*-benzyl-C-(1'-dibenzylphosphonomethyl)-α-D-glucopyranoside (2)

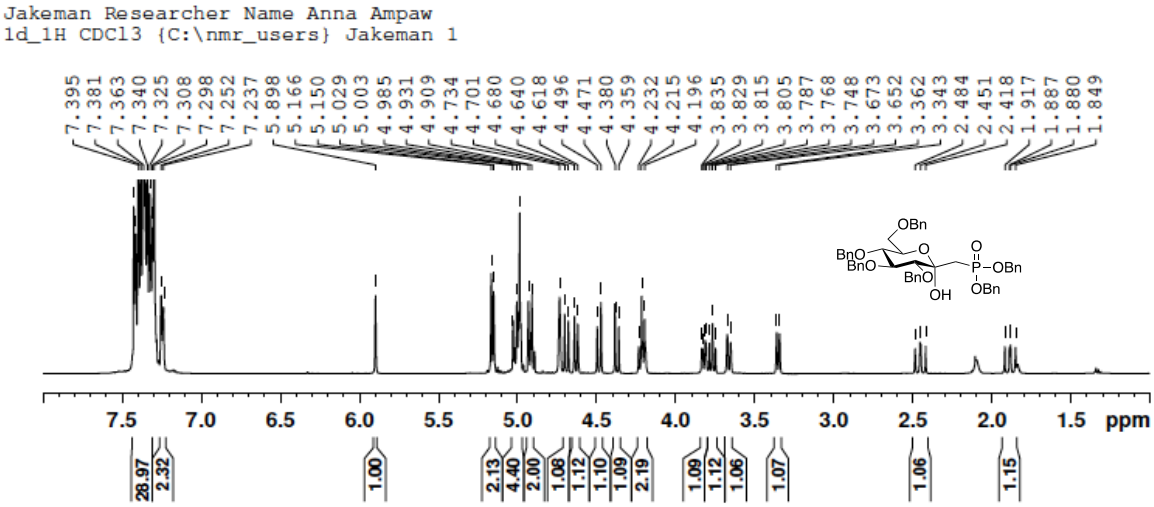

^{13}C NMR. 2,3,4,6-Tetra-*O*-benzyl-C-(1'-dibenzylphosphonomethyl)-α-D-glucopyranoside (2)

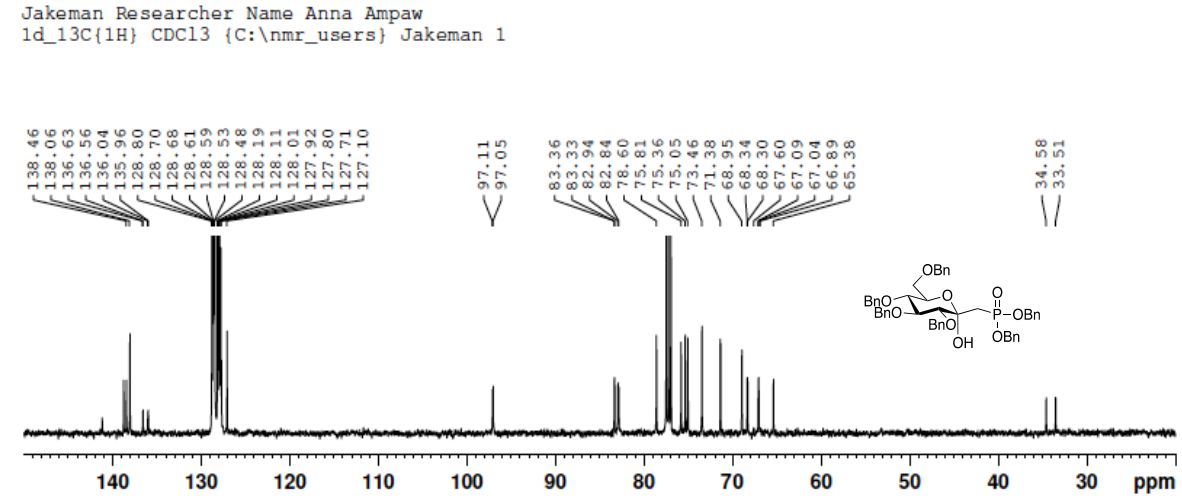

^{31}P NMR. 2,3,4,6-Tetra-*O*-benzyl-C-(1'-dibenzylphosphonomethyl)-α-D-glucopyranoside (2)

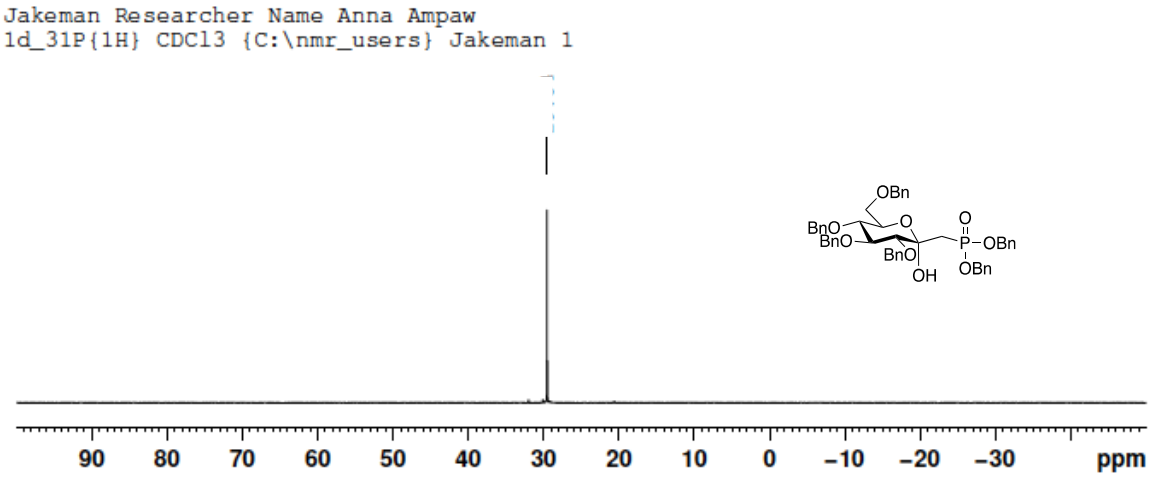

^{1}H NMR. Dibenzyl (*E/Z*)-*C*-(1-deoxy-2,3,4,6-tetra-*O*-benzyl-D-glucopyranosyl-2-ylidene) methanephosphonate (3)

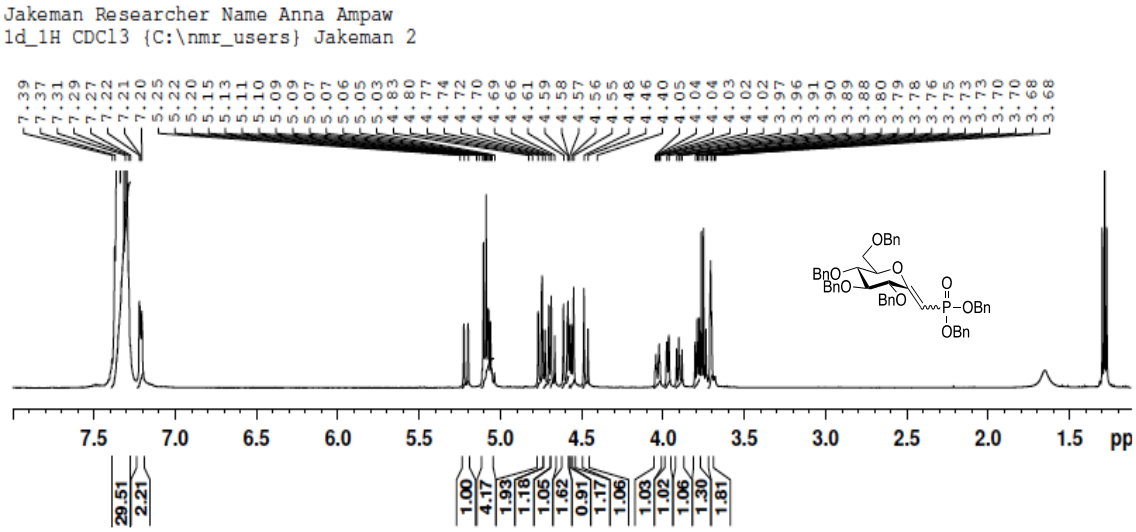

^{13}C NMR. Dibenzyl (*E/Z*)-*C*-(1-deoxy-2,3,4,6-tetra-*O*-benzyl-D-glucopyranosyl-2-ylidene) methanephosphonate (3)

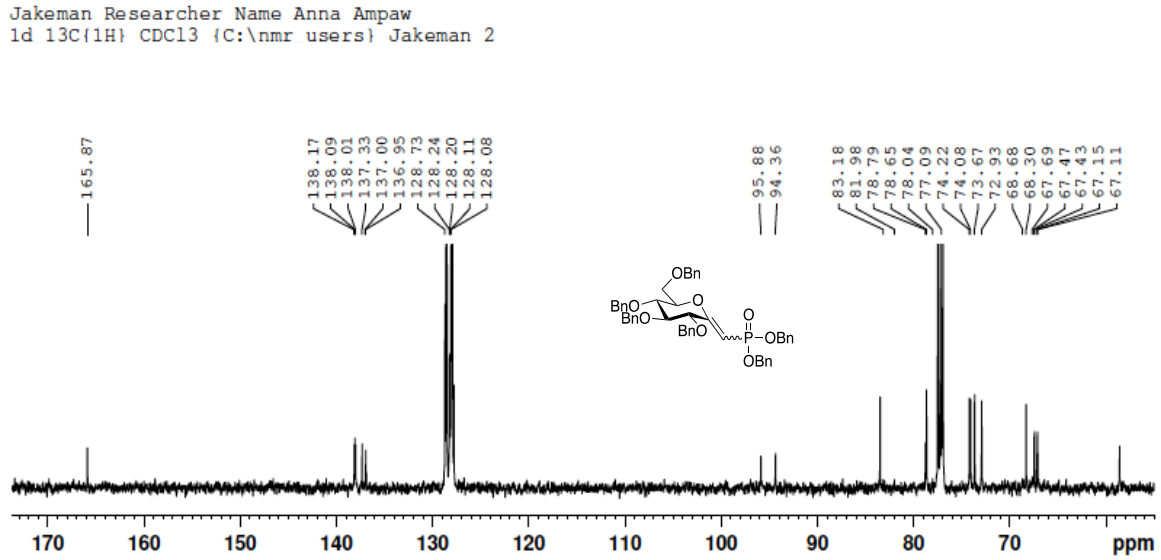

^{31}P NMR. Dibenzyl (*E/Z*)-*C*-(1-deoxy-2,3,4,6-tetra-*O*-benzyl-D-glucopyranosyl-2-ylidene) methanephosphonate (3)

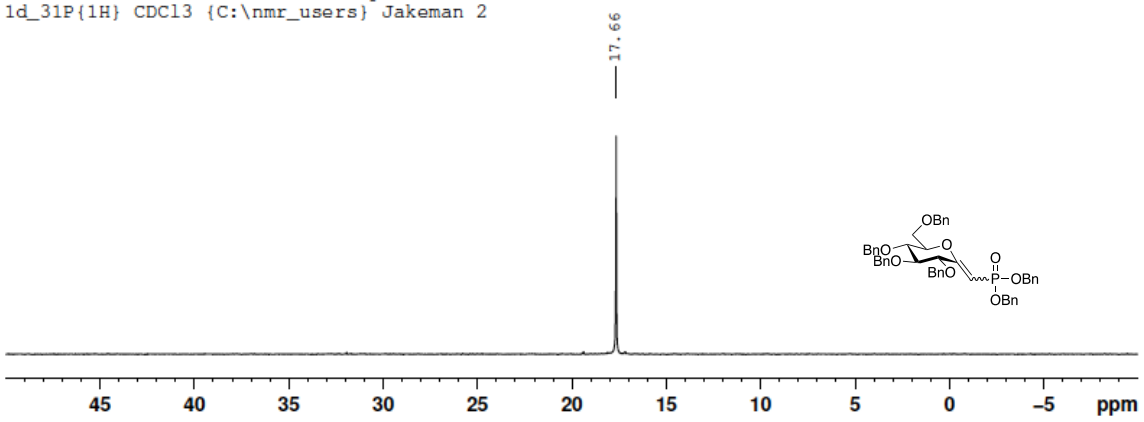

^{1}H NMR. Ammonium *C*-(1-deoxy-β-D-glucopyranosyl) methane phosphonate (5)

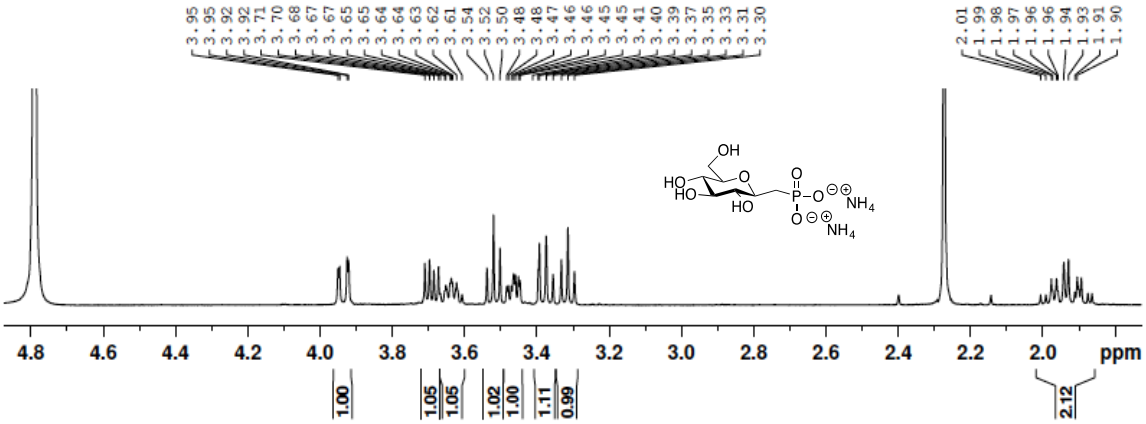

^{13}C NMR. Ammonium *C*-(1-deoxy-β-D-glucopyranosyl) methane phosphonate (5)

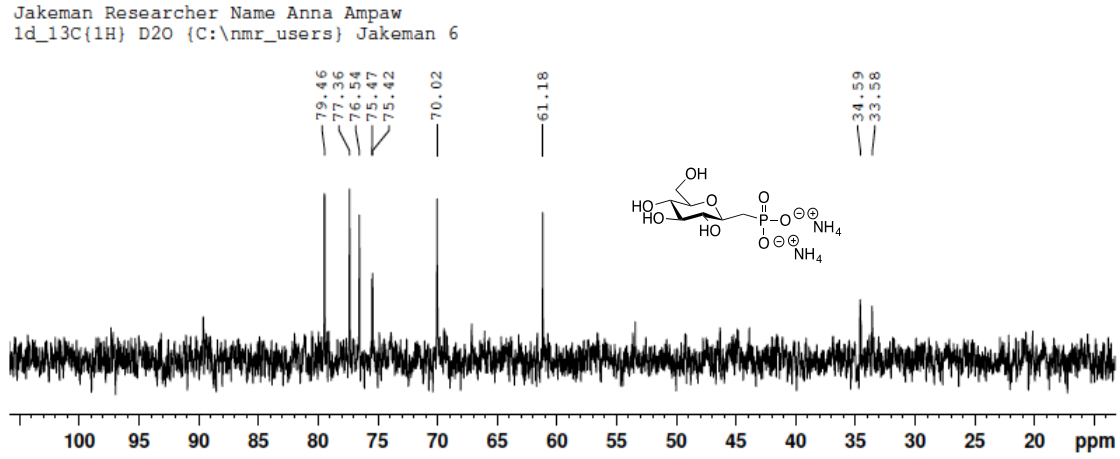

^{31}P NMR. Ammonium *C*-(1-deoxy-β-D-glucopyranosyl) methane phosphonate (5)

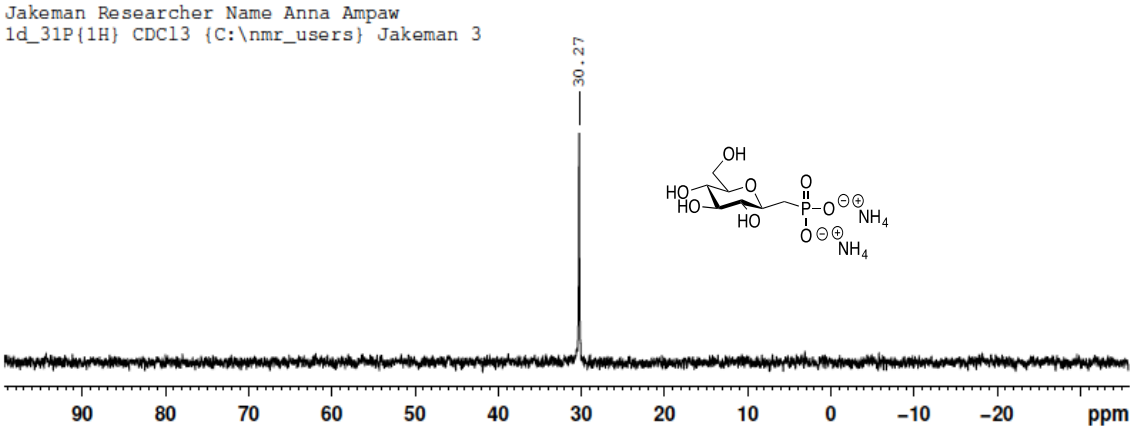

^{1}H NMR. Dibenzyl (*E/Z*)-*C*-(1-deoxy-2,3,4-tri-*O*-benzyl-D-glucopyranosyl-2-ylidene) methanephosphonate (6)

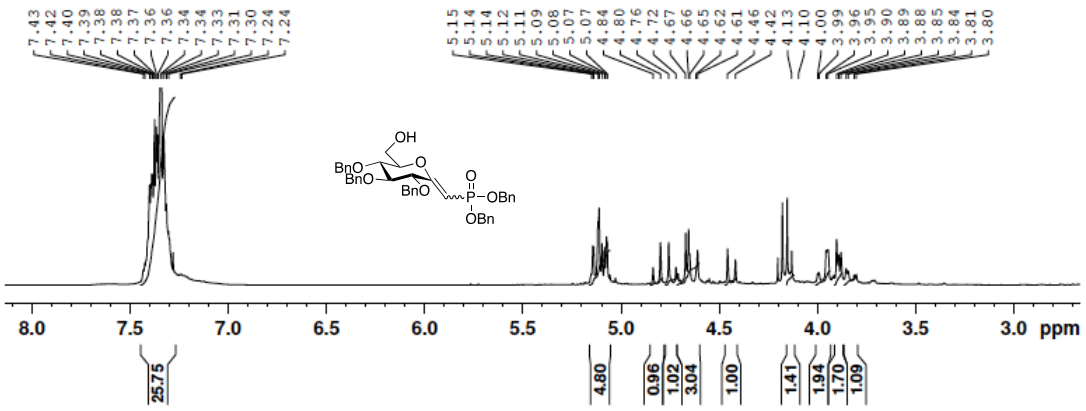

^{13}C NMR. Dibenzyl (*E*/*Z*)-*C*-(1-deoxy-2,3,4-tri-*O*-benzyl-D-glucopyranosyl-2-ylidene) methanephosphonate (6)

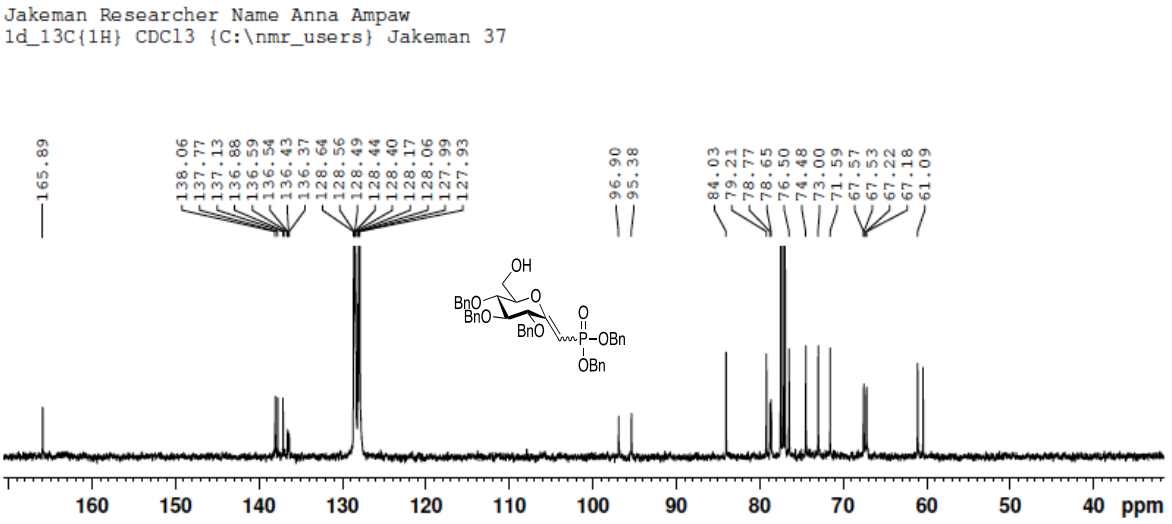

^{31}P NMR. Dibenzyl (*E*/*Z*)-*C*-(1-deoxy-2,3,4-tri-*O*-benzyl-D-glucopyranosyl-2-ylidene) methanephosphonate (6)

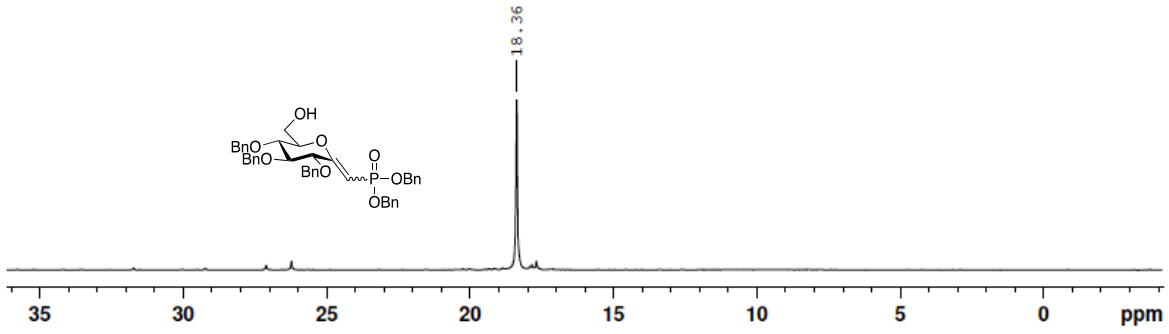

^{1}H NMR. Dibenzyl (*E/Z*)-*C*-(1-deoxy-2,3,4-tetra-*O*-benzyl-6-*O*-diphenylphosphate-D-glucopyranosyl-2-ylidene) methanephosphonate (9)

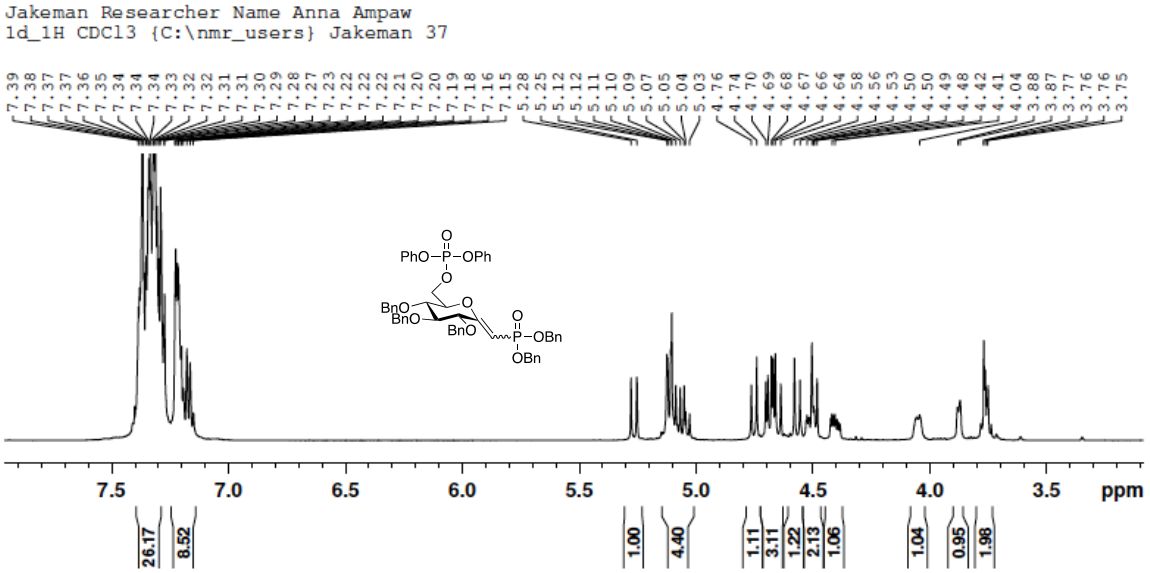

^{13}C NMR. Dibenzyl (*E/Z*)-*C*-(1-deoxy-2,3,4-tetra-*O*-benzyl-6-*O*-diphenylphosphate-D-glucopyranosyl-2-ylidene) methanephosphonate (9)

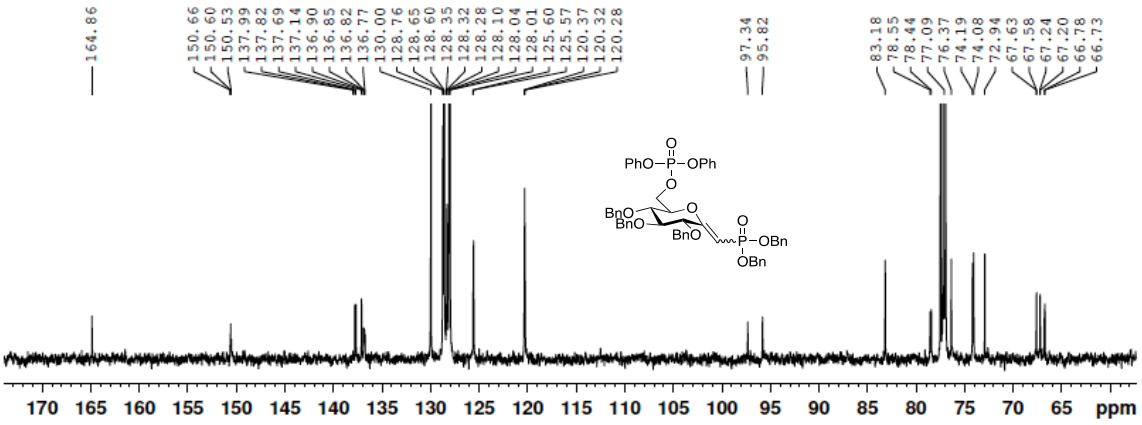

^{31}P NMR. Dibenzyl (*E/Z*)-*C*-(1-deoxy-2,3,4-tetra-*O*-benzyl-6-*O*-diphenylphosphate-D-glucopyranosyl-2-ylidene) methanephosphonate (9)

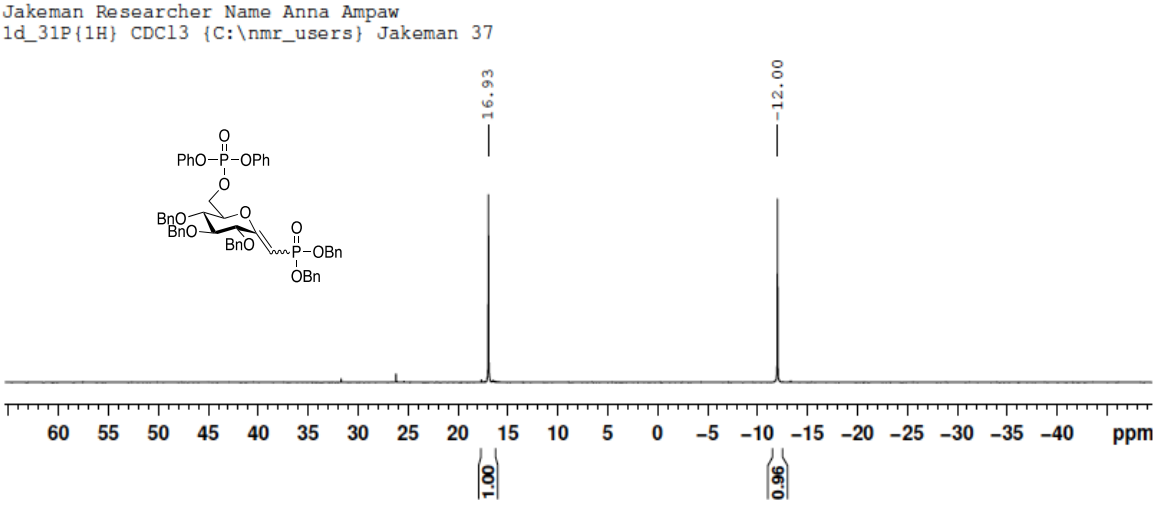

^{1}H NMR.1,2,3,4-Tetra-*O*-acetyl-α-D-glucopyranose (17)

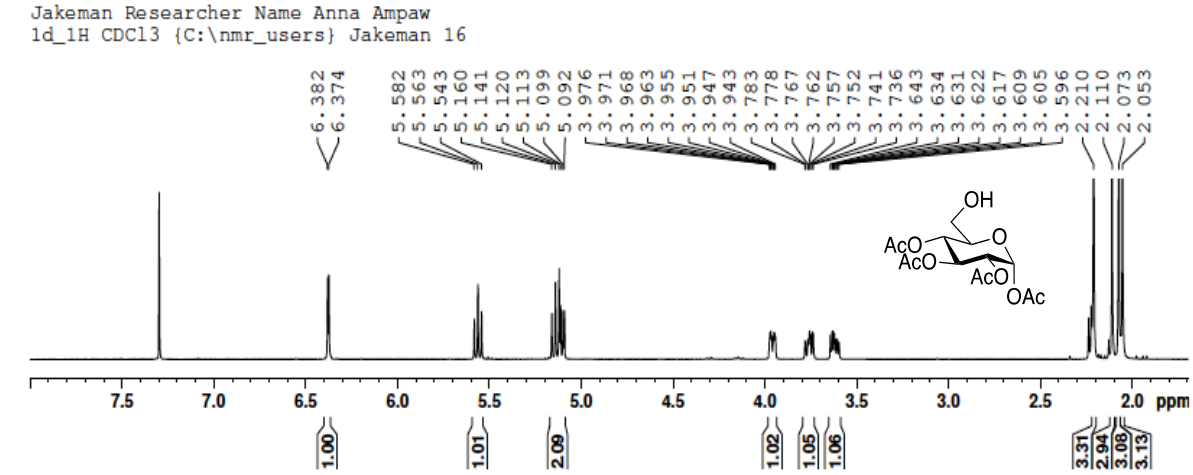

^{13}C NMR.1,2,3,4-Tetra-*O*-acetyl-α-D-glucopyranose (17)

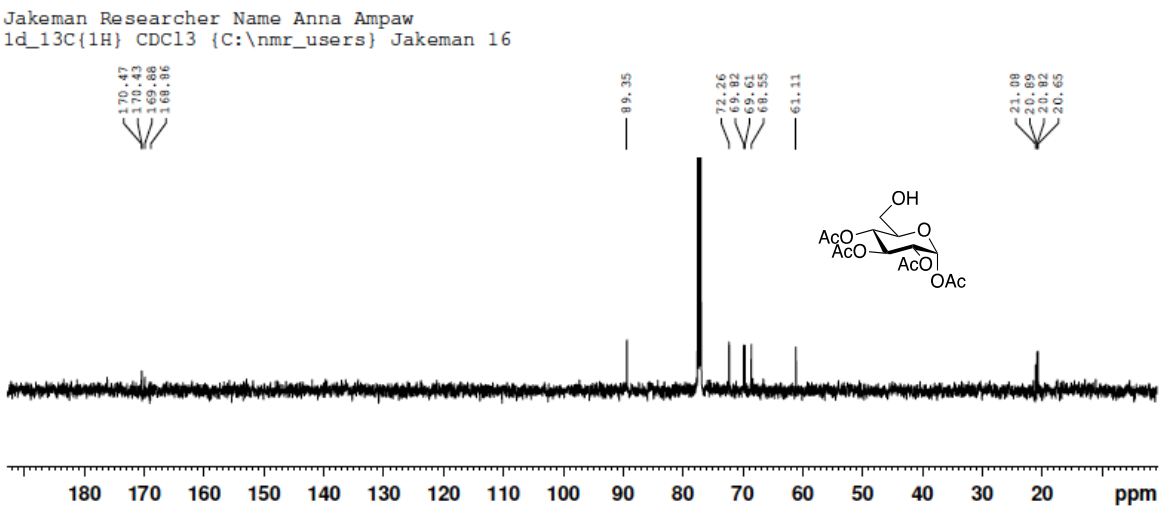

^{1}H NMR. 1,2,3,4-Tetra-*O*-acetyl-α-D-glucopyranosyl-6-diphenylphosphate (18)

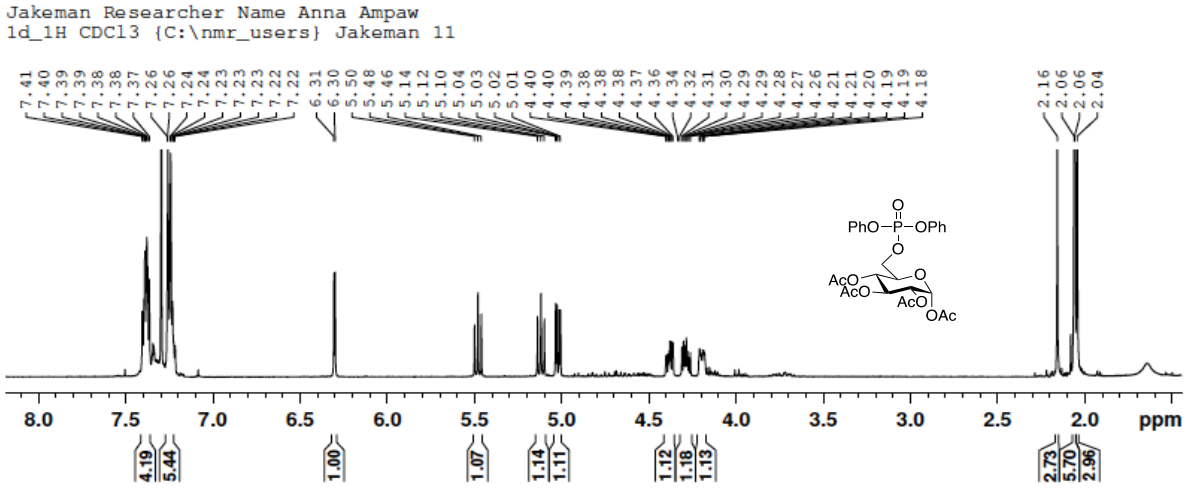

^{13}C NMR. 1,2,3,4-Tetra-*O*-acetyl-α-D-glucopyranosyl-6-diphenylphosphate (18)

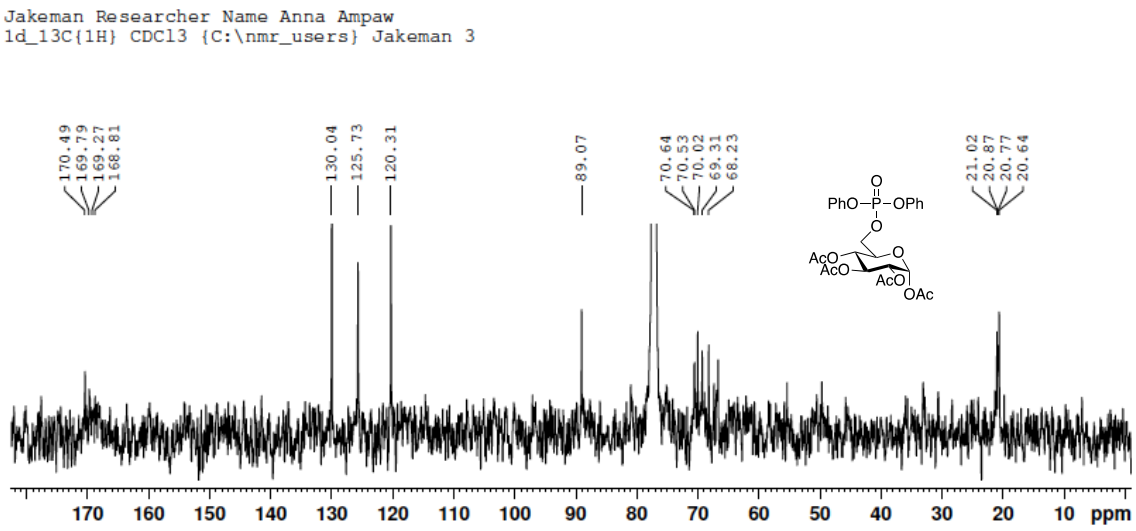

^{31}P NMR. 1,2,3,4-Tetra-*O*-acetyl-α-D-glucopyranosyl-6-diphenylphosphate (18)

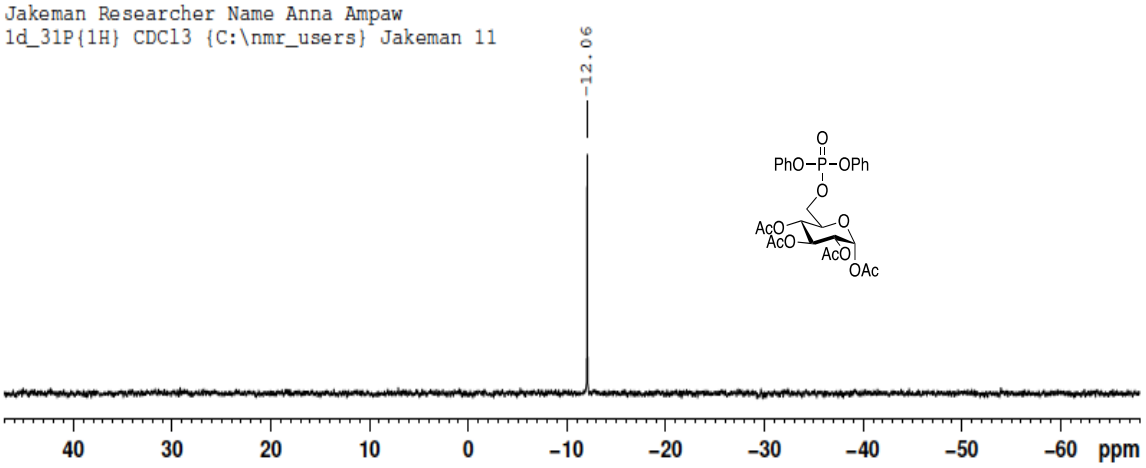

^{1}H NMR.1,2,3,4-Tetra-*O*-acetyl-α-D-glucopyranosyl-6-phosphate (19)

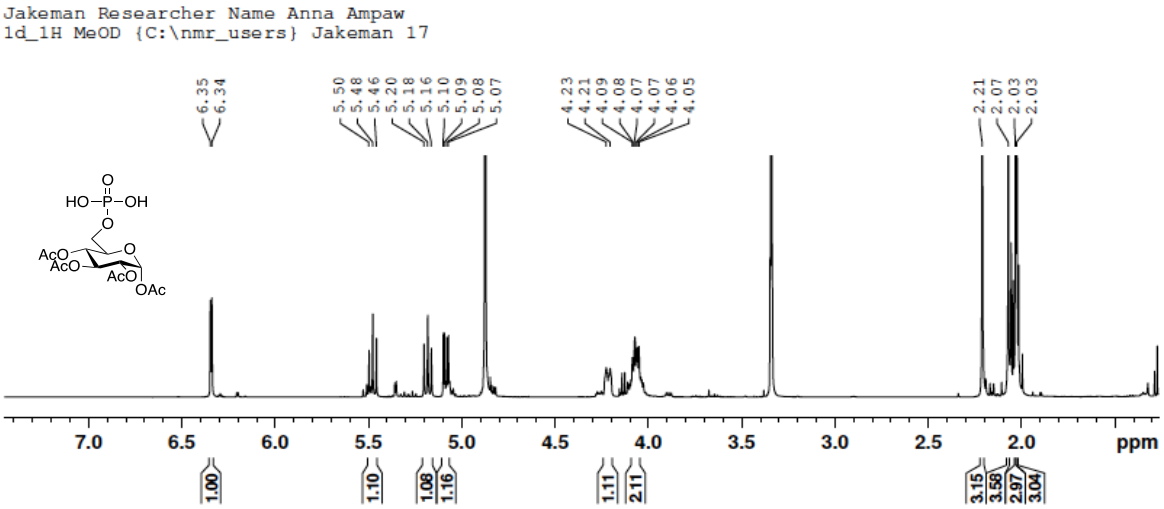

^{13}C NMR.1,2,3,4-Tetra-*O*-acetyl-α-D-glucopyranosyl-6-phosphate (19)

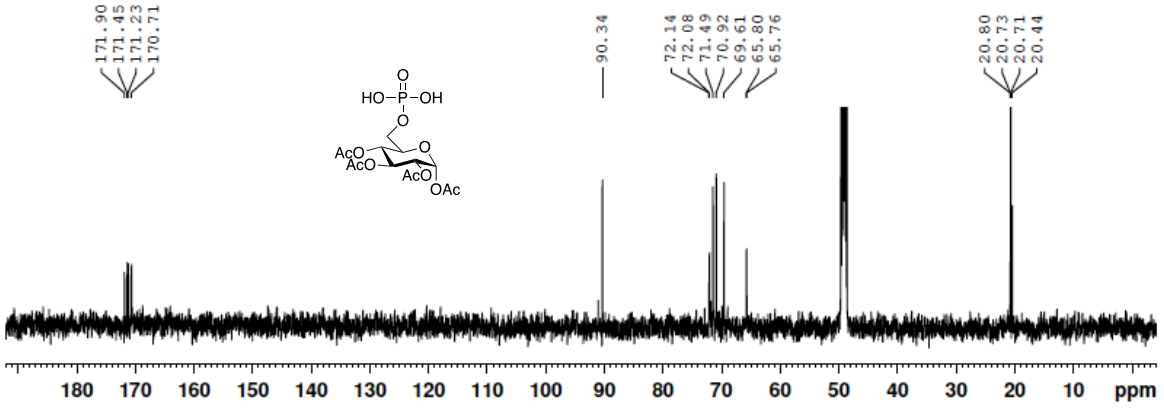

^{31}P NMR.1,2,3,4-Tetra-*O*-acetyl-α-D-glucopyranosyl-6-phosphate (19)

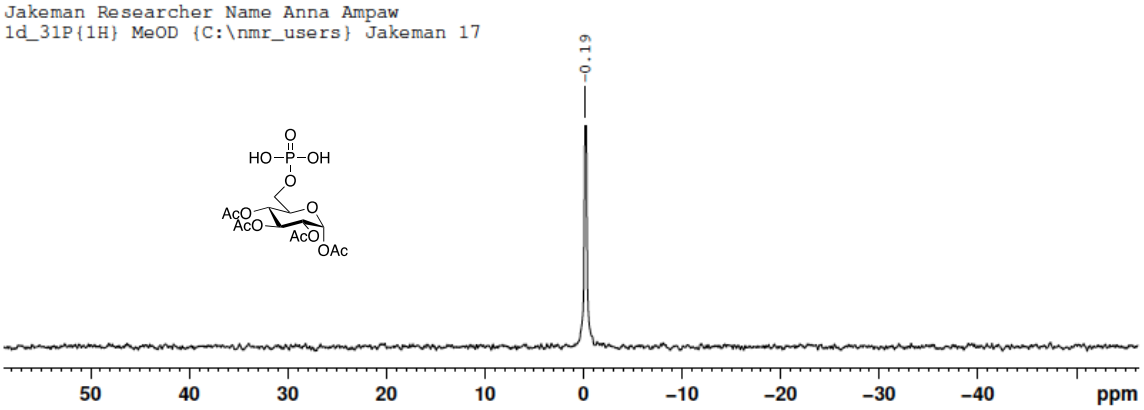

^{1}H NMR. 1,2,3,4-Tetra-*O*-acetyl-α-D-glucopyranosyl 6-[Tri-*n*-butylammonium phosphofluoridate] (20)

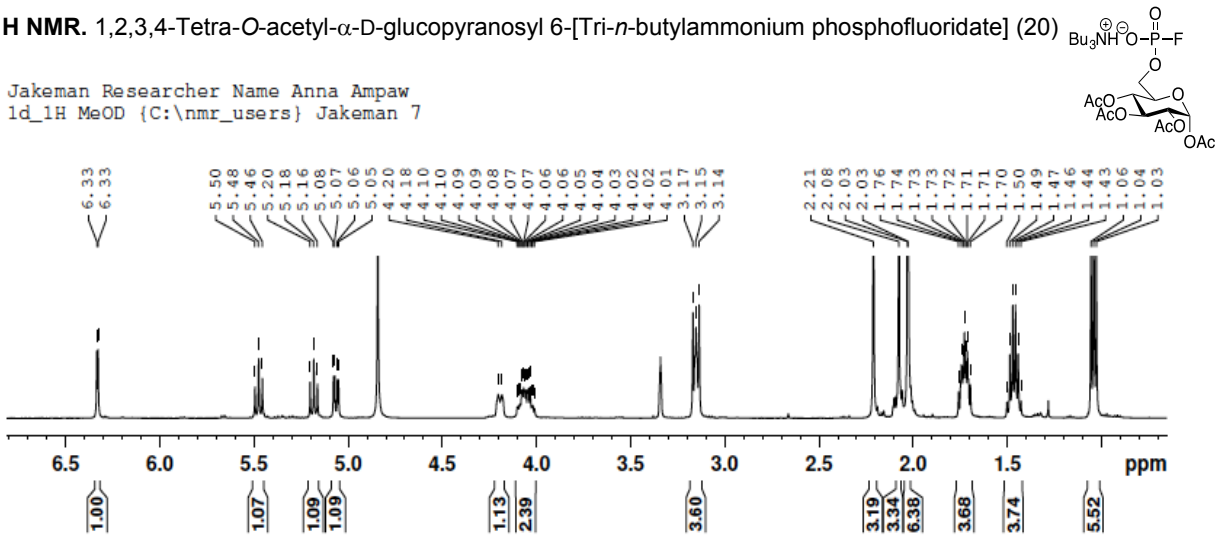

^{13}C NMR. 1,2,3,4-Tetra-*O*-acetyl-α-D-glucopyranosyl 6-[Tri-*n*-butylammonium phosphofluoridate] (20)

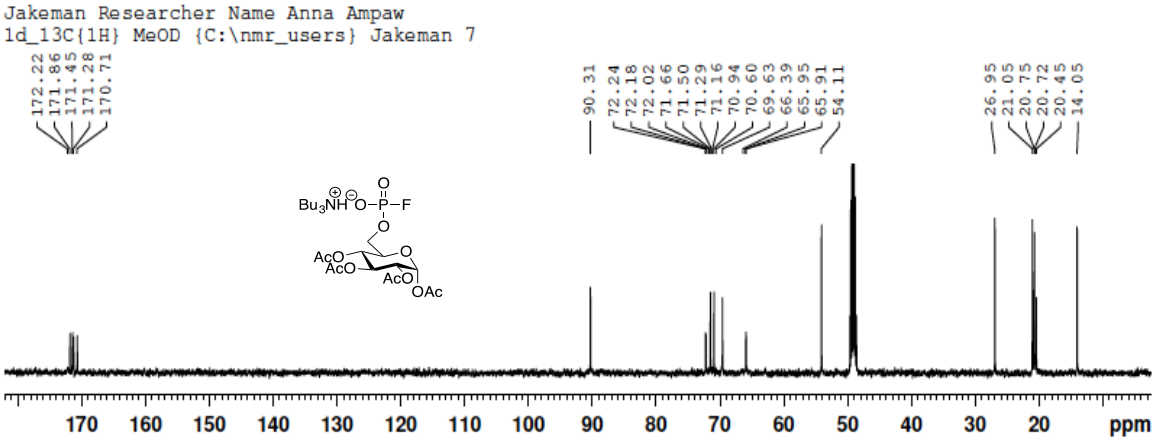

^{31}P NMR. 1,2,3,4-Tetra-*O*-acetyl-α-D-glucopyranosyl 6-[Tri-*n*-butylammonium phosphofluoridate] (20)

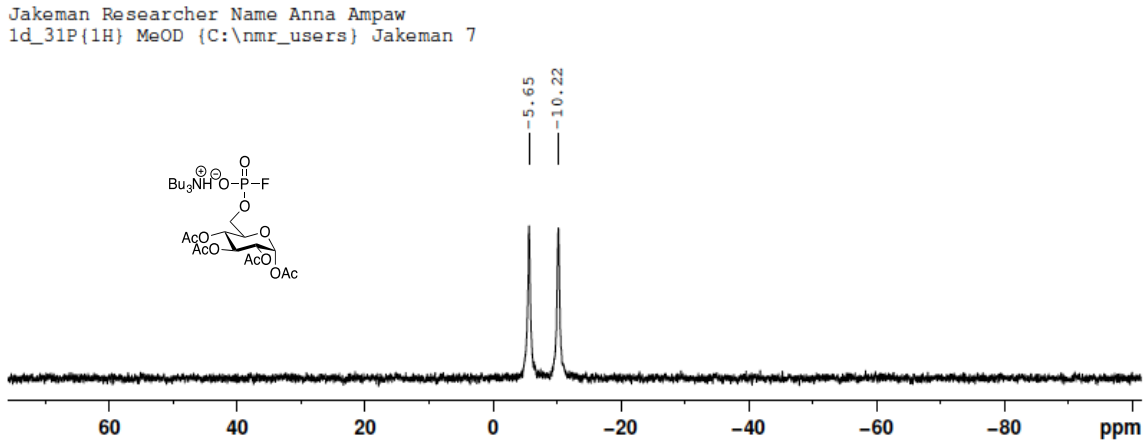

^{19}F NMR. 1,2,3,4-Tetra-*O*-acetyl-α-D-glucopyranosyl 6-[Tri-*n*-butylammonium phosphofluoridate] (20)

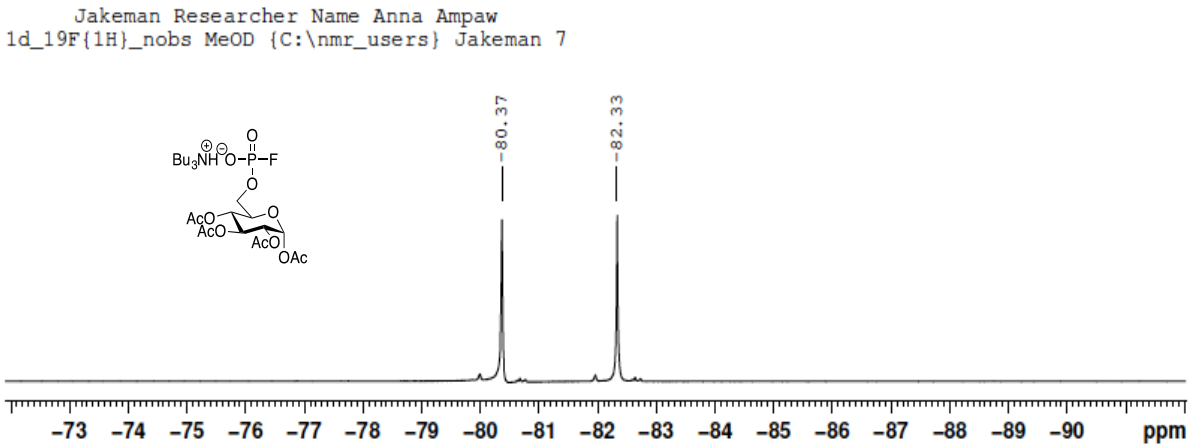

APPENDIX 2. LC-MS/MS DATA

A. XIC of 5FW-modified peptides including W24 (Method A)

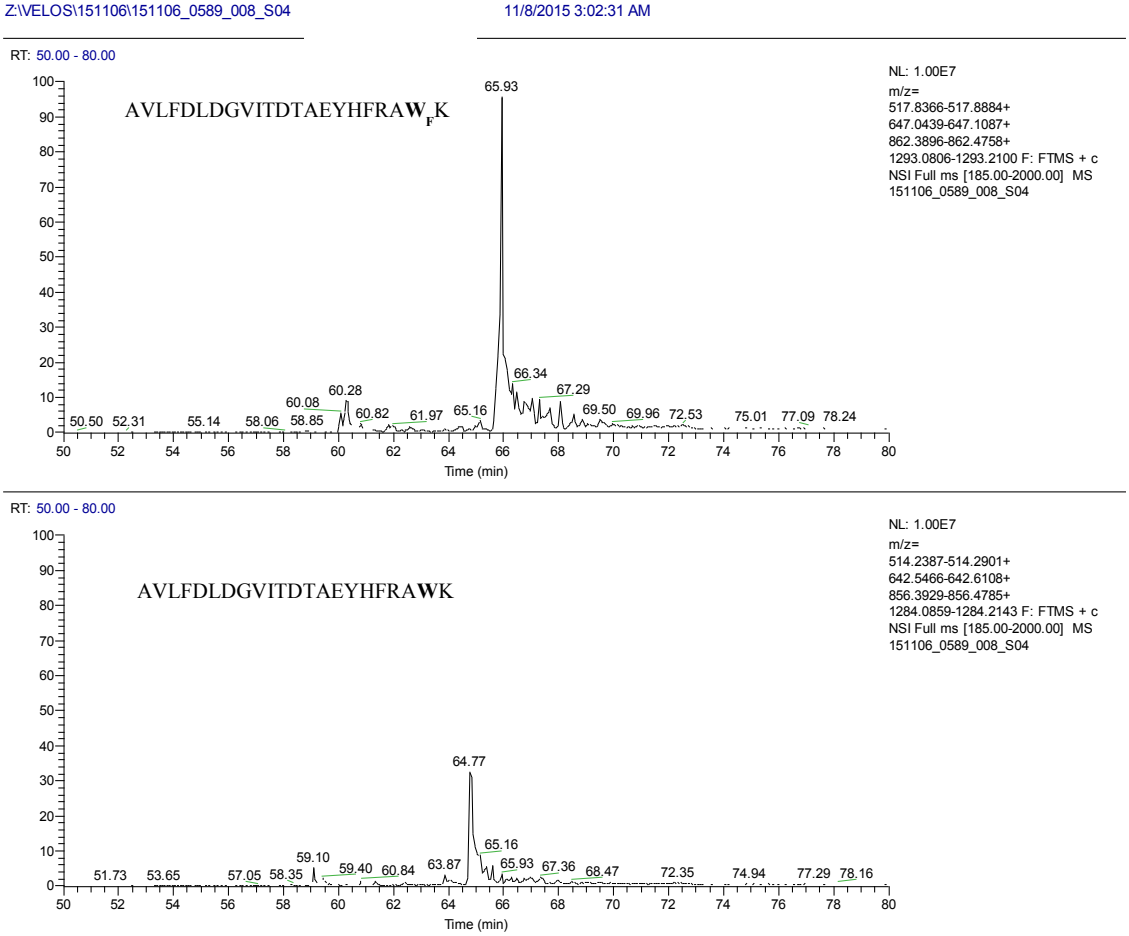

B. XIC of 5FW-modified peptides including W216 (Method A)

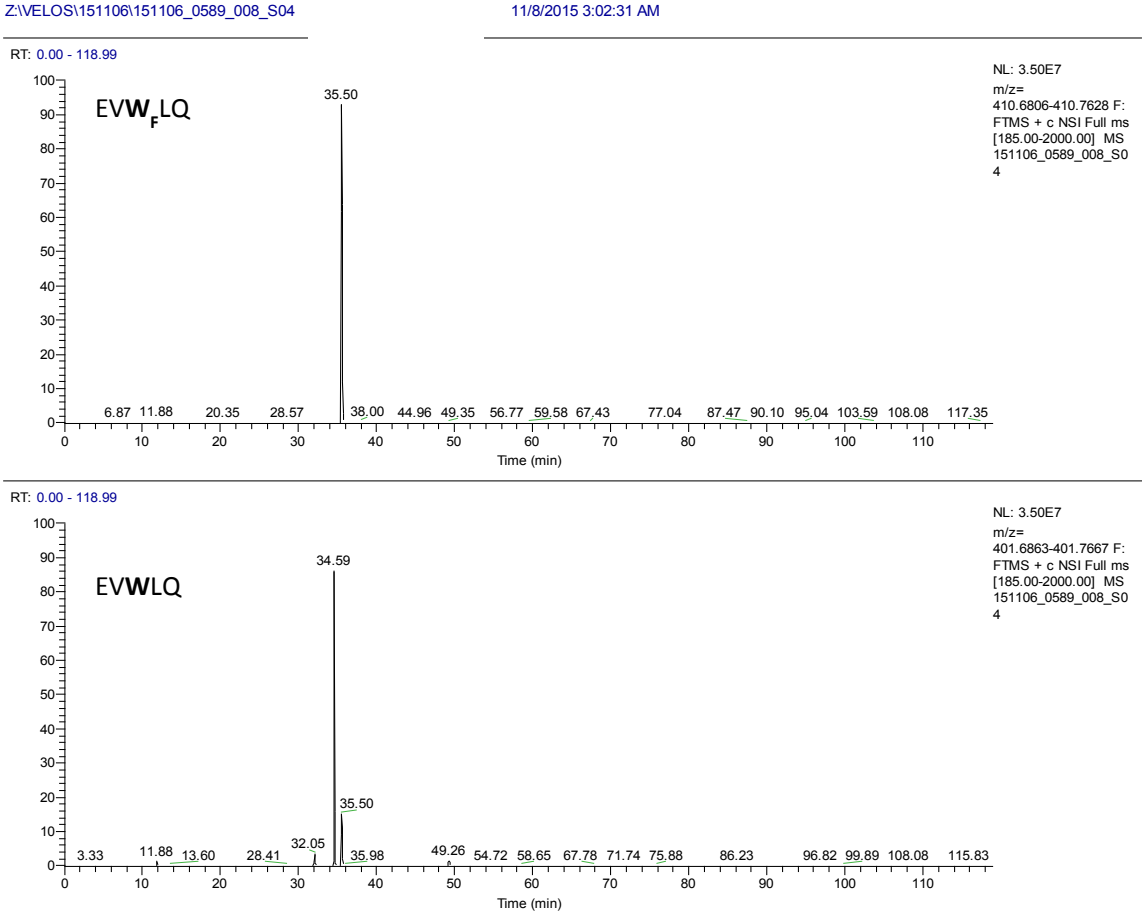

C. XIC of 5FW-modified peptides including W24 (Method B)

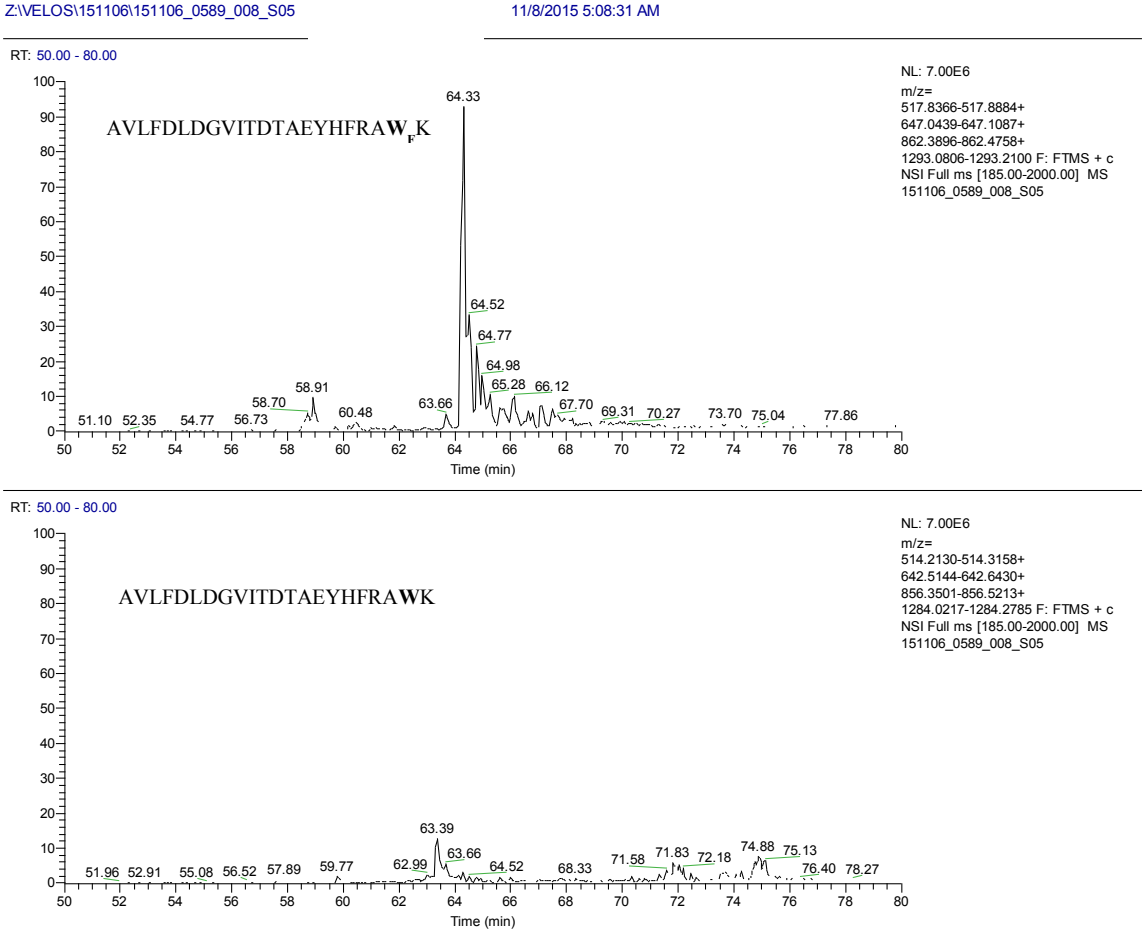

D. XIC of 5FW-modified peptides including W216 (Method B)